

Deep sequence models tend to memorize geometrically; it is unclear why.

Shahriar Noroozizadeh ^{*†}

Machine Learning Department & Heinz College
Carnegie Mellon University
snoroozi@cs.cmu.edu

Vaishnavh Nagarajan [†]

Google Research
vaishnavh@google.com

Elan Rosenfeld

Google Research
elanr@google.com

Sanjiv Kumar

Google Research
sanjivk@google.com

Abstract

Deep sequence models are said to store atomic facts predominantly in the form of *associative* memory: a brute-force lookup of co-occurring entities. We identify a dramatically different form of storage of atomic facts that we term as *geometric* memory. Here, the model has synthesized embeddings encoding novel *global* relationships between all entities, including ones that do not co-occur in training. Such storage is powerful: for instance, we show how it transforms a hard reasoning task involving an ℓ -fold composition into an easy-to-learn 1-step navigation task.

From this phenomenon, we extract fundamental aspects of neural embedding geometries that are hard to explain. We argue that the rise of such a geometry, as against a lookup of local associations, cannot be straightforwardly attributed to typical supervisory, architectural, or optimizational pressures. Counterintuitively, a geometry is learned even when it is more complex than the brute-force lookup.

Then, by analyzing a connection to Node2Vec, we demonstrate how the geometry stems from a spectral bias that—in contrast to prevailing theories—indeed arises naturally despite the lack of various pressures. This analysis also points out to practitioners a visible headroom to make Transformer memory more strongly geometric. We hope the geometric view of parametric memory encourages revisiting the default intuitions that guide researchers in areas like knowledge acquisition, capacity, discovery, and unlearning.

1 Introduction

When succinct high-level patterns explain the data, deep sequence models produce corresponding high-level representations, as seen in natural language [40, 130, 112] and arithmetic tasks [100, 120, 117, 59]. When no such patterns exist (e.g., as in the capitals of countries), models are said to default to a brute-force lookup, known as *associative* memory [139, 20]. These two narratives have so far roughly guided our understanding of how neural networks fit sequential data. We highlight a third behavior missing in this narrative: even when memorizing such incompressible atomic co-occurrences, a deep sequence model can produce powerful representations. This implies a distinct form of parametric memory that we term as *geometric* memory—glimpses of which can be found in recent observations [74, 85, 189]. In opposition to the well-studied associative memory, a geometric memory has synthesized “global” information not explicit in the local co-occurrences, enabling new forms of reasoning. From this behavior, we extract aspects of neural embedding geometries that are hard to explain, raising fundamental questions about memorization in deep sequence models. To these questions, we offer some preliminary answers.

^{*}Work done during internship at Google Research.

[†]Corresponding authors.

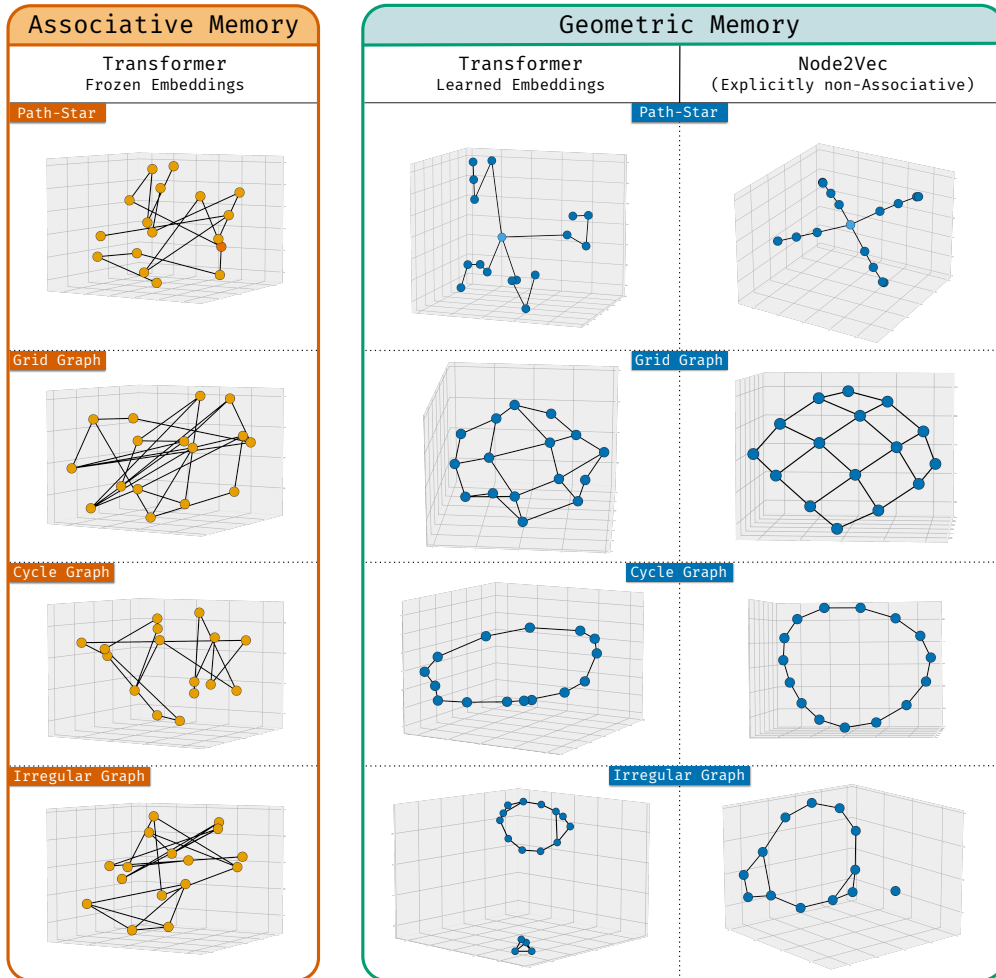


Figure 1: **Associative vs. geometric memory of models trained on various graphs.** There are two dramatically different ways to memorize a dataset of atomic facts. The common view is of associative memory: entities are embedded arbitrarily, and co-occurrences are stored in weight matrices. **(left)**. §2.4: In practice, we find a *geometric* memory: the learned embeddings of a Transformer **(middle)** reflect *global* structure inferred from the *local* co-occurrences in training data. §4: When associative memory is explicitly prohibited (by removing intermediate layers), as in a Node2Vec model **(right)**, a more elegant geometry materializes. This points to a clear headroom to improve the geometric nature of a Transformer’s memory. Details of the Transformer architecture used for this visualization are provided in §B.2.2. Similar geometries for Mamba and neural networks are presented in §C.3.

Our discussion starts at a seemingly tangential point. We begin by consolidating a fragmented set of recent demonstrations [85, 174, 43, 48, 189, 74] that the Transformer exhibits some level of *implicit in-weights reasoning*, i.e., reasoning over knowledge from the weights without emitting an explicit chain of thought. We sharpen these results by crafting a scenario where this ability is unexpected, plays out vividly, and can be cleanly isolated and analyzed. Specifically, we study path-finding on path-star graphs, a (symbolic) implicit reasoning task. The task was adversarially designed [13] to cause failure of next-token trained deep sequence models—Transformer [172] and Mamba [60] models alike. Whereas in the original task, the model is given the graph in-context, here we make the model memorize the graph’s edges in its weights. Where before the model spectacularly failed to learn path-finding even on small graphs, in our in-weights task the model succeeds even on massive graphs.

The success in the in-weights path-star task, we argue, is hard to reconcile within the *associative* view of parametric memory, a convenient and highly effective abstraction of neural network memory, popular in literature [20, 26, 78, 177, 51, 202, 27, 124, 176]. In this abstraction (see Def. 2a), each entity is embedded randomly/near-orthogonally via a “key” function $\Phi(\cdot)$, while associations are

stored in what is effectively a (rotated) adjacency matrix, $\mathbf{W}_{\text{assoc}}$. To perform a “lookup”, one computes the quantity $\Phi(v)^T \mathbf{W}_{\text{assoc}} \Phi(u)$ which is large if *and only if* entities u and v co-occur during training. With such a data structure, our path-finding task requires composing the lookup operation ℓ times (for path length ℓ). Unless there is step-wise supervision for each composition, learning the ℓ -fold composition should be a daunting needle-in-the-haystack task demanding $\exp(\ell)$ time. By the specific design of our task, *every possible form of step-wise guidance is eliminated*. Yet our model appears to find the needle.

This apparent paradox begins to be resolved by a preliminary observation in [78, 85, 189]: that the node embeddings Φ reflect some useful notion of distance; and a separate finding in [74, 153]: that (two-hop) reasoning can emerge from “factorized” parameterizations. We flesh out a unified understanding of these observations and their implications. First, the existence of structured node embeddings implies that models can store atomic facts in an altogether distinct paradigm of parametric memory that we term as geometric memory. This memory is in dramatic contrast to the associative one. In the simplest form of the geometric view (see Def. 2b), the associations are no longer stored verbatim in a lookup table $\mathbf{W}_{\text{assoc}}$, but are (low-rank) factorized into the embeddings as $\Phi_{\text{geom}}(u)^T \Phi_{\text{geom}}(v)$. Our key insight is that these embeddings are no longer arbitrary. Rather, they are carefully arranged such that they encode *global* relationships without explicit supervision to do so: even if entities u and v never appeared in the same context, the dot-product $\Phi_{\text{geom}}(u)^T \Phi_{\text{geom}}(v)$ captures the model’s own notion of multi-hop distance between the pair. This global geometry can open up new forms of reasoning, since what seemed to be a hard-to-learn ℓ -fold composition of local associations is now approximated as an easy-to-learn spatial navigation task. We contrast the associative (Def. 2a) and geometric (Def. 2b) views of memory visually in Fig. 1 and also in Table 1.

The observed geometry raises fundamental questions. Most importantly, there must be competition between the two parametric memories, both equally valid solutions to the training objective; why does the geometric prevail over the associative? To some readers, a geometric bias may seem familiar and intuitive at first sight, but we isolate aspects that cannot be easily explained: the global geometry is learned even when there is no “global” supervision (e.g., a path-finding objective), even when there is no rank constraint, even when the geometry is much harder to find, and even when it is just as succinct as a lookup. Thus, typical pressures from the supervision, architecture or optimization do not explain why a highly non-trivial geometry is synthesized. We term this the *memorization puzzle*. Towards understanding this, we reduce the setup to a minimal Node2Vec architecture, where we find that global geometries emerge from well-known spectral biases in such architectures. But, in contrast to prevailing theories (e.g., Levy and Goldberg [93]; see §5.5), we identify how the spectral bias arises naturally from cross-entropy loss minimization, independent of typically-assumed architectural or optimizational pressures. This gives us a preliminary insight into the natural rise of a geometric memory, albeit in a much simpler model, leaving open a foundational question for deep sequence models. Various practical questions open up too, which we discuss below.

1.1 Implications

Although the evidence of implicit reasoning is so far limited to symbolic tasks, we believe that the geometry we isolate is a clean nucleus of well-established geometries in language modeling [40, 112, 65] and arithmetic tasks [100, 120, 117, 59]. These insights suggest broader directions, both practical and theoretical. First, we find that the embeddings learned by more naive Node2Vec models are more strongly geometric than those of Transformers; in hindsight, this points to a well-specified headroom for making Transformer memory more geometric and less associative in practice. If the geometric bias can be improved in natural language tasks, it would also benefit natural implicit reasoning tasks where results have so far been mixed [135, 21, 185, 186, 16]. Since geometric memory encodes global relationships, it could help discover novel connections between information scattered in a large pretraining set [187] and thus, some types of creativity [22, 45, 119]. On the flip side, the interdependencies in geometric storage may impose limits on knowledge editing, unlearning and accurate retrieval; it may also hallucinate associations [74] (cf. “illusory correlations” in [153]). Another implication of our study is a support for why parametric memory may be superior to in-context memory, echoing Wang et al. [174], Geerts et al. [48]. Finally, the gap between the Transformer and Node2Vec geometries may also be of interest to practitioners in retrieval systems, when choosing between modern generative retrieval models [166, 179, 141] and traditional dual-encoder models [52, 73].

Many foundational directions follow. Foremost are the questions of how associative and geometric memory compete under gradient descent and what aspects of the data or optimization are ideal for the geometry to arise. The examples and analyses in this work may act as sandboxes to study a variety of geometric empirical phenomena: the emergence of “world models” [44, 65, 151], linear representations and superposition in interpretability [112, 130, 40] and why different models share similar representations, i.e., the Platonic representation hypothesis [92, 75]—and *what* these representations are. Finally, we speculate that the associative view forms the default unstated set of intuitions that guide research in numerous areas such as knowledge acquisition, discovery, unlearning, reasoning, storage capacity and scaling laws. The geometric view may inspire researchers to revisit, spell out and widen these latent intuitions. For instance, one may re-examine capacity [106, 81, 105, 80, 87] and scaling laws [10, 115, 144, 128] under a geometric lens and find very different answers.

1.2 Summary of contributions

1. We isolate a clean instance of implicit in-weights reasoning in deep sequence models that succeeds even without any form of stepwise supervision. This isolates a behavior that is hard to explain within the predominant associative view of parametric memory. (§2)
2. We establish an alternative, global *geometric* view of memory in deep sequence models (simple neural networks, Transformers and Mamba). (§2.4)
3. We demonstrate why the geometric memory is surprising: the emergence of geometric over associative memory cannot be attributed to obvious architectural, optimizational or supervisory pressures. With this, we formulate a *memorization puzzle* in sequence modeling. (§3)
4. We connect the global geometry to the spectral bias of Node2Vec dynamics. We empirically intuit how it emerges without typically-assumed pressures, when minimizing the cross-entropy loss. This makes progress towards an open question in Node2Vec. We also highlight significant headroom in the embedding geometry of the current architectures. (§4)

Table 1: Comparison of two forms of parametric memory in a deep sequence model, given a dataset of edges from a graph $\mathcal{G} = (V, E)$

	Associative Memory (Def. 2a)	Geometric Memory (Def. 2b)
Storage mechanism	A lookup table of pairwise edge associations	A graph embedding of the vertices
Embedding Φ	Arbitrary (random or orthogonal); acts as keys for lookup; doesn't reveal the associations in itself	Reveals the graph structure
Simplest neural implementation (of the learned similarity between input token, node u and next-token, node v, denoted by $f(u)[v]$)	$f(u)[v] = \Phi(u)^T \mathbf{W}_{\text{assoc}} \Phi(v)$ where $\mathbf{W}_{\text{assoc}} \approx \sum_{(u,v) \in \mathcal{G}} \Phi(u) \otimes \Phi(v)$ and $\Phi(u) \cdot \Phi(v) \approx 0$ for $u \neq v$.	$f(u)[v] = \Phi_{\text{geom}}(u)^T \Phi_{\text{geom}}(v)$ where Φ_{geom} corresponds to (top) eigenvectors of graph Laplacian.
Relationship to graph \mathcal{G}	$\mathbf{W}_{\text{assoc}}$ can be thought of as adjacency matrix (up to a rotation)	Φ_{geom} can be thought of as <i>low-rank factorization</i> of adjacency matrix; alternatively, the eigenvectors in Φ_{geom} are also components dominant in multi-hop adjacency matrix, \mathbf{A}^ℓ for large ℓ .
Global information	Only local edge information is readily available i.e., $f(u)[v]$ high only for $(u, v) \in E$	Global information readily available i.e., $f(u)[v]$ is proportional to multi-hop distance between u and v in \mathcal{G}
Novel information not present in data	None; only stores seen associations.	Has synthesized novel information by integrating information scattered across multiple datapoints.
Implicit compositional reasoning e.g., path-finding	Intuitively, exponentially hard to learn.	Approximated as an easy-to-learn geometric navigation task.
Accuracy of retrieval	Precise	Approximate
Description length	Number of edges, $ E $	Number of vertices times the embedding dimensionality, $ V m$

Contents

1	Introduction	1
1.1	Implications	3
1.2	Summary of contributions	4
2	Implicit in-weights reasoning is learned	8
2.1	The in-weights path-star task	9
2.2	Success of implicit in-weights reasoning	9
2.3	The contradiction behind learning the hardest token	10
2.4	Two competing data structures for parametric memory	11
3	The memorization puzzle: The emergence of geometric memory is not easy to explain	14
3.1	Supervisory pressure does not explain geometric memory	14
3.2	Capacity or optimizer pressures do not explain geometric memory.	14
3.3	The memorization puzzle	16
4	Geometry arises from naturally-occurring spectral bias, without pressures	19
4.1	Where does the geometry come from?	19
4.2	Where does the global information come from?	19
4.3	Where does the low-rank spectral bias come from?	19
4.4	The importance of weight-tying	22
5	Related work	23
5.1	Analysis of Transformer memory	23
5.2	In-weights reasoning tasks	24
5.3	Failure of end-to-end composition learning	25
5.4	In-context graph tasks	25
5.4.1	In-context vs. in-weights learning	26
5.5	Analyses of graph and word embedding methods	26
5.6	Other foundational works on generalization and memorization	26
6	Limitations	28
7	Conclusions and Future Work	28
A	Detailed background on the path-star task	43
A.1	Failure of next-token learning in the in-context path-star task	43
A.1.1	Where does the path-star-failure argument go wrong in the in-weights setting?	44
B	Experimental setup	46
B.1	Graphs, tokens, and data construction	46

B.2	Model architecture	46
B.2.1	In-weights path-star task experiments	46
B.2.2	Tiny model architectures	46
B.3	Training and optimization	47
B.4	Evaluation protocols and metrics	47
B.5	Implementation and compute	48
C	Experiments on broader settings	49
C.1	Path-star task on Mamba SSM	49
C.2	Other large, harder path-finding graphs	51
C.3	Tiny graphs	53
C.4	Additional experiments on path-star geometry	58
D	Edge supervision and training dynamics	60
D.1	The role of reverse edges	60
D.1.1	The critical role of reverse edges in the large path-star task	60
D.1.2	Tiny graphs with uni-directional edge-memorization	62
D.2	Pause tokens for computational slack	63
D.3	(Not) Interleaving edge-memorization	63
D.4	Effect of weight-untying	64
D.5	Learning order of tokens	65
E	Proofs about representational complexity	66
E.1	Empirical failure of composition learning under associative memory	66
E.2	Succinctness does not break the tie: Proof of Proposition 3d	66
E.3	Weight-tied dual-encoder models can represent certain special or contrived forms of associative memory	67
F	Detailed analysis of spectral bias in Node2Vec	69
F.1	Challenges of analyzing the dynamics	69
F.2	Empirical intuition of the dynamics	69
F.3	Mathematical description	70
F.4	Deriving the dynamics	73

2 Implicit in-weights reasoning is learned

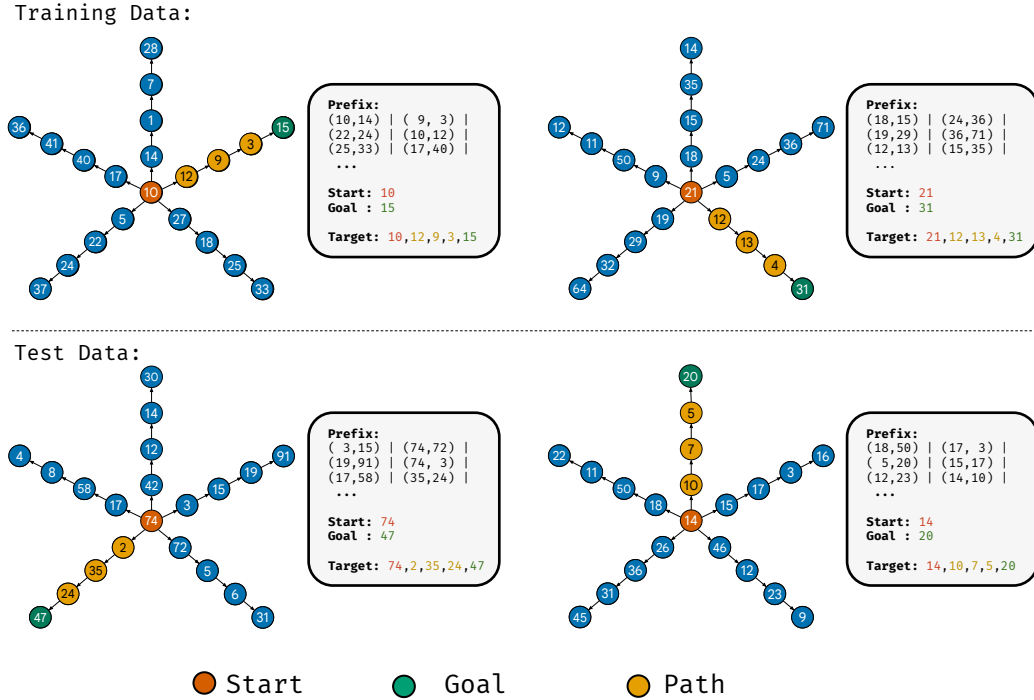


Figure 2: **Overview of in-context path-star task of B&N’24.** Each training and test example corresponds to a fresh, randomly-labeled path-star graph (a tree graph where only the root node branches into d paths of length ℓ). For each example, the prefix specifies a randomized adjacency list (of edge bigrams) of the corresponding graph, followed by $(v_{\text{root}}, v_{\text{goal}})$. The target is the full path $(v_{\text{root}} \rightarrow v_{\text{goal}})$ in that graph.

We investigate planning on a *path-star graph*, a graph designed to be adversarial towards next-token learning [13]. The task has a clear notion of a chain-of-thought, and a well-understood mechanism of failure for learning in-context reasoning. Thus, we hope to repurpose this to cleanly analyze a different type of reasoning—in-weights reasoning—in a way that was not possible in earlier studies of in-weights reasoning.

Background. The path-star topology (Fig. 2) from B&N’24 is a tree graph where multiple *disjoint uniform-length* paths branch outwards from the root. In other words, all internal nodes but the root have exactly one child. In the original version of this task [B&N’24], the model is given a fresh example of this graph in *context* as an adjacency list (with randomized node labeling and edge ordering, but fixed topology), along with a leaf node specified as goal. The model must spell out the nodes in the unique path from the root to the goal in that order. The solution is to notice a simple right-to-left structure: take the unique path back from the leaf node and reverse it. Indeed, this is the implicit chain-of-thought required before emitting the first token.

Yet, on this simple task, left-to-right next-token learners are known to fail in-distribution even on tiny graphs. This failure unfolds in two stages during optimization: (1) On all but the first token, the model fits the data trivially: simply predict the token as the unique child of the previous ground-truth token that is revealed in the context. Then, this starves the first, key decision-making step of gradients from the rest of the path. (2) Consequently, the first token must be learned in isolation, which becomes a computationally hard learning ℓ -hop composition problem (as detailed later). At test-time, this model defaults to guessing a random first token and continuing along that wrong path. We reproduce this failure in Fig. 5 and elaborate on it in §A.

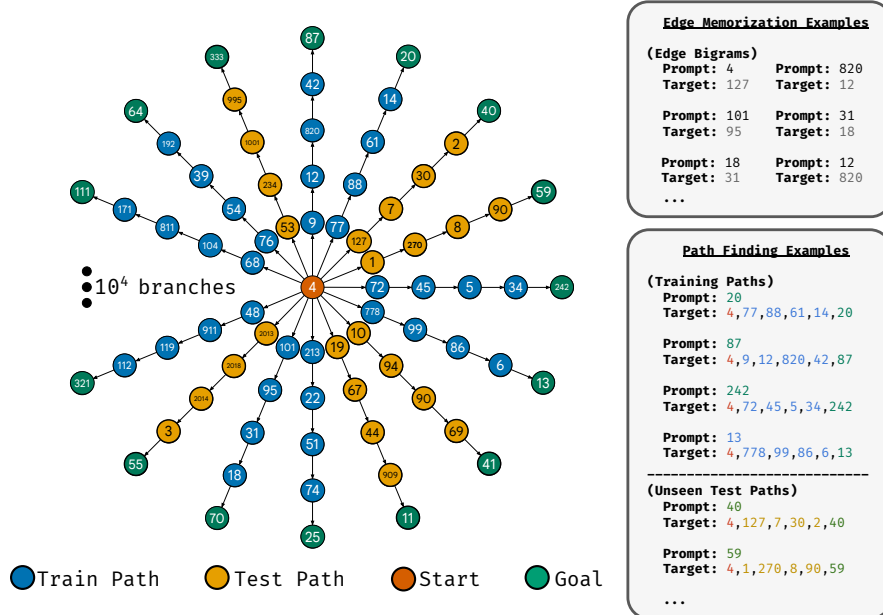


Figure 3: **Overview of our in-weights path-star task.** All examples are derived from a fixed path-star graph. Training involves two types of examples: (i) **edge memorization** examples; (ii) **path-finding** examples, where the prefix is some leaf, and the target is the full path. Test examples are path examples corresponding to a held-out set of leaves.

2.1 The in-weights path-star task

Task definition. For our study, we consider a task inspired by the above task, yet *fundamentally different*. In our task, the graph is stored *in the model weights* rather than *presented in context* (Fig. 3). Here, all examples are generated from a (very large) fixed graph \mathcal{G} (of degree d and path length ℓ), rather than a (small) fresh graph per example. The model is made to memorize the full graph in its weights through “edge-memorization examples”, where the input is some node v , and the next-token target is an adjacent node v' . Separately, path-finding examples are generated from the same graph by picking as input a random leaf node v_{leaf} (a single token) and as target, the unique root-goal path (a sequence from v_{root} to v_{leaf}). The model is trained for path-finding on only a *subset* of such leaves from our fixed graph, and is tested on the remaining “unseen” leaves. By “unseen”, we mean that the paths to these leaves are never seen end-to-end; only the constituent edges are seen individually, which doesn’t trivialize the path-finding task. (Besides this path-star topology, we consider some harder variants, deferred to §C.2.)

Experimental setup. We use a from-scratch, decoder-only Transformer (GPT-mid) [138]; we corroborate all our findings on Mamba in §C.1. For the most stable results, we interleave the edge-memorization and path-finding examples during training as in Fig. 3 and also use pause tokens [57]. We found that it is important to provide both forward and reverse edges for edge-memorization in order to dodge the reversal curse [136, 9], but this may not be necessary for smaller graphs; see §D.1. This reverse augmentation is *not* given for the path-finding examples. Details about the formatting and the hyperparameters are in §B, followed by additional analyses in §D.

2.2 Success of implicit in-weights reasoning

Our first observation is that, despite the adversarially-constructed topology of our graph, and even on path lengths of 6 to 10 hops and graphs as large as 10^4 nodes, our next-token-trained models succeed

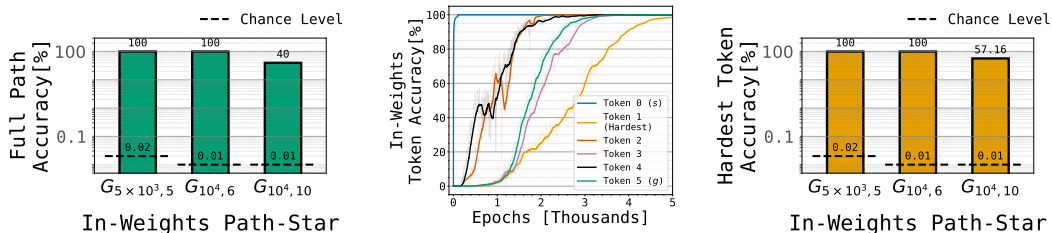


Figure 4: **Success of Transformer in in-weights path-star task. (§2)** (left) A next-token-trained Transformer achieves perfect or highly non-trivial accuracy on large path-star graphs $\mathcal{G}_{d,\ell}$. (middle) **Learning order of tokens.** The tokens of a path are not learned in the reverse order i.e., the model does not learn the right-to-left solution. Thus, gradients from the future tokens are not critical for success. (right) **Success of hardest-token-only task.** In fact, the hardest token (the first) given the leaf is learned in isolation to non-trivial accuracy (Observation 1). Success of this ℓ -fold composition task is hard to explain within the associative memory view (§2.3). Analogous plots for Mamba are in Fig. 14. We invite the reader to contrast these in-weights task results with the in-context task ones in Fig. 5.

at the in-weights path-finding task. We report this in Figs. 4 and 14 (left). This isolates an implicit in-weights reasoning sharper than what exists in the literature. Known instances are on small scales of 200 or fewer entities [85, 48] or on 2-hop tasks [174, 43, 189, 74]. We report success in some harder topologies in §C.2.

Next, we isolate an even sharper instance of success. To arrive at that, we ask: why does the next-token learner succeed on massive in-weights path-star tasks, when back in B&N’24 it failed on even tiny in-context path-star tasks? A possible factor could be that in the in-weights setting, the model does not succumb to trivial left-to-right, next-token shortcuts; thus gradients from farther-away tokens survive, allowing the model to discover the true right-to-left solution. However, we find this is likely not the case since the tokens are not learned in a right-to-left order—we report this in Figs. 4 and 14 (middle) and elaborate on it in §A.1.1. This inspires us to test a harder task where any future-token supervision is manually eliminated: we train the model purely on the first-token loss, conditioned on only the leaf node that is many hops away. Learning the first token—the key decision-making token—in isolation, is (theoretically and empirically) impossible in the in-context path-star task, as B&N’24 show and as reproduced in Fig. 5 (right). In striking contrast in our in-weights task, our model learns this token in isolation, demonstrating an even sharper instance of implicit reasoning:

Observation 1. (Hardest, first token is learned in isolation) *On in-weights path-star graphs of as many as 5×10^4 nodes, when the model is trained on only edge-memorization examples and first-token-training examples from 75% of all the paths, on unseen paths, both the Transformer and Mamba are able to predict the first token when conditioned on held-out leaves, with as much as 100% accuracy (Figs. 4 and 14 (right)).*

That the hardest (first) token is learned, we argue, is difficult to square with the abstraction that parametric memory strictly stores local associations. We explain this in the next subsection.

2.3 The contradiction behind learning the hardest token

Atomic facts are often imagined to be stored in the parameters as local associations, where a matrix acts as a lookup table. We make this concrete. For any tokens u and v , let $f(u)[v]$ denote the logit of a sequence model f on the target v , conditioned on the input u . Then:

Definition 2a. (Local associative parametric memory) *We say that a deep sequence model f has memorized a graph $\mathcal{G} = (V, E)$ associatively iff for any vertices u and v , the logit $f(u)[v]$ is high only on adjacent vertices, $(u, v) \in E$. In its simplest form, this model is typically abstracted as $f(u)[v] = \Phi(u)\mathbf{W}_{\text{assoc}}\Phi(v)$. Here, $\mathbf{W}_{\text{assoc}}$ encodes the adjacencies as $\sum_{(u,v) \in E} \Phi(u) \otimes \Phi(v)$; the embeddings Φ are arbitrary “keys” that by themselves encode no associations in graph \mathcal{G} , e.g., they are orthogonal embeddings [177, 51, 78, 202, 27] or random (and thus, near-orthogonal) embeddings [124, 26, 20, 176].*

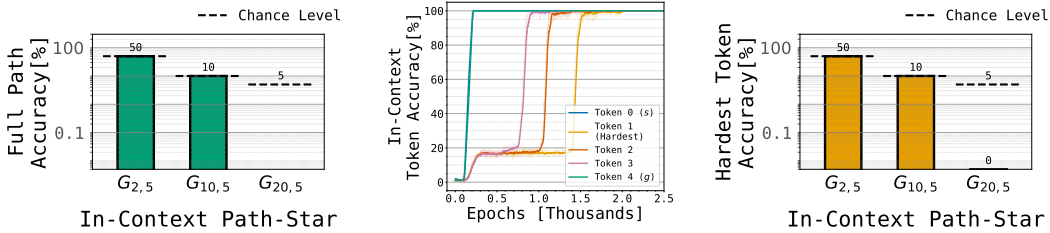


Figure 5: **Failure of Transformer in in-context path-star task. (B&N’24)** We report the failure of next-token Transformers in the in-context version of the path-star task, reproducing results from B&N’24. **(left)** Full path accuracy remains at chance level across different small graph sizes. **(middle)** Learning order of tokens with teacherless (multi-token-trained) objective shows a clear right-to-left learning cascade. **(right)** The hardest (first) token given the leaf fails to be learned in isolation, contrasting sharply with in-weights success shown in Fig. 4.

Observe that, in this abstraction, the first node in our task requires composing a local recall function ℓ -many times: recall the predecessor of v_{leaf} from the weights, namely $v_{\ell-1}$, then the predecessor of that, $v_{\ell-2}$, and so on. In short, one can write $v_1 = \text{Predec}^\ell(v_{\text{leaf}})$.

Hardness of learning compositions. With this structure however, the first-token ℓ -fold composition task should intuitively require $\Omega(\exp(\ell))$ compute to learn—just like the first token was demonstrably hard-to-learn in the in-context path-star task [B&N’24]. One intuition is that the optimization task is a search for a needle in the haystack: there is an $\exp(\ell)$ space of possible discrete compositions, and all but the correct one have an equally miserable loss value; with the loss terrain rendered flat and the gradients uninformative, the learner is forced to sift through the vast hypothesis space to find a needle. As a preliminary corroboration of this intuition, in §E.1, we find that models fail at this task when the embeddings are frozen. We also refer the reader to existing results that empirically demonstrate that compositions are hard to learn [156, 2, 61, 54, 1, 2] and others that theoretically demonstrate hardness [108, 32, 132, 156, 180, 159] (although only in a certain sense; see Remark 2).

The power of step-wise aid. This barrier could be surmounted if, rather than providing supervision from only the end output of the composition, there was supervision from each hop. This could mean providing a data curriculum [149, 180, 188, 5, 36] or providing chain-of-thought supervision [181, 125] or reducing compositionality through various means. Indeed, prior positive results on implicit in-weights reasoning involve one such aid or the other. First, Khona et al. [85] have paths of varying lengths (see their Fig 11), which provides an implicit curriculum; they also provide full path supervision, not just the first-token loss. Furthermore, their test and train paths overlap, reducing compositionality, potentially allowing the model to stitch substrings it has seen (an ability demonstrated as possible [177]). Other results [174, 43, 189, 74] are on 2-hop tasks, implying a friendly exponent.

Our setting, by design, offers none of these aids. Our paths have fixed lengths (hence, no implicit curriculum), are disjoint (so, no test-train overlaps), and require as much as a 10-fold composition (so, a daunting exponent). What we isolate, therefore, is a stronger and more sterile instance of implicit in-weights reasoning, one that is cleanly inconsistent within the associative view of parametric memory.

2.4 Two competing data structures for parametric memory

The paradox begins to resolve with fragmented yet salient observations in literature—[78, 85, 189] and [74]—that we will flesh out more generally. First, [78, 85, 189] find that the embeddings of their tokens reflect some useful notion of distance, aiding their respective implicit reasoning tasks. Independently, [74, 152] find that memorizing associations through an explicitly factorized architecture allows the model to draw unseen (two-hop) inferences. We will generalize these observations to our much larger graphs and many-hop tasks; but first, we point out that these observations are related and lead to profound implications. First, these observations paint an altogether different picture of parametric memory itself: a memory of atomic facts that does not take shape as a lookup over arbitrary embeddings but as a geometry of highly-organized embeddings. While the former directly stores the adjacency matrix \mathbf{A} in the matrix $\mathbf{W}_{\text{assoc}}$ (up to some rotations defined by

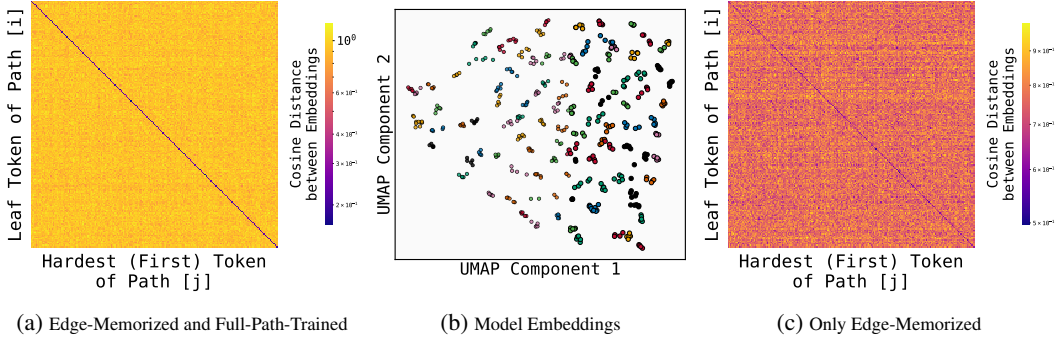


Figure 6: **Evidence of global geometry of Transformer in path-star task.** (a) In the heatmap, entry (i, j) is the cosine distance between the *leaf* embedding of path i (row) and the *first-hop* embedding of path j (col). The clear diagonal line implies that embeddings within each path are more aligned, reflecting global structure. (b) UMAP projection of token embeddings where each point is a node embedding; color indicates path identity. Different paths form separated clusters (see Fig. 27 for clearer image). (c) For a later experiment in §3.1: heatmap for a model trained only on edge-memorization still reveals a level of geometry, although weaker than in (a). Analogous plots for Mamba are in Fig. 15

Φ), the latter “factorizes” the associations into a low-rank form, $\Phi_{\text{geom}}(u)^T \Phi_{\text{geom}}(v)$. Importantly, whereas an associative memory only makes local information accessible, a geometric memory readily exposes global multi-hop relationships (§4 discusses what these global relationships are). We define the notion of geometric memory below, and compare the two forms of memory in Table 1.

Definition 2b. (Global geometric parametric memory) We say that a deep sequence model f has memorized a graph $\mathcal{G} = (V, E)$ geometrically iff for any pairs of vertices u and v , the logit $f(u)[v]$ reflects some notion of multi-hop closeness in \mathcal{G} . At its simplest, this can be abstracted as $f(u)[v] = \Phi_{\text{geom}}(u) \cdot \Phi_{\text{geom}}(v)$, where Φ_{geom} reflects some graph embedding of the vertices.¹²

The resolution. One can view the two parametric memories of Defs. 2a and 2b as two competing data structures, both representable by a deep sequence model, each yielding its own learning complexity for the hardest token (much like how a heap or an array would yield different search complexities). The local associative memory is analogous to a linked list: for the first token, this would incur a (benign) ℓ -hop lookahead step but *learning* this incurs an exponential cost. The geometric memory is powerful in that it reduces this learning complexity all the way to $\Theta(1)$. For instance, we may expect that the embeddings of all nodes in path i are clustered tightly around a unique path vector \mathbf{z}_i . In this data structure, learning the first token given the leaf node is a one-hop task: simply find a one-hop neighbor of the central node that is best-aligned with $\Phi_{\text{geom}}(v_{\text{leaf}}^{(i)})$. As stated below, such a structure indeed materializes both in our massive graphs and in tiny graphs; this geometry turns out to be fundamental to any gradient-descent-trained deep sequence model and not specific to attention or residual connections:

Observation 2. (Evidence of global geometry across various deep sequence models) For our large path-star graphs, the (token) embeddings of the leaf and first node of a path are clustered closer to each other than those of other paths in both the Transformer and Mamba (Fig. 6 and Fig. 15). Similar geometries arise for a variety of small graphs for the Transformer, Mamba and a simple 3-layer neural network model without attention and residual connections—see visualizations in Fig. 1 and Section C.3; §C.3: Figs. 18 to 21) and node-node cosine-similarity heatmaps (§C.3; Figs. 23 and 24).

¹In the simple settings of this paper, the geometric embeddings Φ_{geom} in practice are found in the token embeddings themselves; but more generally, such an embedding may reside in any other layer. We consider even that to be geometric memorization.

²Note that this simplistic abstraction may assign the highest output logit to the input vertex itself (i.e., $\arg \max_v \Phi_{\text{geom}}(u) \cdot \Phi_{\text{geom}}(v) = u$) regardless of whether a self-loop (u, u) exists. To account for this, one may incorporate an auxiliary self-loop-detecting circuit. We treat this as a pedantic detail best ignored for a tidy discussion.

While these geometries help make sense of why implicit reasoning succeeds, it also leaves us with a foundational question of why the model prefers one form of memory over the other. We elaborate on this in the next section.

3 The memorization puzzle: The emergence of geometric memory is not easy to explain

During training, the two types of parametric memory—two equally valid ways to fit the training data—must compete with each other. Why does the geometric memory prevail over the associative? We demonstrate that this behavior is hard to explain.

The reader may offer various plausible explanations for this behavior by borrowing intuition from other well-known phenomena. Some readers may find the rise of a geometry familiar in light of well-known geometries of features in language [40, 130, 112] and arithmetic tasks [100, 120, 117, 59]. Some others may find the phenomenon reminiscent of the competition between memorization and generalization studied in the *generalization* puzzle [195, 122, 17, 23] in regression and classification settings. These settings suggest that representations arise due to pressures from either the supervision or the architecture or the optimizer; such pressures forbid a lookup. Thus, it may be tempting to cite these well-known learning pressures as plausible explanations for what we observe in our sequence models. However, we design experiments refuting such explanations: we show that a geometric representation arises over the associative lookup even in the absence of such learning pressures. Through this analysis, we pose the *memorization puzzle* in sequence modeling.

3.1 Supervisory pressure does not explain geometric memory

Geometric representations arise in various tasks with reasoning objectives, from arithmetic [100, 120, 117, 59] to path-finding [85] to two-hop reasoning [174, 43, 189, 74]. Reasoning supervision has also been shown to act as a regularizer that elicits useful structures in the model’s storage [74]. This trail of findings overwhelmingly directs us to the following guess for why we see a geometry:

Plausible Explanation 3a. (*Pressure from global supervision*) *Perhaps, the model memorizes via a global geometry rather than via local associations due to the supervisory pressure of a multi-hop reasoning objective.*

This hypothesis however is weakened by the distinctive design of the path-star task. First, the test paths are untouched by any path-finding supervision, yet these paths exhibit a global geometry. Next, in the hardest-token-only task, path-finding supervision is applied only on the path end-points; yet a geometry materializes on intermediate nodes (see Fig. 25b). As an even cleaner refutation of this hypothesis, we ablate the reasoning supervision, and train purely on local supervision i.e., on edge memorization:

Refutation 3a. (*Geometry arises even from memorizing local, atomic co-occurrences*) *A global geometry emerges even in locally-supervised models for various architectures, as seen in the heatmaps for the large path-star graph (Figs. 6c and 15c). A locally-supervised model can be subsequently finetuned purely on the hardest-token task and achieve high test accuracy on unseen paths (§D.3). We also note that the geometries seen on the small graphs (Fig. 1; §C.3) are for various architectures trained only on edge-memorization.*

From this, we isolate the following insight: geometries can arise instead of an associative lookup, even when memorizing atomic co-occurrences devoid of any pressure to reason or to find high-level, multi-hop structures in data.

3.2 Capacity or optimizer pressures do not explain geometric memory.

We may seek yet other explanations out of canonical intuitions in theories of generalization. In regression or classification, conventional wisdom was that models learn representations rather than a lookup when there is an explicit capacity pressure e.g., the architecture or the regularizers forbid a lookup. In modern theories since the popularization of the generalization puzzle [122, 195], renewed wisdom has been that this pressure is implicit: even if the model can express a lookup, gradient descent implicitly prefers solutions that are easier-to-find or are more succinct, thus leading to useful representations. It may seem that one of these theories, when imported to the world of sequence models, can tell us why a geometric representation arises over a naive lookup of atomic associations.

We scrutinize (straightforward versions of) both these traditional and modern theories as plausible explanations for the geometry, and we refute them one by one. We begin with the traditional notion of explicit capacity pressures:

Plausible Explanation 3b. (*Explicit capacity pressures*) *Perhaps, the model memorizes geometrically because a lookup of local associations is impossible to represent. This restriction is either due to the parameter count or the design of the architecture, especially the embedding bottleneck.*

This logic can be dismantled as follows. First, we note that our architectures *can* express the associative model. Positive theoretical results in Nichani et al. [124] roughly prove that, with m (frozen) embedding dimensions, and at least m^2 free parameters, an MLP layer can store m^2 many associations. Our models have $m \approx 400$ which means our large graphs *can* be stored associatively in our models.

But maybe, there are yet other explicit pressures—such as normalizations and weight decay—that discourage associative storage. As a definitive refutation of such pressures, we make an empirical demonstration: there are experimental settings (with sufficient capacity and no bottleneck pressure) where geometric memory naturally arises; and in those very settings, an associative memory can be learned with the embeddings frozen and *all else unchanged*. Thus, there is demonstrably no explicit capacity pressure restricting an associative memory—and yet, a geometric one naturally emerges.

Refutation 3b. (*Associative memory can be artificially learned with our architectures*) *On various sequence models (Transformers, Mamba, neural networks) and various tiny graphs in Fig. 1 and §C.3, a geometric memory arises naturally even though the same setup fits the data with frozen embeddings.³*

Thus, explicit capacity pressures are not required to force a geometric memory in place. Maybe then the optimizer has a role to play. For instance, it is known that in classification settings, gradient descent takes longer to discover a lookup of artificially-randomized labels than natural labels [12]; it is also well-known that optimization tends to fit the data in progressively more complex ways [140, 184, 82, 12, 146, 19] and so a lookup would take relatively long to discover than other solutions. A similar effect can be proposed here:

Plausible Explanation 3c. (*Optimization pressure*) *Perhaps, the model memorizes geometrically because an associative storage is harder (e.g., takes longer) to find by gradient descent.*

Refuting this, we argue that in sequence modeling, an associative lookup is significantly easier to find than the geometric one. In fact, during training, *models typically first store the data associatively before storing geometrically*. First, this is already (indirectly) evidenced at various points in literature (although not interpreted this way). In the graph tasks of [189, 174], the Transformer fits atomic facts well before it “groks” to learn circuits/representations that aid two-hop reasoning; in natural language [96] models memorize n-gram statistics well before representations become more organized, giving way to generalization.

A more precise and vivid claim can be made here: Nichani et al. [124] observe that the associative lookup table $\sum_{(u,v) \in E} \Phi(u) \otimes \Phi(v)$ (from Def. 2a) can be found by *one step* of gradient descent given a reasonably large embedding size on the correlation loss, $-\sum_{(u,v) \in E} f(u)[v]$.⁴ We empirically verify this for the cross-entropy loss on our tiny graphs: associative memory forms in 2 steps (Fig. 7); whereas a geometric memory requires 100 steps (Fig. 8).

Our intuition for this “associative first, geometry later” dynamics is that an associative memory merely stores the adjacency matrix \mathbf{A} that is superficially available in the data; a geometric memory requires unearthing implicit information from the data, which requires more iterations—as we will see in §4, this computation corresponds to low-rank factorizing the adjacency matrix, or equivalently, computing a multi-hop adjacency matrix \mathbf{A}^ℓ .

³This fit is purely associative since only one trainable layer exists in these architectures (see §B.2.2).

⁴This “one-step-lookup-table” phenomenon is distinctive of sequence modeling but not of a typical classification/regression task: for the lookup to be learned easily, we want the inputs near-orthogonal. This is true by design of the initial token embeddings of any sequence modeling task, but not necessarily true of the input distribution in classification/regression.

In summary, an associative memory is easier to find than the geometric one, and yet the model (eventually) organizes its memory geometrically:

Refutation 3c. (*Associative memory is easier to find with gradient descent*) *Given sufficient embedding dimensionality and capacity, the associative storage can be discovered by full-batch gradient descent in as little as two steps on all our tiny graphs (Fig. 7) while a geometric memory takes much longer to form (Fig. 8). Similarly, we interpret the earlier findings of [189, 174, 96] as the data being fit associatively early during training, while a geometry (and therefore, reasoning) arising only much later.*

Yet another plausible explanation for the geometry can be derived from the core of modern intuition about generalization, thanks to [122, 195]: gradient descent implicitly finds succinct fits of the data even without being explicitly told to do so. So, even if gradient descent is quick to discover associative memory, over time, perhaps it discovers a geometric organization as it gradually “compresses” the data. Indeed, such compressive or complexity-reducing effects have been brought up in recent analyses of geometry in language [96] and reasoning [174]. We translate this into our terminology:

Plausible Explanation 3d. (*Implicit capacity pressure*) *Perhaps, the model memorizes geometrically (over the course of training) because gradient descent converges to a more succinct fit of the data.*

To refute this, we refute the underlying premise itself: counterintuitively, a geometric storage is not necessarily more succinct than an associative storage. To see why, we first clarify that unlike a typical classification task, or even a typical natural language task, our setting must be recognized as a *memorization* task (in the sense of Feldman [42]): the existence of an edge cannot be statistically surmised from the rest of the training set. Thus, we will show, for certain graphs, straightforward notions of succinctness do not break the tie between the two ways of representing the data.

Concretely, in generalization theories, the complexity of a lookup table is larger than the succinct one *by a factor that scales polynomially with the number of datapoints*. In contrast, in the path-star or cycle memorization task, this gap (measured through bit or norm complexity) can vanish:

Refutation 3d. (*Geometric and associative memory are roughly equally succinct*) *For certain graphs, the complexity of the local associative memory both in terms of bits and ℓ_2 norms is either equal to or at most twice those of the global geometric memory.⁵⁶ Informal proof and more explanations in §E.2.*

Thus, while the familiar geometries of word embedding tasks [40, 130, 112] arise where a lookup is clearly more verbose, similar geometries arise even in tasks where redundancies are absent and a lookup may be just as succinct.

3.3 The memorization puzzle

The above arguments isolate a fundamental aspect of well-known neural geometries that cannot be easily explained by well-known learning pressures. Geometric representations emerge even in an atomic fact-memorization task that lacks statistical redundancies. Attempts to understand this through familiar intuitions from classification/regression tasks—from the lens of ease-of-optimization and succinctness—seem to fail us in the land of sequence models.⁷ This gives rise to what we call the memorization puzzle:

⁵Equality is achieved if there is no weight-tying or if only forward edges are stored.

⁶Note that a geometry appears even when storing only one direction of the edges in the smaller graphs where both forms of storage must be equally succinct; see §D.1.2.

⁷Intuitively, this is because the geometric representations are of a fundamentally different nature from the well-studied *feature* representations in classification/regression tasks (see Remark 3).

Open Question 1: The Memorization Puzzle in Sequence Modeling

Why does a gradient-descent-trained sequence model memorize atomic co-occurrences geometrically, rather than associatively, even in cases where the associative storage is expressible, easier-to-find and just as succinct as the geometric storage?

Answering this requires a more thoughtful argument, perhaps by borrowing other notions of complexity (e.g., flatness [84] or spectral norms [123] or something else not considered so far). One may also consider some other well-understood effects of depth and factorization in neural networks [74, 11]; although, we cast doubt even on these effects; see Remark 1.

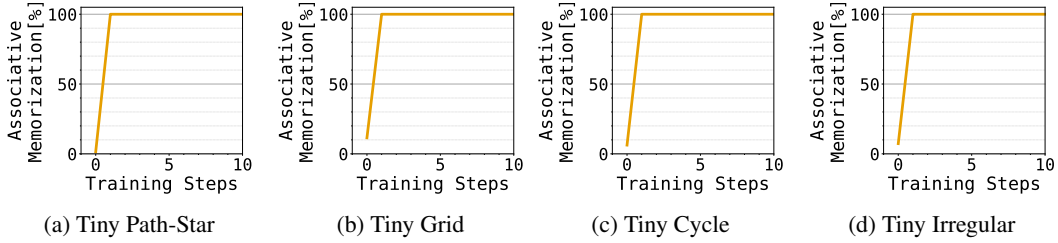


Figure 7: **Associative memory can be discovered quickly by gradient descent, given a sufficiently wide model, and a sufficiently large learning rate:** For the various tiny graphs described in §C.3, and for our TinyNN model (with frozen embedding/unembedding layers and one wide trainable weight matrix to prevent a geometry from taking over; see §B.2.2), we report memorization over timesteps of training with *full-batch* gradient descent and constant learning rate of 0.1. For each vertex, we compute what fraction of its k neighbors appear in the top k next token probabilities; this is averaged across vertices (where k varies across vertices). This value, which quantifies associative memorization, reaches its maximum within 2 steps of gradient descent; compare this to the longer time for geometric memory to form in Fig. 8. This is evidence for our Refutation 3c: ease-of-discovery does *not* dictate what memory is formed.

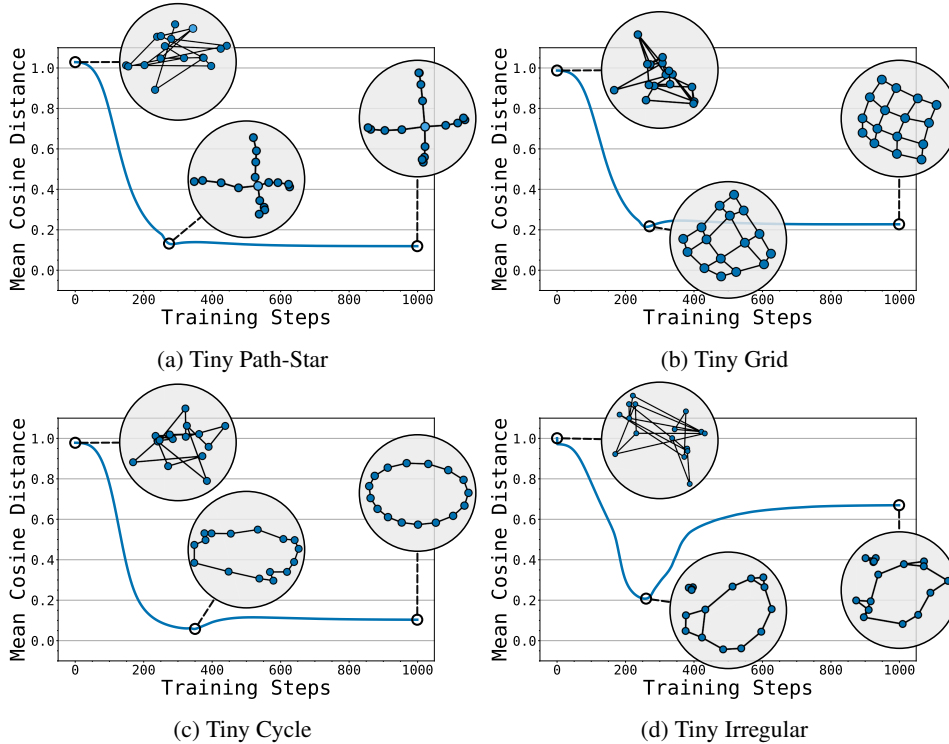


Figure 8: **Geometric memorization takes much longer for gradient descent to discover:** For the same architecture as in Fig. 7 but with learnable embeddings, we roughly quantify geometric memorization over time via cosine distance across *all* pairs of vertices, alongside 2D visualizations. Observe that the geometries emerge after about a 200 steps or more, compared to the 2 steps required for associative memory in Fig. 7. This is evidence for Refutation 3c. While this is for learning rate 0.001 (where the geometries are cleanest), the observation holds for larger learning rates too; please see Fig. 22.

4 Geometry arises from naturally-occurring spectral bias, without pressures

Setting aside the competition with the associative memory, we can still ask questions about the geometry: what is the geometry, how does it correspond to global information, and how does it arise without explicit pressures? Recall that we find these geometries not only in models with attention layers, but also in Mamba and in classical deep networks; to focus on the core phenomenon, we study the simplest yet non-trivial multi-layered gradient-descent-trained model: a 2-layer linear network consisting only of an embedding and unembedding layer (weight-tied), trained on the same loss (cross entropy) and the same dataset (of local edges). Equivalently, this is a one-layer, 1-hop Node2Vec model. Here, associative memory is architecturally prohibited,⁸ so we can pursue a clean analysis of the geometry alone.

4.1 Where does the geometry come from?

A precise characterization of what embeddings are learned even in such simple models is an open question. But a rich line of work—with key assumptions about various pressures outlined shortly—points to a *low-rank spectral bias*: the learned embeddings often align with the top (non-degenerate) eigenvectors of the negative graph Laplacian (roughly given by $\mathbf{A} - \mathbf{D}$, the difference between the adjacency and the diagonal degree matrix). Our figures corroborate this: the Node2Vec embeddings in Fig. 1 right column match the top eigenvectors—called the Fiedler vector(s)—in Fig. 9 left column.

This leads us to a few key insights. First, given the similarity in the geometries of Node2Vec and our deep sequence models (Transformer, Mamba and neural networks), such a spectral bias must indeed be at the heart of all such deep models, regardless of architectural quirks like self-attention and residual connections. However, the Node2Vec geometries turn out to be more well-organized than that which the Transformer exhibited (in Fig. 1 middle column). Thus, we conjecture a similar spectral geometry in Transformers but—in hindsight—mildly adulterated by the competition with local associative memory.

Conjecture 1. (*Adulterated spectral bias*) *The geometric memory of a Transformer has significant headroom in the quality of its geometry; we conjecture that this is because a gradient-descent-trained Transformer has spectral bias that is adulterated with some level of associative memory.*

4.2 Where does the global information come from?

Another key insight is that the top eigenvectors, which are known to encode global structures in the graph, are the very source of global information that aided our reasoning task. Intuitively, the top eigenvectors of the adjacency matrix \mathbf{A} are also the directions that become dominant in the ℓ -hop adjacency matrix \mathbf{A}^ℓ , directions that translate to global information. An alternative perspective is to view geometric memory as having factorized the adjacency matrix \mathbf{A} while (softly) filtering out the lower eigenvectors; this extra computation has produced new information not superficially available in the adjacency data.

In effect, we view Transformers as approximating the global geometry of a Node2Vec. Although only an approximation, the implications are profound: the Transformer comes with the power to *reason* over the global geometry, an ability lacking in Node2Vec-style models.

4.3 Where does the low-rank spectral bias come from?

While the geometry stems from a low-rank spectral bias, it is not clear where the bias itself comes from. Going back to Node2Vec theories (see §5.5), the literature suggests that Node2Vec-like models rely on the top eigenvectors under the assumptions of an explicit pressure of a bottleneck [93, 66, 165, 76, 152, 153, 14] or explicit regularization [83, 199] or an explicitly multi-hop supervision [137]. Our setting defies all these assumptions.

We hypothesize that these analyses inadvertently introduce explicit pressures in an attempt to simplify the dynamics e.g., nearly all analyses are on simpler-to-analyze losses such as the squared-error or a negative-sampling loss. On the other hand, the (more complex-to-analyze) cross-entropy loss is known to provide implicit pressures in certain other settings, such as in classification where it

⁸Node2Vec with weight-tying cannot implement associative memory at least in the form we care about. A more contrived form is possible; see §E.3.

induces margin-maximization [162]; it is also the loss of choice in modern language models. Thus, we undertake an analysis of this loss, without assuming any explicit pressures. We emphasize that closed-form expressions here have remained an open question.

A priori, one would expect the unregularized cross-entropy-based Node2Vec system to behave in one of few ways: the system may diverge (to drive the probabilities to 0 or 1), or may converge but only in direction (like in logistic regression [162]); the converged direction in turn, may be degenerate (e.g., node representations collapse to a single value) or not. Through empirical analysis, we suggest that none of these are true. Instead, the system appears to converge to a zero-gradient solution. It does so by elegantly achieving two properties, one of which is a low-rank spectral bias:

Observation 3. (How spectral bias emerges without typical pressures) *In a 1-layer, 1-hop Node2Vec model with the embedding $\mathbf{V} \in \mathbb{R}^{n \times m}$ of n nodes, with the dynamics denoted as $\dot{\mathbf{V}}(t) = \eta \mathbf{C}(t) \mathbf{V}(t)$ (where $\mathbf{C}(t) \in \mathbb{R}^{n \times n}$ is a time-dependent co-efficient matrix), the converged solution for our small graphs is such that (a) the columns of embedding matrix \mathbf{V} span the graph’s Fiedler-like vectors⁹, and (b) the co-efficient matrix \mathbf{C} has those same vectors in its null space (Fig. 9). Crucially, this dynamic does not need a low rank constraint; the embedding size m can be larger than the graph.*

Why do the dynamics play out this way? We provide in §F an empirically-informed intuition (and a partial proof) for a “self-stabilizing” dynamic. The system gradually filters out lower eigenvectors from the embedding matrix \mathbf{V} , while increasing their presence in the co-efficient matrix \mathbf{C} , zeroing out the gradients $\mathbf{C}\mathbf{V}$ over time. We leave open a formal analysis of convergence, its rate, and whether this can be characterized into a form of max-margin-style bias.

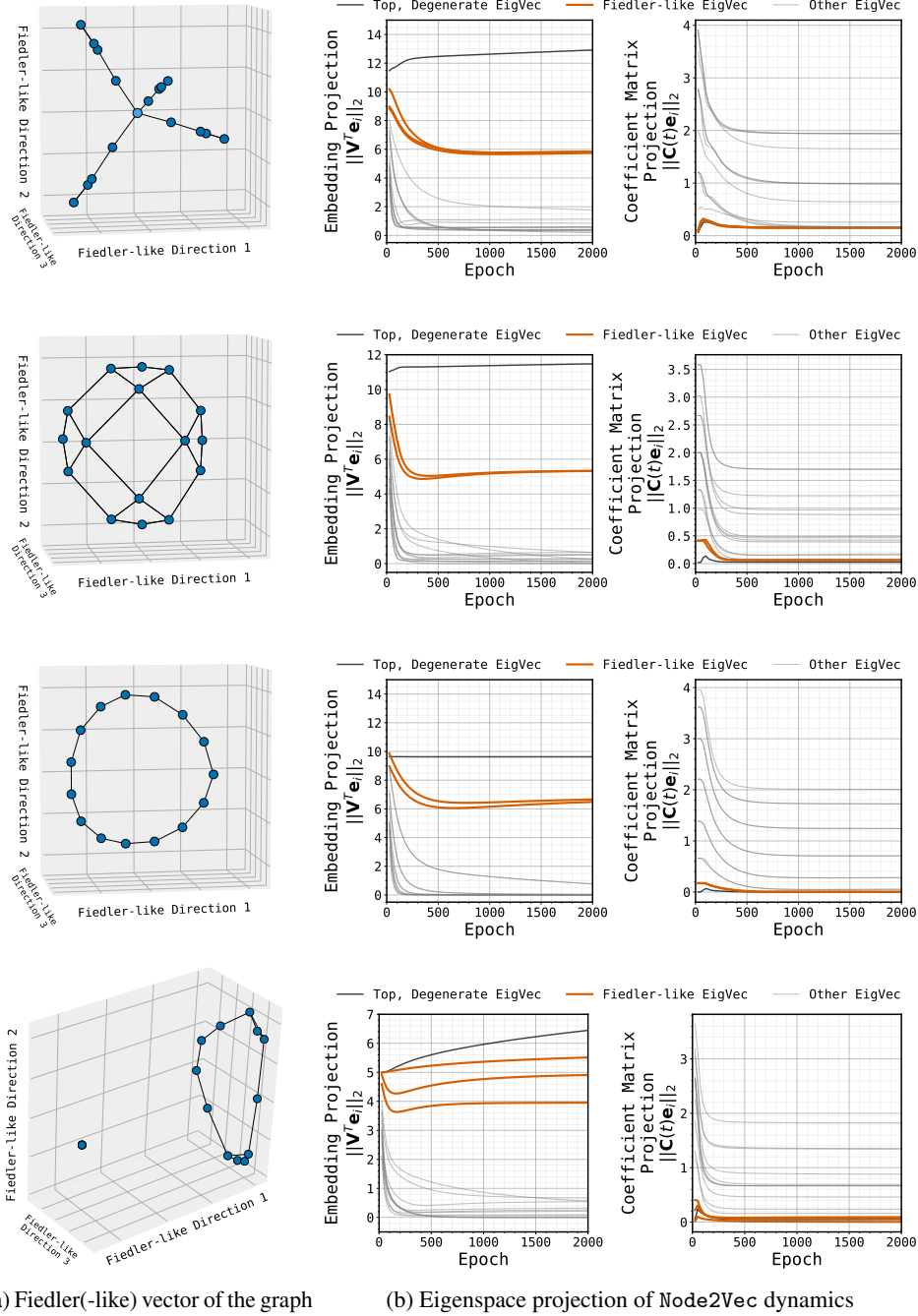
We emphasize that this two-layer analysis does not divulge anything about the competition between associative and geometric memories. That requires a study of deeper models, where the dynamics of different spectral components begin cross-interfering. What this two-layer analysis does is make progress on an open question for the simplest model possible. It also gives us an idea of how and what global information can arise naturally out of local supervision, devoid of any supervisory, bottleneck-driven, or regularizing pressure. These spectral dynamics must be central to any gradient-descent-trained deep sequence model.

With the above insights from Node2Vec, we revisit our original deep sequence models where the geometric memory is in competition with, and adulterated by, associative memory (as noted in §4.1); here, we pose the following concrete question(s) in quantifying this competition:

Open Question 2: Characterizing and Controlling the Geometric Bias

- (i) *To what precise extent does a deep sequence model memorize different parts of a graph dataset geometrically vs. associatively?*
- (ii) *What local or global notions of **graph complexity**—such as the graph spectrum, connectivity, node & vertex count and degree—and what aspects of optimization—such as the architecture, learning rate, training time —control this bias?*
- (iii) *What interventions in the data, architecture or optimization can be made to make memorization more geometric or more associative as desired in practice?*

⁹We use “Fiedler-like” to denote not just the second-top eigenvectors of the negative Laplacian matrix, but also some of the subsequent top eigenvectors.



(a) Fiedler(-like) vector of the graph

(b) Eigenspace projection of Node2Vec dynamics

Figure 9: **Spectral geometry arises in Node2Vec without low-rank pressure (Observation 3) for tiny Path-Star, Grid, Cycle, and Irregular Graphs (top to bottom).** (a) The Fiedler-like vectors of the graphs encode global structure; this structure mirrors the Node2Vec embeddings shown in Fig. 1. (b; left) The evolution of eigenvector projections during training. (middle) The embedding matrix V contracts into space spanned by the **Fiedler-like eigenvectors**, evidenced by the projection norm $\|V^T e_i\|_2$ converging to a stable, non-zero value; projections of **other eigenvectors** diminish towards zero. (b; right) Concurrently, the null space of the co-efficient matrix C subsumes the Fiedler-like eigenvectors, in that the norm $\|C e_i\|_2$ converges to 0. This spectral bias arises without a low dimensional constraint assumed in literature (embedding size $m = 100$, much larger than nodes in graph).

4.4 The importance of weight-tying

Our Node2Vec model shares weights between the two layers, reflecting the *de facto* practice of tying unembedding and embedding matrices in language models. This convention coincidentally plays a unique role in memory: without it, the geometries do not seem visible, at least on the face of it (see Fig. 10 for Node2Vec and Fig. 11 for Transformer, and the corresponding multi-hop cosine-similarities in Fig. 33 and Fig. 34).

We give an explanation for this. A weight-untied two-layer model must factorize the adjacency matrix not as an eigenvalue decomposition (EVD) but as a singular value decomposition (SVD)—this intuitively follows from analyses of weight-untied Word2Vec-style models [199, 83, 152]. The eigenvalues of the adjacency matrix range both positive and negative; the SVD “folds up” the negative eigendirections—all strong eigendirections, both the most positive and most negative, become top singular directions (see [197] for relevant facts on spectral graph theory). The most negative eigendirections however assign zig-zagging values to adjacent nodes (e.g., $+1$ and -1 as we walk along a path). This manifests as the unruly figures in Figs. 10 and 11.

This raises various questions. First, although visually unruly, these zig-zagging eigendirections are highly-structured: they approximate a bipartite cut of the graph. Thus, they correspond to a form of geometric memory distinct from the “global” one, best termed as a *bipartite* geometric memory. Next, while the “global” geometry endows the model with navigational powers (as witnessed in §2), what benefits does the bipartite memory bring to a model’s reasoning abilities?

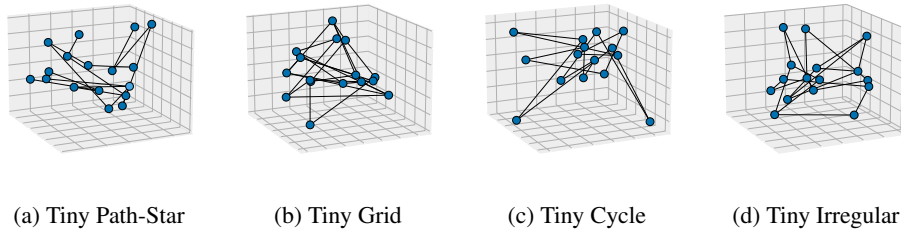


Figure 10: **Embeddings of weight-untied Node2Vec do not show a clean geometry in the top directions.** Corresponding multi-hop cosine similarities are in Fig. 33.

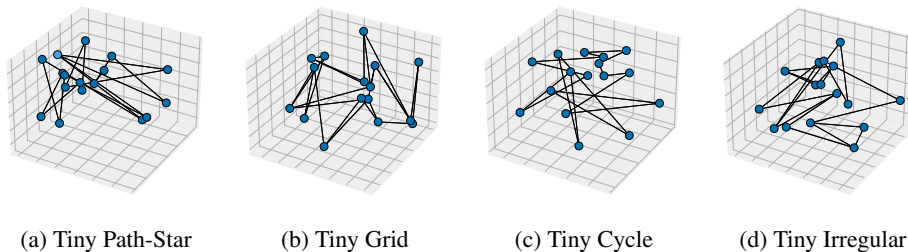


Figure 11: **Embeddings of a weight-untied Transformer do not show a clean geometry in the top directions.** Corresponding multi-hop cosine similarities are in Fig. 34.

5 Related work

Our work consolidates fragments of a nascent phenomenon and brings together distinct lines of theoretical and empirical work on memorization, learning compositional functions, and interpreting model representations. We elaborate on each of these threads below.

5.1 Analysis of Transformer memory

Associative memory. The concept of associative memory dates back to theories of how information is stored in the brain [101, 182]. These ideas have since been explicitly modeled through various architectures such as Hopfield networks [70, 142], energy-based models [89], and other modern Transformer-style inventions [91, 69]. Closest to us are works that analyze how architectures implicitly behave as associative memory storage, such as in autoencoders [139] or Transformers [20, 26, 124, 49, 154, 164]. Others have established connections between the attention mechanism and Hopfield networks [142, 161]. We emphasize that this view is sufficient to understand Transformer behavior on disjoint facts, evidenced by the rich empirical literature built on this view. The geometric view only seems necessary when the facts become interdependent.

Geometric memory as node representations. Although, geometric memory has not been explicitly labeled as a distinct form of parametric memory, we find scattered observations of it in literature in weaker forms. [78, 85, 189] show that nodes in graph-like datasets are embedded in a geometric way that encodes distances. These settings involve some form of global supervision or latent high-level structure, while we find that such a geometry can arise even with atomic facts. Jiang et al. [78] further juxtapose these structured embeddings against associative memory. However, they suggest that the structure becomes relevant only in the underparameterized setting, and that an associative memory suffices as an abstraction in the overparameterized setting; we find this is not the case. Independently, on two-hop datasets, [189, 174] report how models first “memorize” the training data, before “generalizing” on their reasoning task; under the hood, this translates to associative and geometric memorization respectively.

Geometric memory as factorized knowledge. Recall that the geometric memory can be viewed as storing a low-rank factorization of the adjacency matrix. The advantages of such factorizations is again scattered in literature. Saxe et al. [153, 152] prove that a two-layer model naturally learns an SVD factorization of input-output associations. This is a powerful result demonstrating the value of depth in learning hierarchical representations; but the global, multi-hop nature of these representations was not highlighted. Also, unlike our setting, theirs requires explicit pressures to demonstrate a low rank spectral bias (either through a bottleneck or early-stopping) for they study the squared-error loss.¹⁰ More recently, Huang et al. [74] point out that two-hop reasoning emerges if and only if the key-query matrices in an attention layer are kept separate (as against being collapsed into a single matrix); we show that such favorable effects occur in more general architectures without attention layers. They also highlight the role of an implicit regularization effect from their reasoning supervision; we emphasize that this does not resolve our memorization puzzle—see Remark 1.

We also interpret these prior analyses [153, 74] as a study of how 2-layered models memorize a special type of graphs: *bipartite* graphs (although they do not express it as such).¹¹ Importantly, as noted in our own analysis in §4, such 2-layered models do not capture the competition between associative and geometric memory.¹² For that, a study of deeper models is required, where the dynamics along the various spectral components become entangled; to keep them untangled, unnatural assumptions about the initializations need to be made, as shown in [152]. Another nuance in these prior 2-layered analyses is the lack of weight-tying, which creates significant differences in what is learned, as we identify in §4.4.

¹⁰Under their squared error loss (applied without a softmax layer), a fully-trained 2-layered model would learn the 1-hop adjacency matrix perfectly, with no global, multi-hop information revealed in the logits. Although the associations are stored in a factorized form, the final hidden representations do not filter out the lower directions.

¹¹Concretely, [153] study mappings between “entity” tokens and binary feature vectors; we translate this as a bipartite graph where “entity” nodes are connected to various “feature” nodes. [74] study a mapping between “subject” nodes and “answer” nodes.

¹²At least not in its full glory; in 2-layered weight-tied models, there is only a contrived form of associative memory (Lemma 5); if weight-untied, a natural form can arise in a single step (Lemma 4).

Remark 1. (*Implicit regularization in matrix factorization is an insufficient explanation of geometric memory*) Huang et al. [74] attribute the success of reasoning to implicit regularization effects that arise in matrix completion tasks; we argue that these effects do not explain why a geometry arises over associative storage in our experiments. The “matrix completion” view in [74] is that during training the model attempts to fit certain observed entries in a 2-hop adjacency matrix \mathbf{A}^2 ; any test query in effect demands that the model “complete” a missing 2-hop entry. While many minima exist in such underdetermined matrix completion tasks, it is known [62, 11] that gradient descent on a deep factorized model finds the least nuclear norm matrix consistent with the observed entries. However, our edge-memorization-only task is a well-determined task that requires storing the adjacency matrix \mathbf{A} as is, without any missing entries to infer; thus no such implicit pressure must exist. Yet a geometry arises in this task as shown in Refutation 3a. While it is still possible that there is a certain nuclear norm minimization effect even in edge-memorization tasks—perhaps because the logits themselves are not well-determined—the connection is not as obvious as it may seem.

Expressive capacity. Theoretical works have quantified bounds on the expressive capacity of models when it comes to memorizing sequences [106, 81, 105, 80, 87] as opposed to associations between pairs of bigrams. These do not comment on the learning dynamics. These works typically assume that the token embeddings are all well-separated from each other (an assumption that empirically breaks in our setting). In light of the geometric view, it is necessary to restate expressive capacity bounds in terms of geometric capacity of a network and the “geometric complexity” of the dataset.

Empirical analyses. Other works [10, 115, 144, 128] have performed careful empirical analyses of scaling laws for memorization, and quantified memorization in terms of “bits per parameter count”, known as bit complexity [171], which is related to our notion of bit count in Refutation 3d. All these analyses are worth revisiting with the newfound lens of a geometric memory. Zucchet et al. [203] empirically analyze the dynamics behind how facts are memorized in a model. Others [99, 196] have proposed methodological improvements to acquiring knowledge in a Transformer; of relevance to us is the finding in Zhang et al. [196] that training a model simultaneously on both facts and question-answering is a better way to integrate knowledge into the parameters.

Mechanistic interpretability. There have been mechanistic investigations into how Transformers perform fact recall [104, 50] and where facts are stored in a transformer [49] and how it can be edited [201, 111]. Similar attempts have been made in traditional classifier networks [15, 107, 163]. Directly related to us are the works of Khona et al. [85] and Yao et al. [188], Biran et al. [21] who perform a mechanistic interpretability analysis of how multi-hop recall works.

5.2 In-weights reasoning tasks

Synthetic graph tasks. Our work consolidates positive results of in-weights reasoning in literature, and presents a stronger instance of it, removing various confounders that make composition-learning easy. Khona et al. [85] report successful path-finding on 200 nodes-large in-weights graphs, with varying path lengths and test-train overlap. Others [174, 43, 189, 74] report positive results on much shorter 2-hop tasks over a thousand entities or fewer. Geerts et al. [48] look at in-weights transitive inference, a special type of ℓ -fold composition query where the model is trained on local comparisons and is queried on more distant comparisons. On settings with 7 objects, Geerts et al. [48] find a clear difference between an in-context version of their task (where the model struggles) and an in-weights version (where the model succeeds). Our task of finding the first node is a much harder *search* task akin to finding the smallest node in an ordered relationship. Nagarajan et al. [119] discuss the limitations of next-token prediction, including on open-ended in-weights tasks, in lower data regimes. The fact that their next-token predictor achieves non-trivial performance on their in-weights task could be attributed to the effects of a geometric memory. Tangentially related is the positive finding in Yin and Wang [191] that the Transformer can compose in-weights knowledge given in-context demonstrations. It is worth noting that the (theoretical) arguments in both these works [119, 191] rest on the associative memory view.

As a negative result, Wang et al. [177] report that, on in-weights graphs of less than 500 nodes, models are only able to infer already-seen paths or sub-paths, but not beyond them. We suspect this may stem from the fact that their model is only trained on the paths themselves (while our work and Khona et al. [85] make the model memorize edge bigrams).

Multi-hop question-answering. A line of work has looked at how pretrained models respond to two-hop questions in natural language e.g., “What is the calling code of the birthplace of Frida Kahlo?” (example from Press et al. [135]). Results here have been limited [135, 21] or mixed [185, 186, 16]. Success has been shown on synthetic knowledge provided there is exponential amounts of data, or a curriculum, or very long amounts of training [188, 174]. Orthogonally, Wang et al. [178] identify that such in-weights implicit reasoning can be hurt by scaling up the parameters, perhaps due to “excessive memorization”, which we interpret as associative memorization. It is possible that some of these negative results may be attributed to the reversal curse [18, 9], or the lack of extended computation e.g., we use pause tokens [57]. But a dedicated study of this gap between our synthetic settings and these settings is important and left for future work.

Reversal curse and (a)symmetric knowledge. The reversal curse [18, 9] is a well-known out-of-distribution, in-weights failure mode of next-token-trained Transformers. Such models are unable to recall u given v , when trained to recall v given u , suggesting asymmetric storage in parametric memory. Fixes for the reversal curse have involved reversed or permuted data augmentation [64, 102, 88, 55]. In our settings, we find that reverse edges are critical to elicit implicit reasoning in our large path-star tasks (see §D.1), but is not necessary to elicit a geometry in the smaller graphs.¹³ Various theories have been proposed to understand this failure [97, 202, 173], which may be worth revisiting under a geometric view. One may also view our contrast between associative and geometric memory (of a generic graph data) as a generalization of the aforementioned contrast between the asymmetric and symmetric knowledge storage (of a more specific, disjoint set of associations). Future work may discover a nuanced connection between our work and the reversal curse.

5.3 Failure of end-to-end composition learning

While ℓ -fold composition functions are surprisingly easy to *express* in transformers [149], empirical results have time and again demonstrated that they are hard to *learn* through gradient-based methods, both in traditional deep network settings [156, 2, 61, 54, 1, 2] and more recently in language models too [125, 98, 34, 134, 194, 143, 34, 71, 160]. Others [13, 72, 157] demonstrate how next-token learning can trap training at a stage where composition learning becomes a problem. Theoretical works have attempted to formalize these failures by demonstrating limits due to expressivity [108, 32, 132] or sample complexity [156] or computational complexity [181, 72] or in terms of statistical queries [180].

Remark 2. (Theoretical hardness of learning compositions) *Existing theoretical hardness results typically only show that some worst-case function in a class of compositional functions is hard-to-learn; no proclamations are made about how hard it is to learn a fixed function we care about. Indeed, with contrived initial conditions, a singleton function class can be provably learned [4, 3, 118]. Yet, in practice, learning a fixed function is hard, proving which has been an open question—until the recent negative results of Abbe et al. [6], Shoshani and Shamir [159]. These show how the (fixed) full parity function is hard to learn with gradient descent which, through a reduction, proves that in-context composition tasks are hard to learn [72]. We leave it as an open question to link our in-weights composition task to one of these hardness results.*

5.4 In-context graph tasks

Graph tasks have been studied extensively in the setting where each context corresponds to a unique graph. We emphasize that this is a very different setting. Indeed, a takeaway from our work is to be deliberate not to conflate insights from the in-context setting with that of the in-weights setting (a distinction that is rarely made explicit in literature).

While Bachmann and Nagarajan [13] identify the path-star topology as a failure case for next-token learning, Frydenlund [46, 47] demarcate the extent of this failure in the same in-context setting, whereas Brinkmann et al. [24] report positive path-finding results in other graph topologies. Others [150, 148, 190] study Transformers in various in-context graph tasks like search and counting. Connections between in-context graph tasks and spectral biases exist [35, 129] but should not be confused with the spectral bias in in-weights tasks. While all these works study symbolic graph tasks, other works have empirically identified the limitations on graphs described in natural language

¹³It appears that the observations on small graphs in Khona et al. [85] do not require memorizing the reverse edges, which aligns with our findings on small graphs.

[63, 175, 37]. Kim et al. [86], Ying et al. [193] propose algorithmic ideas for encoding graphs as inputs to Transformers. Finally, various failures [114, 39, 168, 169, 170, 158] have been reported on in-context tasks, including planning tasks, framed as word problems.

5.4.1 In-context vs. in-weights learning

The dichotomy between drawing information from context vs. drawing information from the weights has been studied in various angles. Some have looked at this from the aspect of two competing circuits relying on one source vs. the other [29, 28, 121, 33]. Others have looked at it in the context of the learning paradigms of in-context learning and finetuning the weights [116, 90]. Closer to us, the stark in-context vs. in-weights disparity when it comes to handling global relationships has been emphasized in Wang et al. [174], Geerts et al. [48], for which our results provide further evidence.

5.5 Analyses of graph and word embedding methods

Much attention has been given to characterizing what embeddings are learned by various contrastive losses such as Node2Vec. Most of these are on losses simpler than the cross-entropy loss, with the exception of a recent line of work [199, 198, 167] which studies the geometry of cross-entropy-trained (weight-untied) Word2Vec models. However, certain assumptions are made, such as freezing one of the layers [167] or heuristically approximating via a regularized proxy model [199]. Curiously, [199] find that their system only directionally converges, while the weights themselves diverge; we however point out that it’s reasonable to expect the model to converge to a zero-gradient solution. Regardless, [199] suggest an insightful connection to the converged direction to support vector machines; this may inspire better characterizations of what solution is found by our unregularized Node2Vec system.

The connection to a graph spectrum has been made in many other analyses. These analyses focus on a simpler loss called the negative sampling loss where the closed form expression for the inner products is straightforward (namely, the so-called pointwise mutual information (PMI) matrix, as discovered in Levy and Goldberg [93]). This analysis does not however tell us what exactly the embeddings are. The connection between these embeddings and the graph spectrum has been established in adjacent settings, like with DeepWalk [137] (where the objective is explicitly multi-hop), in low-rank settings like SimCLR [66, 165] or with quadratic losses with early stopping [83] or the softmax loss with rank 1 [76]. Other analyses of Node2Vec focus on specific types of graphs such as stochastic block models [38, 67]. We refer the reader to Goyal and Ferrara [56] for a survey of graph embedding methods. Finally, we clarify that these methods and our insights must not be confused with graph neural networks [192, 200], where the graphs are not stored in parametric memory, but presented as input.

5.6 Other foundational works on generalization and memorization

Spectral and simplicity bias. The type of spectral bias we study in memorization and sequence modeling must be distinguished from the one studied in generalization and traditional classification and regression settings [140, 184, 82, 12, 146, 19]. In these earlier studies, the spectrum is that of a continuous function or a decision boundary (e.g., say, the Fourier components of a polynomial), whereas the spectrum we are concerned with is of a discrete, combinatorial object, namely the graph adjacency matrix. This corresponds to a difference in the nature of representations as remarked below.

Remark 3. (On the nature of representations in classification vs. sequence modeling) *The geometric representations learned in our setting (i.e., sequence modeling of atomic facts) are of a fundamentally different nature from that learned in the classification/regression setting. The representations in classification/regression correspond to features inherent to each datapoint, such as the edges detected in an image. No such features are inherent to a one-hot token; a token’s representation is synthesized from its co-occurrence patterns with other tokens. This difference is central to why the analogy between the generalization puzzle and the memorization puzzle breaks down in §3.2, both in terms of succinctness and ease of discovery with gradient descent.*

Memorization. Our work is also orthogonal to the seminal works of Zhang et al. [195], Neyshabur et al. [122] who were concerned with classical generalization tasks that possess statistical redundancies. Their argument is that explicit pressures cannot explain why representations arise in such

tasks, but implicit pressures may. Our memorization task on the other hand is in sequence modeling, and lacks statistical redundancies; both explicit and implicit pressures do not suffice to explain the geometric representations. Our work is also orthogonal to the foundational work of Feldman [42] who argue that memorizing the quirks of a training set can be *necessary* for generalization in long tail datasets.

Linear representation hypothesis. A long-studied geometric concept in language models is the concept of linear representations in analogies [130, 131, 40, 112]. The introduction of certain concepts often takes a linear direction, surprisingly, independent of context i.e., going from *cow* to *calf* takes the same direction as *cat* to *kitten*, independent of the source in the context, (*cow*, *cat*). This linear structure, is related, but neither reducible to nor reducible from geometric memorization. Many theories have been proposed to model the linear geometry and semantics of these embeddings [53, 7, 41, 8, 68, 79]. These studies are orthogonal since their contribution lies in identifying what structures exist in word-context relationships for such geometries to arise in the embeddings. This is akin to identifying structures in the adjacency matrix, while our analysis is agnostic to such structures. There are many other complementary analyses of these embeddings, both theoretical [58] and empirical [113, 31, 30, 94].

6 Limitations

1. Our positive result of implicit in-weights reasoning is on a purely symbolic task, and on a specific graph topology (path-star, and tree-star in §C.2). It is unclear how well this generalizes to other topologies, and to graphs of other sizes.
2. Whether our insights extend to natural language is highly non-trivial, since the way the entities are tokenized and the way relationships are presented are much more unstructured.
3. We use small to mid-sized Transformers trained from scratch (GPT-mid). We have not explored the effect of large model sizes or of large-scale pretraining.
4. We emphasize that all our arguments are empirical and informal (or left as propositions), and lack a precise, fuller characterization of our observations.
 - (a) Perhaps, a slightly more nuanced form of architectural or statistical pressure (e.g., more nuanced norm complexity such as flatness of the loss) may indeed explain why associative memory is less preferred by the model.
 - (b) Conversely, perhaps the lack of pressures in the learning setup is indeed why the Transformer learns a sub-optimal kind of geometric memory compared to Node2Vec.
5. Although we illustrate a clear contrast between associative and geometric memory in their caricatured forms (i.e., as $\Phi(u)^T \mathbf{W}_{\text{assoc}} \Phi(v)$ vs. $\Phi_{\text{geom}}(u) \cdot \Phi_{\text{geom}}(v)$), it is unclear how to conceptually disentangle these two modes of storage in a given multi-layered deep network.

7 Conclusions and Future Work

While the associative view of parametric memory is a simple and highly effective view of neural networks, we isolate an instance of implicit in-weights reasoning that necessitates a geometric view. The emergence of this geometry is not easily explained by various pressures in the learning setup, raising fundamental questions about neural network training. Making some progress into this, we attribute this to a spectral bias that arises even with local supervision and even independent of the embedding dimensionality.

Various practical questions arise out of these findings. The elegant geometries of Node2Vec models indicate that Transformer memory can be made much more geometric. It is also unclear whether Transformers exhibit such desirable behaviors in more complex graph topologies. Importantly, empirical works on implicit reasoning in natural language have so far been mixed. More careful empirical research and ideation may be needed to make the geometric view more broadly applicable. Orthogonally, our findings are of relevance to making choices between parametric vs. contextual memory, and also between generative retrieval vs. dual encoder retrieval models.

Our work raises the foundational question of when and how associative and geometric memory compete with each other during optimization, and what factors—such as graph connectivity, training time, learning rate, weight decay—can foster one over the other. To answer these, our insights into the spectral bias need to be extended from Node2Vec-style architectures (where associative memory is prohibited) to deep sequence models (where associative memory becomes a competitor). We also hope that our simple examples can be useful for orthogonal conceptual studies on interpretability, world models, and in characterizing convergent representations across model families. Broadly, we expect these findings to inspire revisiting unstated associative assumptions underlying research on knowledge and memory in language models.

Acknowledgments. We would like to thank Gaurav Ghosal, Gintare Karolina Dziugaite, George H Chen, Christina Baek, Jacob Springer and Omar Salemhamed for valuable feedback on earlier versions of this draft. We are also grateful to Andrej Risteski, Alberto Bietti, Ekdeep Singh Lubana and Andrew Lampinen for discussions and pointers to related work.

References

- [1] Emmanuel Abbe and Enric Boix-Adsera. On the non-universality of deep learning: quantifying the cost of symmetry. In *Advances in Neural Information Processing Systems*, volume 35, pages 17188–17201. Curran Associates, Inc., 2022.
- [2] Emmanuel Abbe and Colin Sandon. Poly-time universality and limitations of deep learning. *arXiv preprint arXiv:2001.02992*, 2020.
- [3] Emmanuel Abbe and Colin Sandon. On the universality of deep learning. *Advances in Neural Information Processing Systems*, 33:20061–20072, 2020.
- [4] Emmanuel Abbe, Pritish Kamath, Eran Malach, Colin Sandon, and Nathan Srebro. On the power of differentiable learning versus pac and sq learning. *Advances in Neural Information Processing Systems*, 34:24340–24351, 2021.
- [5] Emmanuel Abbe, Elisabetta Cornacchia, and Aryo Lotfi. Provable advantage of curriculum learning on parity targets with mixed inputs. *Advances in Neural Information Processing Systems*, 36:24291–24321, 2023.
- [6] Emmanuel Abbe, Elisabetta Cornacchia, Jan Hązła, and Donald Kougang-Yombi. Learning high-degree parities: The crucial role of the initialization. In *The Thirteenth International Conference on Learning Representations*, 2025. URL <https://openreview.net/forum?id=OuNIWgGGif>.
- [7] Carl Allen and Timothy M. Hospedales. Analogies explained: Towards understanding word embeddings. In Kamalika Chaudhuri and Ruslan Salakhutdinov, editors, *Proceedings of the 36th International Conference on Machine Learning, ICML 2019, 9-15 June 2019, Long Beach, California, USA*, volume 97 of *Proceedings of Machine Learning Research*, pages 223–231. PMLR, 2019. URL <http://proceedings.mlr.press/v97/allen19a.html>.
- [8] Carl Allen, Ivana Balazevic, and Timothy M. Hospedales. What the vec? towards probabilistically grounded embeddings. In Hanna M. Wallach, Hugo Larochelle, Alina Beygelzimer, Florence d’Alché-Buc, Emily B. Fox, and Roman Garnett, editors, *Advances in Neural Information Processing Systems 32: Annual Conference on Neural Information Processing Systems 2019, NeurIPS 2019, December 8-14, 2019, Vancouver, BC, Canada*, pages 7465–7475, 2019.
- [9] Zeyuan Allen-Zhu and Yuanzhi Li. Physics of language models: Part 3.2, knowledge manipulation. *CoRR*, abs/2309.14402, 2023. doi: 10.48550/ARXIV.2309.14402. URL <https://doi.org/10.48550/arXiv.2309.14402>.
- [10] Zeyuan Allen-Zhu and Yuanzhi Li. Physics of language models: Part 3.3, knowledge capacity scaling laws. In *The Thirteenth International Conference on Learning Representations, ICLR 2025, Singapore, April 24-28, 2025*. OpenReview.net, 2025.
- [11] Sanjeev Arora, Nadav Cohen, Wei Hu, and Yuping Luo. Implicit regularization in deep matrix factorization. In *Advances in Neural Information Processing Systems 32: Annual Conference on Neural Information Processing Systems 2019, NeurIPS 2019, December 8-14, 2019, Vancouver, BC, Canada*, pages 7411–7422, 2019.
- [12] Devansh Arpit, Stanisław Jastrzębski, Nicolas Ballas, David Krueger, Emmanuel Bengio, Maxinder S. Kanwal, Tegan Maharaj, Asja Fischer, Aaron Courville, Yoshua Bengio, and Simon Lacoste-Julien. A closer look at memorization in deep networks. In Doina Precup and Yee Whye Teh, editors, *Proceedings of the 34th International Conference on Machine Learning*, volume 70 of *Proceedings of Machine Learning Research*, pages 233–242. PMLR, 06–11 Aug 2017.
- [13] Gregor Bachmann and Vaishnavh Nagarajan. The pitfalls of next-token prediction. In *Proceedings of the 41st International Conference on Machine Learning*, volume 235 of *Proceedings of Machine Learning Research*, pages 2296–2318, 2024.
- [14] Pierre Baldi and Kurt Hornik. Neural networks and principal component analysis: Learning from examples without local minima. *Neural Networks*, 2(1):53–58, 1989. doi: 10.1016/0893-6080(89)90014-2. URL [https://doi.org/10.1016/0893-6080\(89\)90014-2](https://doi.org/10.1016/0893-6080(89)90014-2).
- [15] Robert J. N. Baldock, Hartmut Maennel, and Behnam Neyshabur. Deep learning through the lens of example difficulty. In Marc’Aurelio Ranzato, Alina Beygelzimer, Yann N. Dauphin,

-
- Percy Liang, and Jennifer Wortman Vaughan, editors, *Advances in Neural Information Processing Systems 34: Annual Conference on Neural Information Processing Systems 2021, NeurIPS 2021, December 6-14, 2021, virtual*, pages 10876–10889, 2021.
- [16] Mikita Balesni, Tomek Korbak, and Owain Evans. Lessons from studying two-hop latent reasoning, 2025. URL <https://arxiv.org/abs/2411.16353>.
- [17] Peter L. Bartlett. The sample complexity of pattern classification with neural networks: The size of the weights is more important than the size of the network. *IEEE Trans. Inf. Theory*, 44(2):525–536, 1998.
- [18] Lukas Berglund, Meg Tong, Maximilian Kaufmann, Mikita Balesni, Asa Cooper Stickland, Tomasz Korbak, and Owain Evans. The reversal curse: LLMs trained on "a is b" fail to learn "b is a". In *The Twelfth International Conference on Learning Representations, ICLR 2024, Vienna, Austria, May 7-11, 2024*. OpenReview.net, 2024. URL <https://openreview.net/forum?id=GPKTIktA0k>.
- [19] Alberto Bietti and Julien Mairal. On the inductive bias of neural tangent kernels. *Advances in Neural Information Processing Systems*, 32, 2019.
- [20] Alberto Bietti, Vivien Cabannes, Diane Bouchacourt, Hervé Jégou, and Léon Bottou. Birth of a transformer: A memory viewpoint. In *Advances in Neural Information Processing Systems 36: Annual Conference on Neural Information Processing Systems 2023, NeurIPS 2023, New Orleans, LA, USA, December 10 - 16, 2023*, 2023.
- [21] Eden Biran, Daniela Gottesman, Sohee Yang, Mor Geva, and Amir Globerson. Hopping too late: Exploring the limitations of large language models on multi-hop queries. In Yaser Al-Onaizan, Mohit Bansal, and Yun-Nung Chen, editors, *Proceedings of the 2024 Conference on Empirical Methods in Natural Language Processing, EMNLP 2024, Miami, FL, USA, November 12-16, 2024*, pages 14113–14130, 2024.
- [22] Margaret A. Boden. *The Creative Mind - Myths and Mechanisms (2. ed.)*. Routledge, 2003.
- [23] Leo Breiman. Reflections after refereeing papers for nips. In *The Mathematics of Generalization*, pages 11–15. CRC Press, 2018.
- [24] Jannik Brinkmann, Abhay Sheshadri, Victor Levoso, Paul Swoboda, and Christian Bartelt. A mechanistic analysis of a transformer trained on a symbolic multi-step reasoning task. In *Findings of the Association for Computational Linguistics, ACL 2024, Bangkok, Thailand and virtual meeting, August 11-16, 2024*, pages 4082–4102. Association for Computational Linguistics, 2024.
- [25] Mikhail S Burtsev, Yuri Kuratov, Anton Peganov, and Grigory V Sapunov. Memory transformer. *arXiv preprint arXiv:2006.11527*, 2020.
- [26] Vivien Cabannes, Elvis Dohmatob, and Alberto Bietti. Scaling laws for associative memories. In *The Twelfth International Conference on Learning Representations, ICLR 2024, Vienna, Austria, May 7-11, 2024*. OpenReview.net, 2024. URL <https://openreview.net/forum?id=Tzh6xAJS11>.
- [27] Vivien Cabannes, Berfin Simsek, and Alberto Bietti. Learning associative memories with gradient descent. In *Forty-first International Conference on Machine Learning, ICML 2024, Vienna, Austria, July 21-27, 2024*. OpenReview.net, 2024. URL <https://openreview.net/forum?id=A9fLbXLRTK>.
- [28] Stephanie C. Y. Chan, Ishita Dasgupta, Junkyung Kim, Dharshan Kumaran, Andrew K. Lampinen, and Felix Hill. Transformers generalize differently from information stored in context vs in weights. [abs/2210.05675](https://arxiv.org/abs/2210.05675), 2022. doi: 10.48550/ARXIV.2210.05675. URL <https://doi.org/10.48550/arXiv.2210.05675>.
- [29] Stephanie C. Y. Chan, Adam Santoro, Andrew K. Lampinen, Jane X. Wang, Aaditya K. Singh, Pierre H. Richemond, James L. McClelland, and Felix Hill. Data distributional properties drive emergent in-context learning in transformers. In *Advances in Neural Information Processing Systems 35: Annual Conference on Neural Information Processing Systems 2022, NeurIPS 2022, New Orleans, LA, USA, November 28 - December 9, 2022*, 2022.
- [30] Tyler A. Chang, Zhuowen Tu, and Benjamin K. Bergen. The geometry of multilingual language model representations. In Yoav Goldberg, Zornitsa Kozareva, and Yue Zhang, editors, *Proceedings of the 2022 Conference on Empirical Methods in Natural Language Processing*,

-
- EMNLP 2022, Abu Dhabi, United Arab Emirates, December 7-11, 2022*, pages 119–136. Association for Computational Linguistics, 2022. doi: 10.18653/V1/2022.EMNLP-MAIN.9. URL <https://doi.org/10.18653/v1/2022.emnlp-main.9>.
- [31] Boli Chen, Yao Fu, Guangwei Xu, Pengjun Xie, Chuanqi Tan, Mosha Chen, and Liping Jing. Probing BERT in hyperbolic spaces. In *9th International Conference on Learning Representations, ICLR 2021, Virtual Event, Austria, May 3-7, 2021*. OpenReview.net, 2021.
- [32] Lijie Chen, Binghui Peng, and Hongxun Wu. Theoretical limitations of multi-layer transformer. *arXiv preprint arXiv:2412.02975*, 2024.
- [33] Sitao Cheng, Liangming Pan, Xunjian Yin, Xinyi Wang, and William Yang Wang. Understanding the interplay between parametric and contextual knowledge for large language models, 2024. URL <https://arxiv.org/abs/2410.08414>.
- [34] Karl Cobbe, Vineet Kosaraju, Mohammad Bavarian, Mark Chen, Heewoo Jun, Lukasz Kaiser, Matthias Plappert, Jerry Tworek, Jacob Hilton, Reiichiro Nakano, Christopher Hesse, and John Schulman. Training verifiers to solve math word problems. *arXiv preprint arXiv:2110.14168*, 2021.
- [35] Andrew Cohen, Andrey Gromov, Kaiyu Yang, and Yuandong Tian. Spectral journey: How transformers predict the shortest path. *CoRR*, abs/2502.08794, 2025. doi: 10.48550/ARXIV.2502.08794. URL <https://doi.org/10.48550/arXiv.2502.08794>.
- [36] Elisabetta Cornacchia and Elchanan Mossel. A mathematical model for curriculum learning for parities. In *Proceedings of the 40th International Conference on Machine Learning*, volume 202 of *Proceedings of Machine Learning Research*, pages 6402–6423. PMLR, 23–29 Jul 2023. URL <https://proceedings.mlr.press/v202/cornacchia23a.html>.
- [37] Xinnan Dai, Qihao Wen, Yifei Shen, Hongzhi Wen, Dongsheng Li, Jiliang Tang, and Caihua Shan. Revisiting the graph reasoning ability of large language models: Case studies in translation, connectivity and shortest path, 2025. URL <https://arxiv.org/abs/2408.09529>.
- [38] Andrew Davison, S. Carlyle Morgan, and Owen G. Ward. Community detection guarantees using embeddings learned by node2vec. In *Advances in Neural Information Processing Systems 38: Annual Conference on Neural Information Processing Systems 2024, NeurIPS 2024, Vancouver, BC, Canada, December 10 - 15, 2024*, 2024.
- [39] Nouha Dziri, Ximing Lu, Melanie Sclar, Xiang Lorraine Li, Liwei Jiang, Bill Yuchen Lin, Sean Welleck, Peter West, Chandra Bhagavatula, Ronan Le Bras, et al. Faith and fate: Limits of transformers on compositionality. *Advances in Neural Information Processing Systems*, 36, 2024.
- [40] Nelson Elhage, Tristan Hume, Catherine Olsson, Nicholas Schiefer, Tom Henighan, Shauna Kravec, Zac Hatfield-Dodds, Robert Lasenby, Dawn Drain, Carol Chen, Roger Grosse, Sam McCandlish, Jared Kaplan, Dario Amodei, Martin Wattenberg, and Christopher Olah. Toy models of superposition, 2022. URL <https://arxiv.org/abs/2209.10652>.
- [41] Kawin Ethayarajh, David Duvenaud, and Graeme Hirst. Towards understanding linear word analogies. In *Proceedings of the 57th Conference of the Association for Computational Linguistics, ACL 2019, Florence, Italy, July 28- August 2, 2019, Volume 1: Long Papers*, pages 3253–3262. Association for Computational Linguistics, 2019.
- [42] Vitaly Feldman. Does learning require memorization? a short tale about a long tail. In *Proceedings of the 52nd Annual ACM SIGACT Symposium on Theory of Computing, STOC 2020, Chicago, IL, USA, June 22-26, 2020*, pages 954–959. ACM, 2020.
- [43] Jiahai Feng, Stuart Russell, and Jacob Steinhardt. Extractive structures learned in pretraining enable generalization on finetuned facts. *arXiv preprint arXiv:2412.04614*, 2024.
- [44] Quentin RV. Ferry, Joshua Ching, and Takashi Kawai. Emergence and function of abstract representations in self-supervised transformers, 2023. URL <https://arxiv.org/abs/2312.05361>.
- [45] Giorgio Franceschelli and Mirco Musolesi. On the creativity of large language models. *CoRR*, abs/2304.00008, 2023.

-
- [46] Arvid Frydenlund. The mystery of the pathological path-star task for language models. In *Proceedings of the 2024 Conference on Empirical Methods in Natural Language Processing, EMNLP 2024, Miami, FL, USA, November 12-16, 2024*, pages 12493–12516. Association for Computational Linguistics, 2024.
- [47] Arvid Frydenlund. Language models, graph searching, and supervision adulteration: When more supervision is less and how to make more more. In Wanxiang Che, Joyce Nabende, Ekaterina Shutova, and Mohammad Taher Pilehvar, editors, *Proceedings of the 63rd Annual Meeting of the Association for Computational Linguistics (Volume 1: Long Papers)*, Vienna, Austria, July 2025. Association for Computational Linguistics. URL <https://aclanthology.org/2025.acl-long.1409/>.
- [48] Jesse Geerts, Stephanie Chan, Claudia Clopath, and Kimberly Stachenfeld. Relational reasoning and inductive bias in transformers trained on a transitive inference task, 2025. URL <https://arxiv.org/abs/2506.04289>.
- [49] Mor Geva, Roei Schuster, Jonathan Berant, and Omer Levy. Transformer feed-forward layers are key-value memories. In *Proceedings of the 2021 Conference on Empirical Methods in Natural Language Processing, EMNLP 2021, Virtual Event / Punta Cana, Dominican Republic, 7-11 November, 2021*, pages 5484–5495. Association for Computational Linguistics, 2021.
- [50] Mor Geva, Jasmijn Bastings, Katja Filippova, and Amir Globerson. Dissecting recall of factual associations in auto-regressive language models. In *Proceedings of the 2023 Conference on Empirical Methods in Natural Language Processing, EMNLP 2023, Singapore, December 6-10, 2023*, pages 12216–12235. Association for Computational Linguistics, 2023.
- [51] Gaurav Rohit Ghosal, Tatsunori Hashimoto, and Aditi Raghunathan. Understanding finetuning for factual knowledge extraction. In *Forty-first International Conference on Machine Learning, ICML 2024, Vienna, Austria, July 21-27, 2024*. OpenReview.net, 2024. URL <https://openreview.net/forum?id=cPsn9Ac0Yh>.
- [52] Daniel Gillick, Sayali Kulkarni, Larry Lansing, Alessandro Presta, Jason Baldrige, Eugene Ie, and Diego Garcia-Olano. Learning dense representations for entity retrieval. In Mohit Bansal and Aline Villavicencio, editors, *Proceedings of the 23rd Conference on Computational Natural Language Learning, CoNLL 2019, Hong Kong, China, November 3-4, 2019*, pages 528–537. Association for Computational Linguistics, 2019.
- [53] Alex Gittens, Dimitris Achlioptas, and Michael W. Mahoney. Skip-gram - zipf + uniform = vector additivity. In Regina Barzilay and Min-Yen Kan, editors, *Proceedings of the 55th Annual Meeting of the Association for Computational Linguistics, ACL 2017, Vancouver, Canada, July 30 - August 4, Volume 1: Long Papers*, pages 69–76. Association for Computational Linguistics, 2017.
- [54] Tobias Glasmachers. Limits of end-to-end learning. In *Proceedings of The 9th Asian Conference on Machine Learning, ACML 2017*, volume 77 of *Proceedings of Machine Learning Research*, pages 17–32. PMLR, 2017.
- [55] Olga Golovneva, Zeyuan Allen-Zhu, Jason Weston, and Sainbayar Sukhbaatar. Reverse training to nurse the reversal curse. *CoRR*, abs/2403.13799, 2024. doi: 10.48550/ARXIV.2403.13799. URL <https://doi.org/10.48550/arXiv.2403.13799>.
- [56] Palash Goyal and Emilio Ferrara. Graph embedding techniques, applications, and performance: A survey. *Knowl. Based Syst.*, 151:78–94, 2018. doi: 10.1016/J.KNOSYS.2018.03.022. URL <https://doi.org/10.1016/j.knosys.2018.03.022>.
- [57] Sachin Goyal, Ziwei Ji, Ankit Singh Rawat, Aditya Krishna Menon, Sanjiv Kumar, and Vaishnavh Nagarajan. Think before you speak: Training language models with pause tokens. *The Twelfth International Conference on Learning Representations, ICLR 2024*, 2024.
- [58] Martin Grohe. word2vec, node2vec, graph2vec, x2vec: Towards a theory of vector embeddings of structured data. In Dan Suciu, Yufei Tao, and Zhewei Wei, editors, *Proceedings of the 39th ACM SIGMOD-SIGACT-SIGAI Symposium on Principles of Database Systems, PODS 2020, Portland, OR, USA, June 14-19, 2020*, pages 1–16. ACM, 2020.
- [59] Andrey Gromov. Grokking modular arithmetic, 2023. URL <https://arxiv.org/abs/2301.02679>.

-
- [60] Albert Gu and Tri Dao. Mamba: Linear-time sequence modeling with selective state spaces, 2023.
- [61] Çağlar Gülçehre and Yoshua Bengio. Knowledge matters: Importance of prior information for optimization. *J. Mach. Learn. Res.*, 17:8:1–8:32, 2016.
- [62] Suriya Gunasekar, Blake E. Woodworth, Srinadh Bhojanapalli, Behnam Neyshabur, and Nati Srebro. Implicit regularization in matrix factorization. In *Advances in Neural Information Processing Systems 30: Annual Conference on Neural Information Processing Systems 2017, December 4-9, 2017, Long Beach, CA, USA*, pages 6151–6159, 2017.
- [63] Jiayan Guo, Lun Du, Hengyu Liu, Mengyu Zhou, Xinyi He, and Shi Han. Gpt4graph: Can large language models understand graph structured data ? an empirical evaluation and benchmarking, 2023. URL <https://arxiv.org/abs/2305.15066>.
- [64] Qingyan Guo, Rui Wang, Junliang Guo, Xu Tan, Jiang Bian, and Yujiu Yang. Mitigating reversal curse in large language models via semantic-aware permutation training. In Lun-Wei Ku, Andre Martins, and Vivek Srikumar, editors, *Findings of the Association for Computational Linguistics, ACL 2024, Bangkok, Thailand and virtual meeting, August 11-16, 2024*, pages 11453–11464. Association for Computational Linguistics, 2024. doi: 10.18653/V1/2024.FINDINGS-ACL.680. URL <https://doi.org/10.18653/v1/2024.findings-acl.680>.
- [65] Wes Gurnee and Max Tegmark. Language models represent space and time. In *The Twelfth International Conference on Learning Representations, ICLR 2024, Vienna, Austria, May 7-11, 2024*. OpenReview.net, 2024. URL <https://openreview.net/forum?id=jE8xbmvFin>.
- [66] Jeff Z. HaoChen, Colin Wei, Adrien Gaidon, and Tengyu Ma. Provable guarantees for self-supervised deep learning with spectral contrastive loss. In *Advances in Neural Information Processing Systems 34: Annual Conference on Neural Information Processing Systems 2021, NeurIPS 2021, December 6-14, 2021, virtual*, pages 5000–5011, 2021.
- [67] Christopher Harker and Aditya Bhaskara. Convergence guarantees for the deepwalk embedding on block models. In *Forty-first International Conference on Machine Learning, ICML 2024, Vienna, Austria, July 21-27, 2024*. OpenReview.net, 2024. URL <https://openreview.net/forum?id=xwxUbBHC1q>.
- [68] Tatsunori B. Hashimoto, David Alvarez-Melis, and Tommi S. Jaakkola. Word embeddings as metric recovery in semantic spaces. *Trans. Assoc. Comput. Linguistics*, 4:273–286, 2016. doi: 10.1162/TACL_A_00098. URL https://doi.org/10.1162/tacl_a_00098.
- [69] Benjamin Hoover, Yuchen Liang, Bao Pham, Rameswar Panda, Hendrik Strobelt, Duen Horng Chau, Mohammed Zaki, and Dmitry Krotov. Energy transformer. In A. Oh, T. Naumann, A. Globerson, K. Saenko, M. Hardt, and S. Levine, editors, *Advances in Neural Information Processing Systems*, volume 36, pages 27532–27559. Curran Associates, Inc., 2023. URL https://proceedings.neurips.cc/paper_files/paper/2023/file/57a9b97477b67936298489e3c1417b0a-Paper-Conference.pdf.
- [70] J J Hopfield. Neural networks and physical systems with emergent collective computational abilities. *Proceedings of the National Academy of Sciences*, 79(8):2554–2558, 1982. doi: 10.1073/pnas.79.8.2554. URL <https://www.pnas.org/doi/abs/10.1073/pnas.79.8.2554>.
- [71] Cheng-Yu Hsieh, Chun-Liang Li, Chih-Kuan Yeh, Hootan Nakhost, Yasuhisa Fujii, Alexander Ratner, Ranjay Krishna, Chen-Yu Lee, and Tomas Pfister. Distilling step-by-step! outperforming larger language models with less training data and smaller model sizes. *arXiv preprint arXiv:2305.02301*, 2023.
- [72] Edward S. Hu, Kwangjun Ahn, Qinghua Liu, Haoran Xu, Manan Tomar, Ada Langford, Dinesh Jayaraman, Alex Lamb, and John Langford. The belief state transformer. In *The Thirteenth International Conference on Learning Representations, ICLR 2025, Singapore, April 24-28, 2025*. OpenReview.net, 2025.
- [73] Po-Sen Huang, Xiaodong He, Jianfeng Gao, Li Deng, Alex Acero, and Larry P. Heck. Learning deep structured semantic models for web search using clickthrough data. In Qi He, Arun Iyengar, Wolfgang Nejdl, Jian Pei, and Rajeev Rastogi, editors, *22nd ACM International Conference on Information and Knowledge Management, CIKM'13, San Francisco, CA, USA, October 27 - November 1, 2013*, pages 2333–2338. ACM, 2013.

-
- [74] Yixiao Huang, Hanlin Zhu, Tianyu Guo, Jiantao Jiao, Somayeh Sojoudi, Michael I Jordan, Stuart Russell, and Song Mei. Generalization or hallucination? understanding out-of-context reasoning in transformers. In *Advances in Neural Information Processing Systems 39: Annual Conference on Neural Information Processing Systems 2025, NeurIPS 2025*, 2025.
- [75] Minyoung Huh, Brian Cheung, Tongzhou Wang, and Phillip Isola. Position: The platonic representation hypothesis. In *Forty-first International Conference on Machine Learning, ICML 2024, Vienna, Austria, July 21-27, 2024*. OpenReview.net, 2024. URL <https://openreview.net/forum?id=BH8TYy0r6u>.
- [76] Ariel Jaffe, Yuval Kluger, Ofir Lindenbaum, Jonathan Patsenker, Erez Peterfreund, and Stefan Steinerberger. The spectral underpinning of word2vec, 2020.
- [77] Erik Jenner, Shreyas Kapur, Vasil Georgiev, Cameron Allen, Scott Emmons, and Stuart J. Russell. Evidence of learned look-ahead in a chess-playing neural network. In *Advances in Neural Information Processing Systems 38: Annual Conference on Neural Information Processing Systems 2024, NeurIPS 2024, Vancouver, BC, Canada, December 10 - 15, 2024*, 2024.
- [78] Yibo Jiang, Goutham Rajendran, Pradeep Ravikumar, and Bryon Aragam. Do llms dream of elephants (when told not to)? latent concept association and associative memory in transformers. In *Advances in Neural Information Processing Systems 38: Annual Conference on Neural Information Processing Systems 2024, NeurIPS 2024, Vancouver, BC, Canada, December 10 - 15, 2024*, 2024.
- [79] Yibo Jiang, Goutham Rajendran, Pradeep Kumar Ravikumar, Bryon Aragam, and Victor Veitch. On the origins of linear representations in large language models. In *Forty-first International Conference on Machine Learning, ICML 2024*, 2024.
- [80] Tokio Kajitsuka and Issei Sato. Are transformers with one layer self-attention using low-rank weight matrices universal approximators? In *The Twelfth International Conference on Learning Representations, ICLR 2024, Vienna, Austria, May 7-11, 2024*. OpenReview.net, 2024. URL <https://openreview.net/forum?id=nJnky5K944>.
- [81] Tokio Kajitsuka and Issei Sato. On the optimal memorization capacity of transformers. In *The Thirteenth International Conference on Learning Representations, ICLR 2025, Singapore, April 24-28, 2025*. OpenReview.net, 2025. URL <https://openreview.net/forum?id=UGVYez1LcZ>.
- [82] Dimitris Kalimeris, Gal Kaplun, Preetum Nakkiran, Benjamin Edelman, Tristan Yang, Boaz Barak, and Haofeng Zhang. Sgd on neural networks learns functions of increasing complexity. *Advances in neural information processing systems*, 32, 2019.
- [83] Dhruva Karkada, James B. Simon, Yasaman Bahri, and Michael R. DeWeese. Closed-form training dynamics reveal learned features and linear structure in word2vec-like models, 2025. URL <https://arxiv.org/abs/2502.09863>.
- [84] Nitish Shirish Keskar, Dheevatsa Mudigere, Jorge Nocedal, Mikhail Smelyanskiy, and Ping Tak Peter Tang. On large-batch training for deep learning: Generalization gap and sharp minima. In *5th International Conference on Learning Representations, ICLR 2017, Toulon, France, April 24-26, 2017, Conference Track Proceedings*. OpenReview.net, 2017. URL <https://openreview.net/forum?id=H1oyR1Ygg>.
- [85] Mikail Khona, Maya Okawa, Jan Hula, Rahul Ramesh, Kento Nishi, Robert P. Dick, Ekdeep Singh Lubana, and Hidenori Tanaka. Towards an understanding of stepwise inference in transformers: A synthetic graph navigation model. In *Forty-first International Conference on Machine Learning, ICML 2024, Vienna, Austria, July 21-27, 2024*. OpenReview.net, 2024.
- [86] Jinwoo Kim, Dat Nguyen, Seonwoo Min, Sungjun Cho, Moontae Lee, Honglak Lee, and Seunghoon Hong. Pure transformers are powerful graph learners. In *Advances in Neural Information Processing Systems 35: Annual Conference on Neural Information Processing Systems 2022, NeurIPS 2022, New Orleans, LA, USA, November 28 - December 9, 2022*, 2022.
- [87] Junghwan Kim, Michelle Kim, and Barzan Mozafari. Provable memorization capacity of transformers. In *The Eleventh International Conference on Learning Representations*, 2023. URL <https://openreview.net/forum?id=8JCG5xJCTPR>.

-
- [88] Ouail Kitouni, Niklas Nolte, Diane Bouchacourt, Adina Williams, Mike Rabbat, and Mark Ibrahim. The factorization curse: Which tokens you predict underlie the reversal curse and more. *CoRR*, abs/2406.05183, 2024. doi: 10.48550/ARXIV.2406.05183. URL <https://doi.org/10.48550/arXiv.2406.05183>.
- [89] Dmitry Krotov and John J. Hopfield. Dense associative memory for pattern recognition. In Daniel D. Lee, Masashi Sugiyama, Ulrike von Luxburg, Isabelle Guyon, and Roman Garnett, editors, *Advances in Neural Information Processing Systems 29: Annual Conference on Neural Information Processing Systems 2016, December 5-10, 2016, Barcelona, Spain*, pages 1172–1180, 2016. URL <https://proceedings.neurips.cc/paper/2016/hash/eaee339c4d89fc102edd9dbdb6a28915-Abstract.html>.
- [90] Andrew K. Lampinen, Arslan Chaudhry, Stephanie C. Y. Chan, Cody Wild, Diane Wan, Alex Ku, Jörg Bornschein, Razvan Pascanu, Murray Shanahan, and James L. McClelland. On the generalization of language models from in-context learning and finetuning: a controlled study, 2025. URL <https://arxiv.org/abs/2505.00661>.
- [91] Hung Le, Truyen Tran, and Svetha Venkatesh. Self-attentive associative memory. In Hal Daumé III and Aarti Singh, editors, *Proceedings of the 37th International Conference on Machine Learning*, volume 119 of *Proceedings of Machine Learning Research*, pages 5682–5691. PMLR, 13–18 Jul 2020. URL <https://proceedings.mlr.press/v119/le20b.html>.
- [92] Andrew Lee, Melanie Weber, Fernanda Viégas, and Martin Wattenberg. Shared global and local geometry of language model embeddings. In *Second Conference on Language Modeling*, 2025. URL <https://openreview.net/forum?id=aJDykpJAYF>.
- [93] Omer Levy and Yoav Goldberg. Neural word embedding as implicit matrix factorization. In Zoubin Ghahramani, Max Welling, Corinna Cortes, Neil D. Lawrence, and Kilian Q. Weinberger, editors, *Advances in Neural Information Processing Systems 27: Annual Conference on Neural Information Processing Systems 2014, December 8-13 2014, Montreal, Quebec, Canada*, pages 2177–2185, 2014.
- [94] Bohan Li, Hao Zhou, Junxian He, Mingxuan Wang, Yiming Yang, and Lei Li. On the sentence embeddings from pre-trained language models. In Bonnie Webber, Trevor Cohn, Yulan He, and Yang Liu, editors, *Proceedings of the 2020 Conference on Empirical Methods in Natural Language Processing, EMNLP 2020, Online, November 16-20, 2020*, pages 9119–9130. Association for Computational Linguistics, 2020.
- [95] Hongyu Li, Liang Ding, Meng Fang, and Dacheng Tao. Revisiting catastrophic forgetting in large language model tuning. In *Findings of the Association for Computational Linguistics: EMNLP 2024, Miami, Florida, USA, November 12-16, 2024*, pages 4297–4308. Association for Computational Linguistics, 2024.
- [96] Melody Zixuan Li, Kumar Krishna Agrawal, Arna Ghosh, Komal Kumar Teru, Adam Santoro, Guillaume Lajoie, and Blake A Richards. Tracing the representation geometry of language models from pretraining to post-training. 2025.
- [97] Zhengkai Lin, Zhihang Fu, Kai Liu, Liang Xie, Binbin Lin, Wenxiao Wang, Deng Cai, Yue Wu, and Jieping Ye. Delving into the reversal curse: How far can large language models generalize? In *Advances in Neural Information Processing Systems 38: Annual Conference on Neural Information Processing Systems 2024, NeurIPS 2024, Vancouver, BC, Canada, December 10 - 15, 2024*, 2024.
- [98] Wang Ling, Dani Yogatama, Chris Dyer, and Phil Blunsom. Program induction by rationale generation: Learning to solve and explain algebraic word problems. In *Proceedings of the 55th Annual Meeting of the Association for Computational Linguistics, ACL 2017, Vancouver, Canada, July 30 - August 4, Volume 1: Long Papers*, pages 158–167. Association for Computational Linguistics, 2017.
- [99] Junnan Liu, Qianren Mao, Weifeng Jiang, and Jianxin Li. Knowformer: Revisiting transformers for knowledge graph reasoning. In *Forty-first International Conference on Machine Learning, ICML 2024, Vienna, Austria, July 21-27, 2024*. OpenReview.net, 2024. URL <https://openreview.net/forum?id=EncFNR3hxM>.
- [100] Ziming Liu, Ouail Kitouni, Niklas Nolte, Eric J. Michaud, Max Tegmark, and Mike Williams. Towards understanding grokking: An effective theory of representation learning. In *Advances in Neural Information Processing Systems 35: Annual Conference on Neural Information*

Processing Systems 2022, NeurIPS 2022, New Orleans, LA, USA, November 28 - December 9, 2022, 2022.

- [101] H. C. Longuet-Higgins, D. J. Willshaw, and O. P. Buneman. Theories of associative recall. *Quarterly Reviews of Biophysics*, 3(2):223–244, 1970. doi: 10.1017/S0033583500004583.
- [102] Zhicong Lu, Li Jin, Peiguang Li, Yu Tian, Linhao Zhang, Sirui Wang, Guangluan Xu, Changyuan Tian, and Xunliang Cai. Rethinking the reversal curse of LLMs: a prescription from human knowledge reversal. In *Proceedings of the 2024 Conference on Empirical Methods in Natural Language Processing*, November 2024.
- [103] Yun Luo, Zhen Yang, Fandong Meng, Yafu Li, Jie Zhou, and Yue Zhang. An empirical study of catastrophic forgetting in large language models during continual fine-tuning, 2025. URL <https://arxiv.org/abs/2308.08747>.
- [104] Ang Lv, Kaiyi Zhang, Yuhan Chen, Yulong Wang, Lifeng Liu, Ji-Rong Wen, Jian Xie, and Rui Yan. Interpreting key mechanisms of factual recall in transformer-based language models. *CoRR*, abs/2403.19521, 2024.
- [105] Liam Madden, Curtis Fox, and Christos Thrampoulidis. Next-token prediction capacity: General upper bounds and a lower bound for transformers. *IEEE Transactions on Information Theory*, pages 1–1, 2025.
- [106] Sadeqh Mahdavi, Renjie Liao, and Christos Thrampoulidis. Memorization capacity of multi-head attention in transformers. In *The Twelfth International Conference on Learning Representations, ICLR 2024, Vienna, Austria, May 7-11, 2024*. OpenReview.net, 2024.
- [107] Pratyush Maini, Michael Curtis Mozer, Hanie Sedghi, Zachary Chase Lipton, J. Zico Kolter, and Chiyuan Zhang. Can neural network memorization be localized? In *International Conference on Machine Learning, ICML 2023, 23-29 July 2023, Honolulu, Hawaii, USA*, volume 202 of *Proceedings of Machine Learning Research*, pages 23536–23557. PMLR, 2023.
- [108] Eran Malach. Auto-regressive next-token predictors are universal learners. *arXiv preprint arXiv:2309.06979*, 2023.
- [109] Leland McInnes, John Healy, and James Melville. Umap: Uniform manifold approximation and projection for dimension reduction. *arXiv preprint arXiv:1802.03426*, 2018.
- [110] Tianyi Men, Pengfei Cao, Zhuoran Jin, Yubo Chen, Kang Liu, and Jun Zhao. Unlocking the future: Exploring look-ahead planning mechanistic interpretability in large language models. In *Proceedings of the 2024 Conference on Empirical Methods in Natural Language Processing, EMNLP 2024, Miami, FL, USA, November 12-16, 2024*, pages 7713–7724. Association for Computational Linguistics, 2024.
- [111] Kevin Meng, David Bau, Alex Andonian, and Yonatan Belinkov. Locating and editing factual associations in GPT. In *Advances in Neural Information Processing Systems 35: Annual Conference on Neural Information Processing Systems 2022, NeurIPS 2022, New Orleans, LA, USA, November 28 - December 9, 2022, 2022*.
- [112] Tomas Mikolov, Wen-tau Yih, and Geoffrey Zweig. Linguistic regularities in continuous space word representations. In Lucy Vanderwende, Hal Daume III, and Katrin Kirchhoff, editors, *Human Language Technologies: Conference of the North American Chapter of the Association of Computational Linguistics, Proceedings, June 9-14, 2013, Westin Peachtree Plaza Hotel, Atlanta, Georgia, USA*, pages 746–751. The Association for Computational Linguistics, 2013.
- [113] David M. Mimno and Laure Thompson. The strange geometry of skip-gram with negative sampling. In Martha Palmer, Rebecca Hwa, and Sebastian Riedel, editors, *Proceedings of the 2017 Conference on Empirical Methods in Natural Language Processing, EMNLP 2017, Copenhagen, Denmark, September 9-11, 2017*, pages 2873–2878. Association for Computational Linguistics, 2017. URL <https://doi.org/10.18653/v1/d17-1308>.
- [114] Ida Momennejad, Hosein Hasanbeig, Felipe Vieira Frujeri, Hiteshi Sharma, Robert Osazuwa Ness, Nebojsa Jojic, Hamid Palangi, and Jonathan Larson. Evaluating cognitive maps and planning in large language models with cogeval. *Advances in Neural Information Processing Systems*, 36, 2023.
- [115] John X. Morris, Chawin Sitawarin, Chuan Guo, Narine Kokhlikyan, G. Edward Suh, Alexander M. Rush, Kamalika Chaudhuri, and Saeed Mahloujifar. How much do language models memorize?, 2025. URL <https://arxiv.org/abs/2505.24832>.

-
- [116] Marius Mosbach, Tiago Pimentel, Shauli Ravfogel, Dietrich Klakow, and Yanai Elazar. Few-shot fine-tuning vs. in-context learning: A fair comparison and evaluation. In Anna Rogers, Jordan L. Boyd-Graber, and Naoaki Okazaki, editors, *Findings of the Association for Computational Linguistics: ACL 2023, Toronto, Canada, July 9-14, 2023*, pages 12284–12314. Association for Computational Linguistics, 2023.
- [117] Tiberiu Musat. Clustering and alignment: Understanding the training dynamics in modular addition, 2024. URL <https://arxiv.org/abs/2408.09414>.
- [118] Ido Nachum and Amir Yehudayoff. On symmetry and initialization for neural networks. In *Latin American Symposium on Theoretical Informatics*, pages 401–412. Springer, 2020.
- [119] Vaishnavh Nagarajan, Chen Henry Wu, Charles Ding, and Aditi Raghunathan. Roll the dice & look before you leap: Going beyond the creative limits of next-token prediction. 2025.
- [120] Neel Nanda, Lawrence Chan, Tom Lieberum, Jess Smith, and Jacob Steinhardt. Progress measures for grokking via mechanistic interpretability. In *The Eleventh International Conference on Learning Representations, ICLR 2023*, 2023.
- [121] Ella Neeman, Roei Aharoni, Or Honovich, Leshem Choshen, Idan Szpektor, and Omri Abend. Disentqa: Disentangling parametric and contextual knowledge with counterfactual question answering. In *Proceedings of the 61st Annual Meeting of the Association for Computational Linguistics (Volume 1: Long Papers), ACL 2023, Toronto, Canada, July 9-14, 2023*, pages 10056–10070. Association for Computational Linguistics, 2023.
- [122] Behnam Neyshabur, Ryota Tomioka, and Nathan Srebro. In search of the real inductive bias: On the role of implicit regularization in deep learning, 2015. URL <https://arxiv.org/abs/1412.6614>.
- [123] Behnam Neyshabur, Srinadh Bhojanapalli, David McAllester, and Nati Srebro. Exploring generalization in deep learning. In *Advances in Neural Information Processing Systems 30: Annual Conference on Neural Information Processing Systems 2017, December 4-9, 2017, Long Beach, CA, USA*, pages 5947–5956, 2017.
- [124] Eshaan Nichani, Jason D. Lee, and Alberto Bietti. Understanding factual recall in transformers via associative memories, 2024. URL <https://arxiv.org/abs/2412.06538>.
- [125] Maxwell I. Nye, Anders Johan Andreassen, Guy Gur-Ari, Henryk Michalewski, Jacob Austin, David Bieber, David Dohan, Aitor Lewkowycz, Maarten Bosma, David Luan, Charles Sutton, and Augustus Odena. Show your work: Scratchpads for intermediate computation with language models. *arXiv preprint arXiv:2112.00114*, 2021.
- [126] Catherine Olsson, Nelson Elhage, Neel Nanda, Nicholas Joseph, Nova DasSarma, Tom Henighan, Ben Mann, Amanda Askell, Yuntao Bai, Anna Chen, et al. In-context learning and induction heads. *arXiv preprint arXiv:2209.11895*, 2022.
- [127] Koyena Pal, Jiuding Sun, Andrew Yuan, Byron C. Wallace, and David Bau. Future lens: Anticipating subsequent tokens from a single hidden state. In *Proceedings of the 27th Conference on Computational Natural Language Learning, CoNLL 2023*. Association for Computational Linguistics, 2023.
- [128] Zhixuan Pan, Shaowen Wang, and Jian Li. Understanding llm behaviors via compression: Data generation, knowledge acquisition and scaling laws, 2025. URL <https://arxiv.org/abs/2504.09597>.
- [129] Core Francisco Park, Andrew Lee, Ekdeep Singh Lubana, Yongyi Yang, Maya Okawa, Kento Nishi, Martin Wattenberg, and Hidenori Tanaka. ICLR: in-context learning of representations. In *The Thirteenth International Conference on Learning Representations, ICLR 2025*. OpenReview.net, 2025.
- [130] Kiho Park, Yo Joong Choe, and Victor Veitch. The linear representation hypothesis and the geometry of large language models. In *Forty-first International Conference on Machine Learning, ICML 2024, Vienna, Austria, July 21-27, 2024*. OpenReview.net, 2024. URL <https://openreview.net/forum?id=UGpGkLzwpP>.
- [131] Kiho Park, Yo Joong Choe, Yibo Jiang, and Victor Veitch. The geometry of categorical and hierarchical concepts in large language models. In *The Thirteenth International Conference on Learning Representations, ICLR 2025, Singapore, April 24-28, 2025*. OpenReview.net, 2025. URL <https://openreview.net/forum?id=bVTM2QKYuA>.

-
- [132] Binghui Peng, Srinu Narayanan, and Christos Papadimitriou. On limitations of the transformer architecture. In *First Conference on Language Modeling*, 2024. URL <https://openreview.net/forum?id=KidynPuLNW>.
- [133] Mohammad Pezeshki, Sékou-Oumar Kaba, Yoshua Bengio, Aaron C. Courville, Doina Precup, and Guillaume Lajoie. Gradient starvation: A learning proclivity in neural networks. In *Advances in Neural Information Processing Systems 34: Annual Conference on Neural Information Processing Systems 2021, NeurIPS 2021, December 6-14, 2021, virtual*, pages 1256–1272, 2021.
- [134] Piotr Piekos, Mateusz Malinowski, and Henryk Michalewski. Measuring and improving bert’s mathematical abilities by predicting the order of reasoning. In *Proceedings of the 59th Annual Meeting of the Association for Computational Linguistics and the 11th International Joint Conference on Natural Language Processing, ACL/IJCNLP 2021, (Volume 2: Short Papers), Virtual Event, August 1-6, 2021*, pages 383–394. Association for Computational Linguistics, 2021.
- [135] Ofir Press, Muru Zhang, Sewon Min, Ludwig Schmidt, Noah A. Smith, and Mike Lewis. Measuring and narrowing the compositionality gap in language models. In Houda Bouamor, Juan Pino, and Kalika Bali, editors, *Findings of the Association for Computational Linguistics: EMNLP 2023, Singapore, December 6-10, 2023*, pages 5687–5711. Association for Computational Linguistics, 2023.
- [136] Chengwen Qi, Bowen Li, Binyuan Hui, Bailin Wang, Jinyang Li, Jinwang Wu, and Yuanjun Laili. An investigation of llms’ inefficacy in understanding converse relations. In Houda Bouamor, Juan Pino, and Kalika Bali, editors, *Proceedings of the 2023 Conference on Empirical Methods in Natural Language Processing, EMNLP 2023, Singapore, December 6-10, 2023*, pages 6932–6953. Association for Computational Linguistics, 2023.
- [137] Jiezhong Qiu, Yuxiao Dong, Hao Ma, Jian Li, Kuansan Wang, and Jie Tang. Network embedding as matrix factorization: Unifying deepwalk, line, pte, and node2vec. In *Proceedings of the Eleventh ACM International Conference on Web Search and Data Mining, WSDM 2018*, page 459–467. ACM, February 2018. doi: 10.1145/3159652.3159706. URL <http://dx.doi.org/10.1145/3159652.3159706>.
- [138] Alec Radford, Jeff Wu, Rewon Child, David Luan, Dario Amodei, and Ilya Sutskever. Language models are unsupervised multitask learners. 2019.
- [139] Adityanarayanan Radhakrishnan, Mikhail Belkin, and Caroline Uhler. Overparameterized neural networks implement associative memory. *Proc. Natl. Acad. Sci. USA*, 117(44):27162–27170, 2020. doi: 10.1073/PNAS.2005013117. URL <https://doi.org/10.1073/pnas.2005013117>.
- [140] Nasim Rahaman, Aristide Baratin, Devansh Arpit, Felix Draxler, Min Lin, Fred Hamprecht, Yoshua Bengio, and Aaron Courville. On the spectral bias of neural networks. In *Proceedings of the 36th International Conference on Machine Learning*, volume 97 of *Proceedings of Machine Learning Research*, pages 5301–5310. PMLR, 09–15 Jun 2019.
- [141] Shashank Rajput, Nikhil Mehta, Anima Singh, Raghunandan Hulikal Keshavan, Trung Vu, Lukasz Heldt, Lichan Hong, Yi Tay, Vinh Q. Tran, Jonah Samost, Maciej Kula, Ed H. Chi, and Mahesh Sathiamoorthy. Recommender systems with generative retrieval. In *Advances in Neural Information Processing Systems 36: Annual Conference on Neural Information Processing Systems 2023, NeurIPS 2023, New Orleans, LA, USA, December 10 - 16, 2023*, 2023.
- [142] Hubert Ramsauer, Bernhard Schöfl, Johannes Lehner, Philipp Seidl, Michael Widrich, Lukas Gruber, Markus Holzleitner, Thomas Adler, David P. Kreil, Michael K. Kopp, Günter Klambauer, Johannes Brandstetter, and Sepp Hochreiter. Hopfield networks is all you need. OpenReview.net, 2021. URL <https://openreview.net/forum?id=tL89RnzTiCd>.
- [143] Gabriel Recchia. Teaching autoregressive language models complex tasks by demonstration. *arXiv preprint arXiv:2109.02102*, 2021.
- [144] Adam Roberts, Colin Raffel, and Noam Shazeer. How much knowledge can you pack into the parameters of a language model? In *Proceedings of the 2020 Conference on Empirical Methods in Natural Language Processing, EMNLP 2020, Online, November 16-20, 2020*,

-
- pages 5418–5426. Association for Computational Linguistics, 2020. doi: 10.18653/V1/2020.EMNLP-MAIN.437. URL <https://doi.org/10.18653/v1/2020.emnlp-main.437>.
- [145] Mark Rofin, Jalal Naghiyev, and Michael Hahn. On the emergence of ”useless” features in next token predictors. In *ICML 2025 Workshop on Assessing World Models*, 2025. URL <https://openreview.net/forum?id=lniwJxd2cT>.
- [146] Basri Ronen, David Jacobs, Yoni Kasten, and Shira Kritchman. The convergence rate of neural networks for learned functions of different frequencies. *Advances in Neural Information Processing Systems*, 32, 2019.
- [147] Elan Rosenfeld and Andrej Risteski. Outliers with opposing signals have an outsized effect on neural network optimization. In *The Twelfth International Conference on Learning Representations*, 2024. URL <https://openreview.net/forum?id=kIZ3S3tel6>.
- [148] Clayton Sanford, Bahare Fatemi, Ethan Hall, Anton Tsitsulin, Seyed Mehran Kazemi, Jonathan Halcrow, Bryan Perozzi, and Vahab Mirrokni. Understanding transformer reasoning capabilities via graph algorithms. abs/2405.18512, 2024.
- [149] Clayton Sanford, Daniel Hsu, and Matus Telgarsky. Transformers, parallel computation, and logarithmic depth. In *Forty-first International Conference on Machine Learning, ICML 2024, Vienna, Austria, July 21-27, 2024*. OpenReview.net, 2024. URL <https://openreview.net/forum?id=QCZabhKQhB>.
- [150] Abulhair Saparov, Srushti Pawar, Shreyas Pimpalgaonkar, Nitish Joshi, Richard Yuanzhe Pang, Vishakh Padmakumar, Seyed Mehran Kazemi, Najoung Kim, and He He. Transformers struggle to learn to search, 2024. URL <https://arxiv.org/abs/2412.04703>.
- [151] Shashata Sawmya, Micah Adler, and Nir Shavit. The birth of knowledge: Emergent features across time, space, and scale in large language models, 2025. URL <https://arxiv.org/abs/2505.19440>.
- [152] Andrew M. Saxe, James L. McClelland, and Surya Ganguli. Exact solutions to the nonlinear dynamics of learning in deep linear neural networks. In *2nd International Conference on Learning Representations, ICLR 2014, Banff, AB, Canada, April 14-16, 2014, Conference Track Proceedings*, 2014. URL <http://arxiv.org/abs/1312.6120>.
- [153] Andrew M. Saxe, James L. McClelland, and Surya Ganguli. A mathematical theory of semantic development in deep neural networks. *Proceedings of the National Academy of Sciences*, 116(23):11537–11546, 2019. doi: 10.1073/pnas.1820226116. URL <https://www.pnas.org/doi/abs/10.1073/pnas.1820226116>.
- [154] Imanol Schlag, Kazuki Irie, and Jürgen Schmidhuber. Linear transformers are secretly fast weight programmers. In Marina Meila and Tong Zhang, editors, *Proceedings of the 38th International Conference on Machine Learning*, volume 139 of *Proceedings of Machine Learning Research*, pages 9355–9366. PMLR, 18–24 Jul 2021.
- [155] Harshay Shah, Kaustav Tamuly, Aditi Raghunathan, Prateek Jain, and Praneeth Netrapalli. The pitfalls of simplicity bias in neural networks. In *Advances in Neural Information Processing Systems 33: Annual Conference on Neural Information Processing Systems 2020, NeurIPS 2020, December 6-12, 2020, virtual*, 2020.
- [156] Shai Shalev-Shwartz and Amnon Shashua. On the sample complexity of end-to-end training vs. semantic abstraction training. *arXiv preprint arXiv:1604.06915*, 2016.
- [157] Shai Shalev-Shwartz and Amnon Shashua. From reasoning to super-intelligence: A search-theoretic perspective, 2025. URL <https://arxiv.org/abs/2507.15865>.
- [158] Parshin Shojaee, Iman Mirzadeh, Keivan Alizadeh, Maxwell Horton, Samy Bengio, and Mehrdad Farajtabar. The illusion of thinking: Understanding the strengths and limitations of reasoning models via the lens of problem complexity, 2025. URL <https://arxiv.org/abs/2506.06941>.
- [159] Itamar Shoshani and Ohad Shamir. Hardness of learning fixed parities with neural networks. *arXiv preprint arXiv:2501.00817*, 2025.
- [160] Kumar Shridhar, Alessandro Stolfo, and Mrinmaya Sachan. Distilling reasoning capabilities into smaller language models. *arXiv preprint arXiv:2212.00193*, 2022.

-
- [161] Matthew Smart, Alberto Bietti, and Anirvan M. Sengupta. In-context denoising with one-layer transformers: connections between attention and associative memory retrieval. In *New Frontiers in Associative Memories*, 2025. URL <https://openreview.net/forum?id=F07wIRq8pK>.
- [162] Daniel Soudry, Elad Hoffer, and Nathan Srebro. The implicit bias of gradient descent on separable data. In *International Conference on Learning Representations*, 2018. URL <https://openreview.net/forum?id=r1q7n9gAb>.
- [163] Cory Stephenson, Suchismita Padhy, Abhinav Ganesh, Yue Hui, Hanlin Tang, and SueYeon Chung. On the geometry of generalization and memorization in deep neural networks. In *9th International Conference on Learning Representations, ICLR 2021, Virtual Event, Austria, May 3-7, 2021*. OpenReview.net, 2021.
- [164] Sainbayar Sukhbaatar, Edouard Grave, Guillaume Lample, Herve Jegou, and Armand Joulin. Augmenting self-attention with persistent memory, 2019. URL <https://arxiv.org/abs/1907.01470>.
- [165] Zhiqian Tan, Yifan Zhang, Jingqin Yang, and Yang Yuan. Contrastive learning is spectral clustering on similarity graph. In *The Twelfth International Conference on Learning Representations, ICLR 2024, Vienna, Austria, May 7-11, 2024*. OpenReview.net, 2024. URL <https://openreview.net/forum?id=hLZQTFGT0A>.
- [166] Yi Tay, Vinh Tran, Mostafa Dehghani, Jianmo Ni, Dara Bahri, Harsh Mehta, Zhen Qin, Kai Hui, Zhe Zhao, Jai Prakash Gupta, Tal Schuster, William W. Cohen, and Donald Metzler. Transformer memory as a differentiable search index. In *Advances in Neural Information Processing Systems 35: Annual Conference on Neural Information Processing Systems 2022, NeurIPS 2022, New Orleans, LA, USA, November 28 - December 9, 2022*, 2022.
- [167] Christos Thrampoulidis. Implicit optimization bias of next-token prediction in linear models. In Amir Globersons, Lester Mackey, Danielle Belgrave, Angela Fan, Ulrich Paquet, Jakub M. Tomczak, and Cheng Zhang, editors, *Advances in Neural Information Processing Systems 38: Annual Conference on Neural Information Processing Systems 2024, NeurIPS 2024, Vancouver, BC, Canada, December 10 - 15, 2024*, 2024.
- [168] Karthik Valmeekam, Matthew Marquez, and Subbarao Kambhampati. Can large language models really improve by self-critiquing their own plans? *arXiv preprint arXiv:2310.08118*, 2023.
- [169] Karthik Valmeekam, Matthew Marquez, Alberto Olmo, Sarath Sreedharan, and Subbarao Kambhampati. Planbench: An extensible benchmark for evaluating large language models on planning and reasoning about change, 2023.
- [170] Karthik Valmeekam, Matthew Marquez, Sarath Sreedharan, and Subbarao Kambhampati. On the planning abilities of large language models - A critical investigation. In *Advances in Neural Information Processing Systems 36: Annual Conference on Neural Information Processing Systems 2023, NeurIPS 2023, New Orleans, LA, USA, December 10 - 16, 2023*, 2023.
- [171] Gal Vardi, Gilad Yehudai, and Ohad Shamir. On the optimal memorization power of relu neural networks. In *The Tenth International Conference on Learning Representations, ICLR 2022, Virtual Event, April 25-29, 2022*. OpenReview.net, 2022. URL <https://openreview.net/forum?id=MkTPtnjeYTV>.
- [172] Ashish Vaswani, Noam Shazeer, Niki Parmar, Jakob Uszkoreit, Llion Jones, Aidan N. Gomez, Lukasz Kaiser, and Illia Polosukhin. Attention is all you need. In *Advances in Neural Information Processing Systems 30: Annual Conference on Neural Information Processing Systems 2017, December 4-9, 2017, Long Beach, CA, USA*, pages 5998–6008, 2017.
- [173] Boshi Wang and Huan Sun. Is the reversal curse a binding problem? uncovering limitations of transformers from a basic generalization failure, 2025. URL <https://arxiv.org/abs/2504.01928>.
- [174] Boshi Wang, Xiang Yue, Yu Su, and Huan Sun. Grokking of implicit reasoning in transformers: A mechanistic journey to the edge of generalization. In *Advances in Neural Information Processing Systems 38: Annual Conference on Neural Information Processing Systems 2024, NeurIPS 2024, Vancouver, BC, Canada, December 10 - 15, 2024*, 2024.

-
- [175] Heng Wang, Shangbin Feng, Tianxing He, Zhaoxuan Tan, Xiaochuang Han, and Yulia Tsvetkov. Can language models solve graph problems in natural language? In *Advances in Neural Information Processing Systems 36: Annual Conference on Neural Information Processing Systems 2023, NeurIPS 2023*, 2023.
- [176] Shuo Wang and Issei Sato. Rethinking associative memory mechanism in induction head. In *Second Conference on Language Modeling*, 2025. URL <https://openreview.net/forum?id=8N5H8DgfPw>.
- [177] Siwei Wang, Yifei Shen, Shi Feng, Haoran Sun, Shang-Hua Teng, and Wei Chen. ALPINE: unveiling the planning capability of autoregressive learning in language models. In *Advances in Neural Information Processing Systems 38: Annual Conference on Neural Information Processing Systems 2024, NeurIPS 2024, Vancouver, BC, Canada, December 10 - 15, 2024*, 2024.
- [178] Xinyi Wang, Shawn Tan, Mingyu Jin, William Yang Wang, Rameswar Panda, and Yikang Shen. Do larger language models imply better generalization? a pretraining scaling law for implicit reasoning, 2025. URL <https://arxiv.org/abs/2504.03635>.
- [179] Yujing Wang, Yingyan Hou, Haonan Wang, Ziming Miao, Shibin Wu, Qi Chen, Yuqing Xia, Chengmin Chi, Guoshuai Zhao, Zheng Liu, Xing Xie, Hao Sun, Weiwei Deng, Qi Zhang, and Mao Yang. A neural corpus indexer for document retrieval. In *Advances in Neural Information Processing Systems 35: Annual Conference on Neural Information Processing Systems 2022, NeurIPS 2022, New Orleans, LA, USA, November 28 - December 9, 2022*, 2022.
- [180] Zixuan Wang, Eshaan Nichani, Alberto Bietti, Alex Damian, Daniel Hsu, Jason D. Lee, and Denny Wu. Learning compositional functions with transformers from easy-to-hard data, 2025. URL <https://arxiv.org/abs/2505.23683>.
- [181] Noam Wies, Yoav Levine, and Amnon Shashua. Sub-task decomposition enables learning in sequence to sequence tasks. In *The Eleventh International Conference on Learning Representations, ICLR 2023*, 2023.
- [182] David J Willshaw, O Peter Buneman, and Hugh Christopher Longuet-Higgins. Non-holographic associative memory. *Nature*, 222(5197):960–962, 1969.
- [183] Wilson Wu, John X. Morris, and Lionel Levine. Do language models plan ahead for future tokens? abs/2404.00859, 2024. doi: 10.48550/ARXIV.2404.00859. URL <https://doi.org/10.48550/arXiv.2404.00859>.
- [184] Zhiqin John Xu. Understanding training and generalization in deep learning by fourier analysis. *arXiv preprint arXiv:1808.04295*, 2018.
- [185] Sohee Yang, Elena Gribovskaya, Nora Kassner, Mor Geva, and Sebastian Riedel. Do large language models latently perform multi-hop reasoning? In *Proceedings of the 62nd Annual Meeting of the Association for Computational Linguistics (Volume 1: Long Papers), ACL 2024, Bangkok, Thailand, August 11-16, 2024*, pages 10210–10229. Association for Computational Linguistics, 2024.
- [186] Sohee Yang, Nora Kassner, Elena Gribovskaya, Sebastian Riedel, and Mor Geva. Do large language models perform latent multi-hop reasoning without exploiting shortcuts? abs/2411.16679, 2024. doi: 10.48550/ARXIV.2411.16679. URL <https://doi.org/10.48550/arXiv.2411.16679>.
- [187] Zitong Yang, Neil Band, Shuangping Li, Emmanuel J. Candès, and Tatsunori Hashimoto. Synthetic continued pretraining. In *The Thirteenth International Conference on Learning Representations, ICLR 2025, Singapore, April 24-28, 2025*. OpenReview.net, 2025.
- [188] Yuekun Yao, Yupei Du, Dawei Zhu, Michael Hahn, and Alexander Koller. Language models can learn implicit multi-hop reasoning, but only if they have lots of training data, 2025. URL <https://arxiv.org/abs/2505.17923>.
- [189] Jiaran Ye, Zijun Yao, Zhidian Huang, Liangming Pan, Jinxin Liu, Yushi Bai, Amy Xin, Liu Weichuan, Xiaoyin Che, Lei Hou, and Juanzi Li. How does transformer learn implicit reasoning?, 2025. URL <https://arxiv.org/abs/2505.23653>.
- [190] Gilad Yehudai, Clayton Sanford, Maya Bechler-Speicher, Orr Fischer, Ran Gilad-Bachrach, and Amir Globerson. Depth-width tradeoffs in algorithmic reasoning of graph tasks with transformers. *arXiv preprint arXiv:2503.01805*, 2025.

-
- [191] Yutong Yin and Zhaoran Wang. Are transformers able to reason by connecting separated knowledge in training data? In *The Thirteenth International Conference on Learning Representations*, 2025. URL <https://openreview.net/forum?id=1Xg4JPPxJ0>.
- [192] Chengxuan Ying, Tianle Cai, Shengjie Luo, Shuxin Zheng, Guolin Ke, Di He, Yanming Shen, and Tie-Yan Liu. Do transformers really perform badly for graph representation? In *Advances in Neural Information Processing Systems 34: Annual Conference on Neural Information Processing Systems 2021, NeurIPS 2021, December 6-14, 2021, virtual*, pages 28877–28888, 2021.
- [193] Chengxuan Ying, Tianle Cai, Shengjie Luo, Shuxin Zheng, Guolin Ke, Di He, Yanming Shen, and Tie-Yan Liu. Do transformers really perform bad for graph representation?, 2021. URL <https://arxiv.org/abs/2106.05234>.
- [194] Eric Zelikman, Yuhuai Wu, Jesse Mu, and Noah D. Goodman. Star: Bootstrapping reasoning with reasoning. In *Advances in Neural Information Processing Systems 35: Annual Conference on Neural Information Processing Systems 2022, NeurIPS 2022, New Orleans, LA, USA, November 28 - December 9, 2022*, 2022.
- [195] Chiyuan Zhang, Samy Bengio, Moritz Hardt, Benjamin Recht, and Oriol Vinyals. Understanding deep learning requires rethinking generalization. In *5th International Conference on Learning Representations, ICLR 2017, Toulon, France, April 24-26, 2017, Conference Track Proceedings*. OpenReview.net, 2017. URL <https://openreview.net/forum?id=Sy8gdB9xx>.
- [196] Ying Zhang, Benjamin Heinzerling, Dongyuan Li, Ryoma Ishigaki, Yuta Hitomi, and Kentaro Inui. Understanding fact recall in language models: Why two-stage training encourages memorization but mixed training teaches knowledge, 2025. URL <https://arxiv.org/abs/2505.16178>.
- [197] Ziwei Zhang. A note on spectral clustering and svd of graph data, 2018. URL <https://arxiv.org/abs/1809.11029>.
- [198] Yize Zhao and Christos Thrampoulidis. On the geometry of semantics in next-token prediction, 2025. URL <https://arxiv.org/abs/2505.08348>.
- [199] Yize Zhao, Tina Behnia, Vala Vakilian, and Christos Thrampoulidis. Implicit geometry of next-token prediction: From language sparsity patterns to model representations, 2025. URL <https://arxiv.org/abs/2408.15417>.
- [200] Jie Zhou, Ganqu Cui, Shengding Hu, Zhengyan Zhang, Cheng Yang, Zhiyuan Liu, Lifeng Wang, Changcheng Li, and Maosong Sun. Graph neural networks: A review of methods and applications. *AI Open*, 1:57–81, 2020.
- [201] Chen Zhu, Ankit Singh Rawat, Manzil Zaheer, Srinadh Bhojanapalli, Daliang Li, Felix Yu, and Sanjiv Kumar. Modifying memories in transformer models, 2020. URL <https://arxiv.org/abs/2012.00363>.
- [202] Hanlin Zhu, Baihe Huang, Shaolun Zhang, Michael I. Jordan, Jiantao Jiao, Yuandong Tian, and Stuart J. Russell. Towards a theoretical understanding of the ‘reversal curse’ via training dynamics. In *Advances in Neural Information Processing Systems 38: Annual Conference on Neural Information Processing Systems 2024, NeurIPS 2024, Vancouver, BC, Canada, December 10 - 15, 2024*, 2024.
- [203] Nicolas Zucchet, Jörg Bornschein, Stephanie Chan, Andrew Lampinen, Razvan Pascanu, and Soham De. How do language models learn facts? dynamics, curricula and hallucinations, 2025. URL <https://arxiv.org/abs/2503.21676>.

Appendix

A Detailed background on the path-star task

A path-star graph $\mathcal{G} = (V, E)$ is a special tree graph from Bachmann and Nagarajan [13] that has a central root named v_{root} with multiple disjoint, uniform-length paths emanating from it. One of the leaf nodes is specified as v_{goal} . The task is to find the unique path from v_{root} to v_{goal} . To solve this task, one may either plan—by searching over the paths and backtracking—or execute a much simpler solution by following the unique path back from v_{goal} , and then outputting the reverse of this path. Although this solution is algorithmically straightforward, and although a Transformer can even be shown to learn this solution under a simple multi-token modification to the objective, the next-token objective itself fails to learn this task even with sufficient amounts of data. Thus, the failure comes from optimization under the next-token objective. In this sense, the path-star task is known to be a minimal textbook adversarial example to next-token learning.

In-context path-star task. In the in-context version of the task, the model is given the prefix $\mathbf{p} = (\text{adj}(\mathcal{G}), v_{\text{root}}, v_{\text{goal}})$ that provides a randomized adjacency list, and indicates the start and goal nodes, in the model’s context. The model must then produce the true path as response, $\mathbf{r} = (v_{\text{root}}, \dots, v_{\text{goal}})$. To cast this as a learning task, we define a distribution $\mathcal{D}_{d,l}$ corresponding to graphs of the same topology, degree d and path length l . To sample $\mathbf{p} \sim \mathcal{D}_{d,l}$, we uniformly sample node values from a vocabulary \mathbb{V} to create the graph G ; given this, we can randomize the adjacency list $\text{adj}(G)$.

Figures 2 and 3 contrast the two evaluation regimes we use throughout: in-weights (edge memorization & path finetuning) versus in-context (graph in the prompt).

A.1 Failure of next-token learning in the in-context path-star task

Next-token learners trained on samples from the above task are known to fail *in-distribution* i.e., even on unseen graphs of the *same* topology (with only variations in the node identities and adjacency list randomization), the model uniformly at random picks a path to follow from the center. The mechanism of failure plays out in two stages during training.

The Clever Hans Cheat. Early on during training, the model fits the later tokens in the target — concretely nodes $v_2, \dots, v_{\text{goal}}$ — as the unique child of the previous token provided in the input during next-token training. This is known as a *Clever Hans cheat*: the model uses a local rule that relies on witnessing part of the ground truth prefix $(\mathbf{p}, r_{<i})$ to predict the next token r_i — as against only using the prefix \mathbf{p} to predict the answer tokens. Arguably, this happens because the cheat is much simpler to learn — as an induction head [126] — than the more complex solutions that rely only on \mathbf{p} (which involves search-and-backtracking or the simpler lookahead-and-reverse). Simpler predictive features are prioritized early in training [12, 155, 147], which starves gradient signals from more complex features [133].

The Indecipherable Token. Therefore, in the second stage towards failure, the model attempts to learn the first token r_i —the key decision-making token—purely based on information about the graph in the prefix \mathbf{p} , and without any gradient signal about the later tokens. This is however a computationally hard “needle-in-the-haystack problem” [181]: the model needs to find a complex end-to-end algorithm with ℓ subroutines in it, without any intermediate supervision for those subroutines. The first token thus becomes “indecipherable” and the model simply memorizes it on the training data; during test-time the model subsequently predicts the first token as a random neighbor, and then continues following down the path by applying the local follow-the-child rule it learned through the Clever Hans cheat.

Fig. 5 (also reproduced in Fig. 13) demonstrates these failure modes empirically, showing that next-token prediction achieves only chance-level performance on path-star graphs of varying sizes, with the first token remaining particularly difficult to learn in isolation.

Observation 4a. (Success of implicit in-weights reasoning) *On in-weights path-star graphs of as many as 5×10^4 nodes, trained on 75% of the total 10^4 paths, both the Transformer and Mamba are able to predict unseen paths when conditioned on held-out leaves with as much as 100% accuracy*

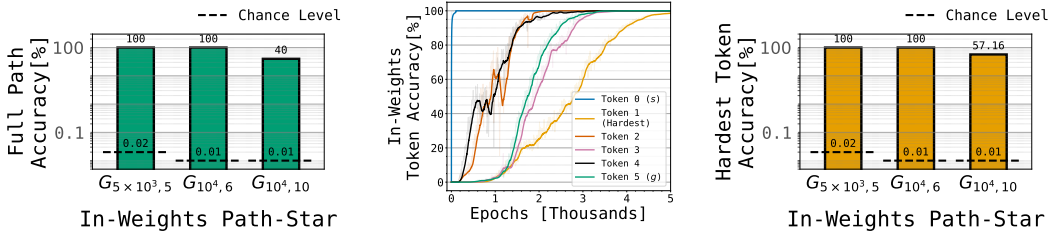


Figure 12: **Success of Transformer in in-weights path-star task.** (left) A next-token-trained Transformer achieves perfect or highly non-trivial accuracy on large path-star graphs $\mathcal{G}_{d,\ell}$ (Observation 4a). (middle) **Learning order of tokens.** The tokens of a path are not learned in the reverse order i.e., the model does not learn the right-to-left solution. Thus, gradients from the future tokens are not critical for success (Observation 4b). (right) **Success of hardest-token-only task.** In fact, the hardest token (the first) given the leaf is learned in isolation to non-trivial accuracy (Observation 1). Success of this ℓ -fold composition task is hard to explain within the associative memory view (§2.3). Analogous plots for Mamba are in Fig. 14. We invite the reader to contrast these in-weights task results with the in-context task ones in Fig. 13.

(see left plot of Fig. 4 for Transformer (also reproduced in Fig. 12), and left plot of Fig. 14 for Mamba) Similar positive results for some harder graph topologies are in §C.2.

Shortly, we will isolate an even stronger instance of implicit reasoning from this task for analysis. To get there, let us scrutinize where the argument of B&N’24 may go differently in the in-weights setting for the model to succeed in Observation 4a.

A.1.1 Where does the path-star-failure argument go wrong in the in-weights setting?

Recall that the path-star failure unfolds in two stages. Perhaps one of these stages does not play out in the in-weights setting. A first possibility could be that the Clever Hans cheat is not picked up here. The cheat was a simple, left-to-right pattern that fits all but the first token as the unique neighbor of the preceding ground-truth token that was present as input. Such left-to-right cheats are simpler than the true right-to-left solution, and thus quickly learned. However, perhaps when the target we train on is an *in-weights* path, the cheat is not easy to learn—say, due to the nature of recalling from parametric memory. A complex cheat may not be learned quickly, allowing gradients from future tokens to reach the first token representation, in turn allowing the correct, right-to-left solution to compete and emerge. Indeed, such gradients, termed as pre-caching gradients [183] have been identified in a line of empirical works in natural language [127, 77, 145, 183, 110]. We summarize this hypothesis out below:

Plausible Explanation 4a. (Model may experience future-token gradients) *The in-weights path-star task is solved (Observation 4a) because Clever Hans cheats are not learned quickly enough, allowing future-token gradients to persist, teaching the model to find the right-to-left solution.*

We can indirectly test for this hypothesis as follows. If the model learned the right-to-left dependencies, it must also learn the tokens in the reverse order: the unique predecessor of the goal node is the easiest to identify (under the right-to-left dependencies) and will thus be learned first; the next-easiest is the next predecessor and so on, until the first node (which depends on all that has been learned so far). Indeed, in the in-context setting of B&N’24 where they explicitly switch off the Clever Hans cheat (under teacherless training), such a reverse-learning cascade is observed (Fig. 5). However, we do not see this in the in-weights setting.

Observation 4b. (No reverse-learning cascade) *The target tokens in the in-weights path-star task are learned in no particular order by the Transformer and Mamba models (see middle plots of Figs. 4 and 14 in contrast with Fig. 5; or see Fig. 35 for side-by-side comparison).*

The above observation weakens Expl. 4a, encouraging us to search for another one. A second possibility is that the second stage of the failure of B&N’24 does not trouble us in the in-weights task. Recall that in this stage, the first token is to be learned in isolation without future-token gradients.

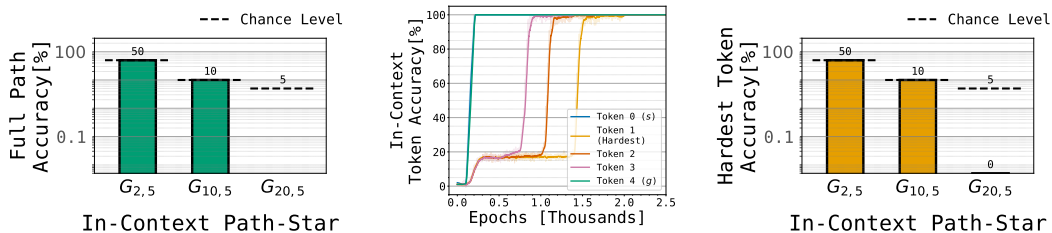


Figure 13: **Failure of Transformer in in-context path-star task. (B&N’24)** We report the failure of next-token Transformers in the in-context version of the path-star task, reproducing results from B&N’24. **(left)** Full path accuracy remains at chance level across different small graph sizes. **(middle)** Learning order of tokens with teacherless (multi-token-trained) objective shows a clear right-to-left learning cascade. **(right)** The hardest (first) token given the leaf fails to be learned in isolation, contrasting sharply with in-weights success shown in Fig. 12.

But this is an ℓ -fold composition task that is theoretically well-understood to be computationally hard (as we elaborate later). Perhaps, that is not the case for our in-weights task:

Plausible Explanation 4b. (First-token may be easy to learn) *Learning the key decision-making token (the first token) in the in-weights path-star task is not computationally hard.*

Testing Expl. 4b is easy: we train the model simply on the first token loss, instead of the loss over the full path sequence. We find that this task is trivial here, affirming Expl. 4b, and isolating a much stronger and cleaner instance of implicit in-weights reasoning.

B Experimental setup

B.1 Graphs, tokens, and data construction

Path-star graphs. We denote by $\mathcal{G}_{d,\ell}$ a path-star graph with central node v_{root} , degree d (number of arms), and path length ℓ per arm. The i -th arm consists of the node sequence $(v_{\text{root}} = v_0^{(i)}, v_1^{(i)}, \dots, v_{\ell-1}^{(i)})$ where the last node in the sequence is $v_{\ell-1}^{(i)} = v_{\text{leaf}}^{(i)}$.

Vocabulary. Each node is represented by a unique numerical token. We reserve several special tokens: [PAUSE] (a compute/pause token), [PAD] (a padding token), optional directional tokens ($>$, $<$), and task-specific prefix tokens ([EDGE], [PATH]). The effective vocabulary size is $|\mathbb{V}| = |\text{nodes}| + 9$.

Edge-memorization datasets for local supervision. We form directed bigrams (u, v) when v is a child of u to define a distribution $\mathcal{D}_{\text{edge}}^{\rightarrow}$. Conversely, we use examples of the form (v, u) where u is the parent of v to define $\mathcal{D}_{\text{edge}}^{\leftarrow}$; and $\mathcal{D}_{\text{edge}}$ is their union. Training sequences of edge bigrams are simple two-token sequences “ uv ” sampled uniformly. All these examples, be it forward or backward, provide only local supervision.

Path-finding datasets. We define a path distribution $\mathcal{D}_{\text{path}}^{\rightarrow}$, where an example is the pair (\mathbf{p}, \mathbf{r})

with $\mathbf{p} = (v_{\text{leaf}}^{(i)}, \overbrace{[\text{PAUSE}], \dots, [\text{PAUSE}]}^{P \text{ tokens}})$ and $\mathbf{r} = (v_{\text{root}}, v_1^{(i)}, \dots, v_{\ell-1}^{(i)})$. The leaf node is sampled uniformly. We finetune on a subset of leaves and *evaluate on held-out leaves*. Unless stated otherwise, decoding is greedy (top-1). The arrow in $\mathcal{D}_{\text{path}}^{\rightarrow}$ denotes that this is the *forward* path; we also experiment with predicting the reverse goal-to-start path, denoted by the distribution $\mathcal{D}_{\text{path}}^{\leftarrow}$.

In-context datasets. Adapted from Bachmann and Nagarajan [13], the prefix contains a randomized adjacency serialization and $(v_{\text{root}}, v_{\text{goal}})$; the target is the full path. Where NTP fails in-context, we use the teacherless objective of Bachmann and Nagarajan [13] for comparison plots (details in §B.3).

B.2 Model architecture

B.2.1 In-weights path-star task experiments

Backbone. The main experiments appearing in §2 use a decoder-only Transformer (GPT-mid) with a causal mask, pre-norm LayerNorm, sinusoidal positional embeddings [172], GELU MLPs, and tied input/output token embeddings. Additionally, experiments in §C.1 employ a Mamba sequence model [60] of comparable scale.

Default Transformer configuration.

- Layers $N_{\text{layer}} = 12$, model width $m_{\text{width}} = 384$, heads $m_{\text{head}} = 8$.
- Dropout 0 on attention and MLP blocks (synthetic setting), label smoothing 0.
- Context length set to accommodate the longest training sequence (edges: 2; paths: $\ell + 1 + N_{\text{pause}}$) with margin.

Mamba configuration. The Mamba models in §C.1 use an equivalent depth and hidden dimension to the Transformer baseline. The sequence model parameters include the state dimension $d_{\text{state}} = 16$, convolution kernel size $d_{\text{conv}} = 4$, and expansion factor $\text{expand} = 2$, which follow the standard values from the original Mamba implementation.

Embedding layer. Token embeddings are stored in $\mathbf{V} \in \mathbb{R}^{|\mathbb{V}| \times m_{\text{width}}}$, with output projection weights tied to \mathbf{V} .

Variants. For larger graphs $\mathcal{G}_{10^4, 10}$, we scaled m_{width} proportionally to 784 in our hyperparameter grid search. For the Mamba architecture, we also varied the expansion factor to 4 and the state dimension to 32.

B.2.2 Tiny model architectures

For toy experiments on small-scale graphs (§C.3, §D.1.2), including the *Tiny Path-Star*, *Tiny Grid*, *Tiny Cycle*, and *Tiny Irregular* graphs, we used reduced-size architectures.

Models. We evaluated three model types: (1) a Transformer (TinyGPT), (2) a feed-forward neural network with the same configuration but without residual connection or attention and (TinyNN) (3) a Mamba model (TinySSM) of comparable scale to (1). Exact configurations are described below.

Configuration.

- For all graphs, all models used a single layer ($N_{\text{layer}} = 1$), but the model specifications differed across graph types.

For TinyGPT and TinySSM in particular:

- For *Tiny Path–Star* and *Tiny Grid*, TinyGPT used embedding dimension $m_{\text{width}} = 32$ with $m_{\text{head}} = 8$, and TinySSM used embedding dimension 8 with $d_{\text{state}} = 2$, $d_{\text{conv}} = 2$, and $\text{expand} = 1$.
- For *Tiny Cycle*, TinyGPT used embedding dimension 16 with 8 heads, while TinySSM matched the same specifications as above (8-dim, $d_{\text{state}} = 2$, $d_{\text{conv}} = 2$, $\text{expand} = 1$).
- For *Tiny Irregular*, TinyGPT again used embedding dimension 16 with 8 heads, and TinySSM used embedding dimension 8 with $d_{\text{state}} = 2$, $d_{\text{conv}} = 4$, and $\text{expand} = 1$.

For TinyNN, we used a large embedding dimension 512 with 1 head for the sake of empirical proofs of Section 3. We elaborate why. First, TinyNN architectures are a clean architecture where one can be certain that freezing the (un)embedding layers results in a purely associative storage; thus they are appropriate for our empirical proofs. Next, in our proofs, we wanted to make two demonstrations. First, that the model memorize geometrically even without bottleneck pressures (as is the case with a large embedding dimension); second, that in sufficiently wide-neck settings, the associative storage is realized within just 2 learning steps (which we find is true here).

We clarify that even when reducing the embedding dimension of TinyNN to match that of TinyGPT (*Tiny Path–Star* and *Tiny Grid*: $m_{\text{width}} = 32$; *Tiny Cycle* and *Tiny Irregular*: $m_{\text{width}} = 16$), we found that the geometric structure still persisted and that the associative memory variant continued to fully memorize the edge bigrams, albeit with longer optimization steps.

Associative memory variants of these architectures. In associative-memory settings (e.g., left-column visualizations in Figure 1), token embeddings were frozen in all these architectures. All models employed weight tying between input and output embeddings. Note that since we employ only one trainable layer in these settings (the embedding/unembedding layers frozen), we can be certain, at least in the case of TinyNN that storage is associative.

B.3 Training and optimization

Objective. We use next-token cross-entropy over the causal prefix. For first-token-only experiments, the loss is restricted to the first target position. Although we train all our models to 50,000 epochs, we *only need about a couple of thousand epochs* to see accuracy gains (e.g., see the per-token accuracy plots in Fig. 4).

Optimizer and schedule. We use the AdamW optimizer with a weight decay of 0.01. The learning rate follows a cosine decay schedule with a linear warm-up. In the two-phased edge-memorization ablation experiment of §D.3, the peak learning rate for edge memorization (Phase 1) is 1×10^{-2} and for path finetuning (Phase 2) is 5×10^{-5} .

Batching. We used a range of different batch sizes of {64, 128, 256, 512, 1024}.

PAUSE tokens. We append $N_{\text{pause}} \in \{0, 2, 4, 6, 10\}$ pauses in $\mathcal{D}_{\text{path}}^{\rightarrow}$ to provide compute budget (no labels on pause positions). The chosen N_{pause} for each $\mathcal{G}_{d,\ell}$ is given in Table 2.

B.4 Evaluation protocols and metrics

Forward vs. reverse. We evaluate forward generation ($v_{\text{root}} \rightarrow v_{\text{leaf}}$) and reverse generation ($v_{\text{leaf}} \rightarrow v_{\text{root}}$). Reverse is algorithmically trivial after edge memorization; forward is the non-trivial case we care about.

Table 2: Default hyperparameters by graph size. Values denote the settings used.

Graph $\mathcal{G}_{d,\ell}$	N_{layer}	m_{width}	m_{head}	N_{pause}	Peak LR
$\mathcal{G}_{5 \times 10^3, 5}$ (In-Weights)	12	384	8	5	5×10^{-5}
$\mathcal{G}_{10^4, 6}$ (In-Weights)	12	384	8	6	5×10^{-5}
$\mathcal{G}_{10^4, 10}$ (In-Weights)	12	784	8	10	5×10^{-5}
$\mathcal{G}_{2, 5}$ (In-Context)	12	384	8	n/a	1×10^{-4}
$\mathcal{G}_{10, 5}$ (In-Context)	12	384	8	n/a	1×10^{-4}
$\mathcal{G}_{20, 5}$ (In-Context)	12	784	8	n/a	1×10^{-4}

Metrics.

- *Exact-match path accuracy / Full path accuracy*: fraction of held-out leaves whose entire path is generated correctly.
- *First-token accuracy / Hardest token accuracy*: accuracy of the first hop (hardest token) given the leaf.
- *Per-token accuracy over epochs / Token accuracy*: accuracy at each target position, tracked through training (used in Fig. 35).

Baselines. Random choice among d branches gives $1/d$ first-token accuracy and near-zero exact-match.

B.5 Implementation and compute

Code is implemented in PyTorch with standard Transformer components. All runs fit on a single modern GPU (e.g., A100-40GB or A100-80GB for the largest batch-size); per-figure training time depends on (d, ℓ) and batch size.

C Experiments on broader settings

In this section, we demonstrate that our findings generalize to various other deep sequence architectures and various other large and smaller graphs.

C.1 Path-star task on Mamba SSM

This section demonstrates that the implicit reasoning on path-star graphs observed for Transformers in §2.1, generalizes to the Mamba SSM architecture [60] too. Fig. 14 is the counterpart of the Transformer accuracy plots in Fig. 4; Fig. 15 is the counterpart to Transformer heatmaps in Fig. 25; Fig. 16 is the counterpart to the UMAP topology of Transformers in Fig. 27. A notable difference here is that the Mamba model presents a strong geometry even when trained only on the edges (as seen in Fig. 15c).

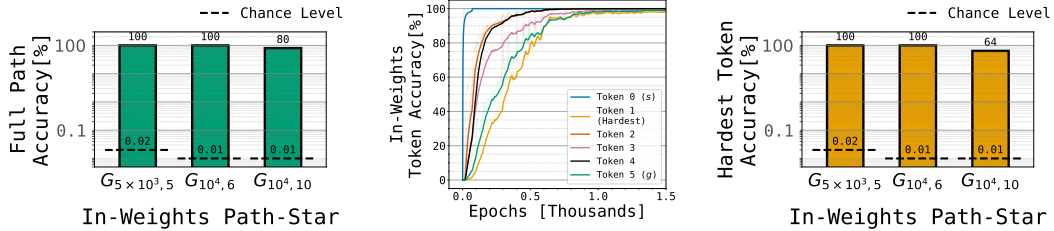


Figure 14: **(left) Success of in-weights path-star task for Mamba.** This figure is a counterpart to Fig. 4. A next-token-trained Mamba achieves perfect or highly non-trivial accuracy on large path-star graphs $\mathcal{G}_{d,\ell}$ (Observation 4a). **(middle) Learning order of tokens.** The tokens of a path are not learned in the reverse order i.e., the model does not learn the right-to-left solution. Thus, gradients from the future tokens are not critical for success (Observation 4b). **(right) Success of hardest-token-only task.** In fact, the hardest token (the first token) given the leaf is learned in isolation to non-trivial accuracy (Observation 1). Success of this ℓ -fold composition task is hard to explain within the associative memory (§2.3).

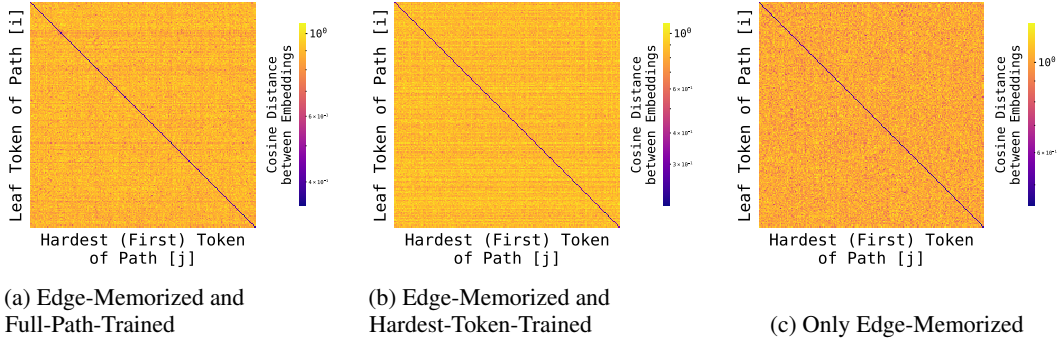


Figure 15: **Evidence of global geometry in path-star task for Mamba.** This figure is a counterpart to Figs. 6 and 25 for the Mamba SSM architecture. Recall that entry (i, j) is the mean cosine distance between the leaf token in (an unseen) path i (row) and first/hardest token on (an unseen) path j (col). Each heatmap corresponds to a different training objective: Left: trained on edges and path-finding task ($\mathcal{D}_{\text{edge}} \cup \mathcal{D}_{\text{path}}^{\rightarrow}$); Middle: trained on edges and hardest-token-finding task (not presented in the main paper); Right: edges only ($\mathcal{D}_{\text{edge}}$). We find that even on these unseen paths, the leaf and first token embeddings cluster together, regardless of whether path-finding supervision exists. Interestingly, compared to the Transformer in Fig. 25, the Mamba trained only on local supervision (right) exhibits a much stronger geometry.

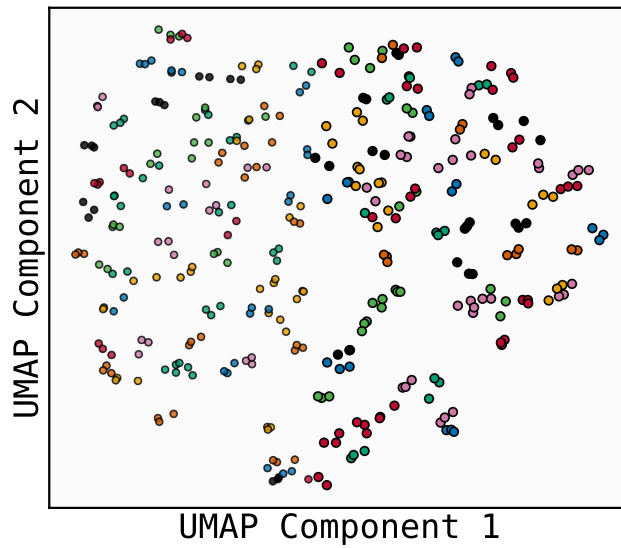


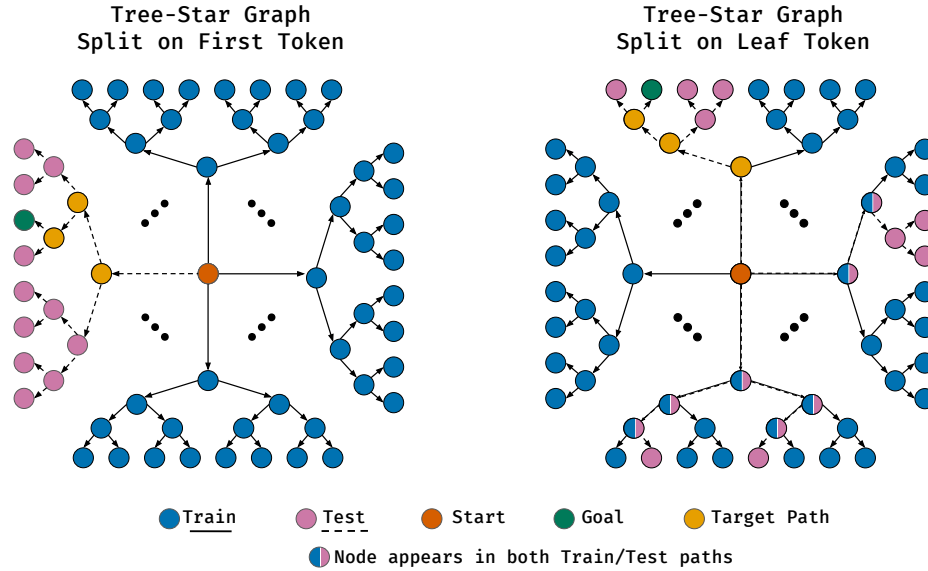
Figure 16: UMAP **projection of token embeddings of Mamba exhibits path-star topology**. We corroborate the UMAP [109] observations from the Transformer (Fig. 27) in Mamba SSM here. Each point is a node embedding; color indicates path identity. Different paths form separated clusters (although this clustering is weaker than for a Transformer); the central node v_{root} is excluded since it is shared across all paths. The graph has degree 10^4 and path length 6 (including the root). Axes are UMAP components (arbitrary units). Note that we have re-used each color for multiple paths.

C.2 Other large, harder path-finding graphs

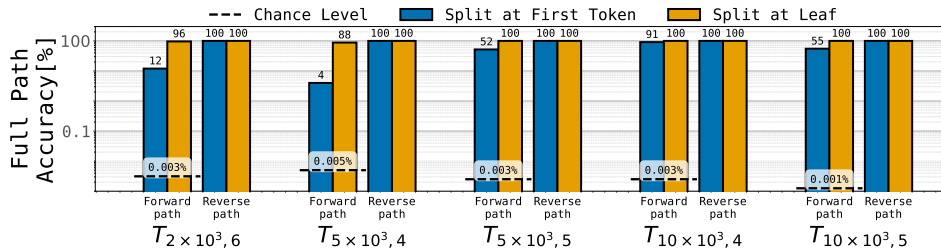
Next, we consider variants of the path-finding graph. While the path-star graph is adversarially constructed in certain ways, there is only one decision-making step, which makes planning simpler in a certain way. To make the task harder, we introduce a branching at every node along each path. (Similar tree variants have been considered in [47] for the in-context task, but we are interested in in-weights tasks.)

In the *tree-star* graph, $\mathcal{T}_{d,\ell}$, there is a central node with degree d and each child node except the leaf has a fixed degree of 2, as visualized in Fig. 17a. The path-length from the root to any leaf is ℓ . In this graph, two types of learning tasks can be considered, depending on how we split the test and training paths. For a no-overlap setting, we could sample all training paths from one subset of trees, and the test paths from the remaining trees; we call this the *split at first token* setting, since the test/train split is determined by the first token. A second setting—with some test-train overlap—is one where we reserve some leaves as training goals, and the rest as test-goals. Here, on any test path, a prefix may have participated in a training path. We call this the *split at leaf* setting. Note that in both variants, all nodes will be sampled as part of the edge-memorization task.

In Fig. 17b, we find that on both variants the Transformer achieves non-trivial path-finding accuracy, generalizing our results beyond the path-star task. However, we note that the test-train split at the first token is much harder to succeed at, likely due to no overlaps.



(a) In-Weights Tree-Star



(b) Task Success

Figure 17: **Transformer achieves non-trivial accuracy on the harder in-weights tree-star task.** The tree-star task of §C.2 introduces decision-making at every step of the path, not just the first token. There are two variants of this task based on the test-train split. In the *split on first token* variant (**top-left**), we reserve some of the trees for generating training paths, and the rest for test paths. In the *split on leaf token* variant (**top-right**), we reserve some leaves for training and the rest for testing; some nodes may be sampled for path-finding during both test and train time. In both tasks, we have visualized a single target path. In the **bottom** figure, we report non-trivial path-finding accuracies on both tasks, above random chance defined as $1/\text{num_leaves}$.

C.3 Tiny graphs

Besides the large path-star graph (of §2) and tree-star graphs (of C.2), we also report the embeddings learned on four tinier graphs for various architectures (details in B.2.2); the figures here are an extension of the Transformer embeddings in Fig. 1. In these experiments, we train the models purely on local supervision (the edges, presented in both directions) to 100% edge-memorization accuracy: for each vertex, we ensure that its d neighbors appear in the top d softmax probabilities. The graphs include (a) a tiny path-star graph with four paths of length 4, (b) a 4×4 grid graph, (c) a 15-node cycle graph and (d) an irregular graph with two asymmetric components. Each visualization includes the embeddings from: an associative memory model (implemented with a neural network with only one trainable matrix sandwiched between (un)embedding layers), a Node2Vec model, the eigenvectors of the graph Laplacian, a Transformer’s token embeddings, a neural network’s first layer, and a Mamba SSM’s token embeddings. For the Node2Vec model we use the top eigenvectors, and for the rest we use UMAP [109] to choose the top directions.

We note that these visualizations by themselves do *not* guarantee the presence of global information (a model that embeds each node as its adjacency row can still show similar geometries). As a rigorous test, we provide node-node cosine-similarity heatmaps to examine whether it exhibits multi-hop information. These are in Figs. 23 and 24.

We consolidate the various observations from these figures (Figs. 18 to 24) and our memorization vs. time plots in Fig. 7 here:

Observation 5. *In the tiny graphs of Figs. 18 to 21, on various architectures (Node2Vec, graph spectrum, Transformer, neural network, Mamba SSM), we find that:*

1. *A geometry arises in all these architectures even without global supervision from a path-finding task (Refutation 3a).*
2. *The global information in these geometries can be traced back to the eigenvectors of the graph spectrum (§4).*
3. *The geometry arises in all three deep sequence models (Transformer, Mamba SSM, neural network) even though these models can learn the data associatively using the same learning setup, with just the (un)embedding matrices frozen (Refutation 3b).*
4. *The geometry of the Node2Vec model (which precludes associative memory), is much stronger than the deep sequence models, suggesting that the deep sequence models may be adulterated with associative memory (Conjecture 1).*
5. *Associative storage can be quickly found by gradient descent (Fig. 7), as claimed in Refutation 3c, whereas geometric memorization takes longer to discover (Fig. 22)*
6. *We note that similar geometries arise even with only one direction presented; see §D.1.2. This is the scenario where both types of storage have the same bit and ℓ_2 norm complexity; thus, there are no straightforward implicit pressures that encourage the geometry (Refutation 3d).*

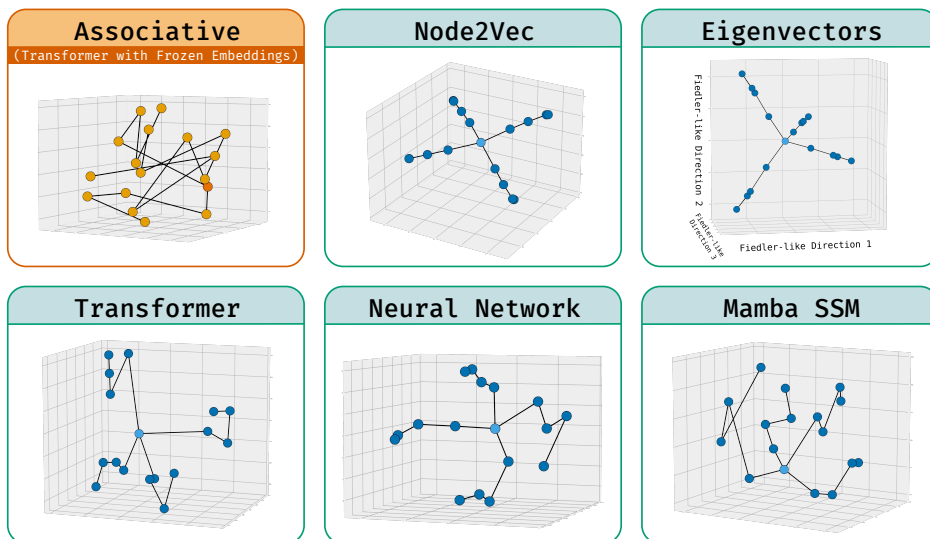


Figure 18: **Tiny path-star**: Geometries of various architectures on a smaller version of the path-star graph. See Observation 5.

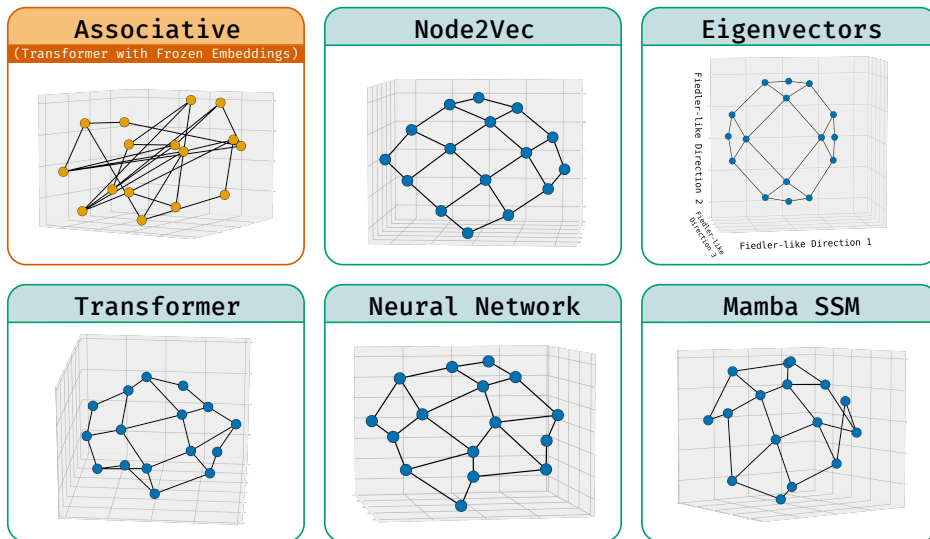


Figure 19: **Tiny grid**: Geometries of various architectures on a small 4×4 grid graph. See Observation 5.

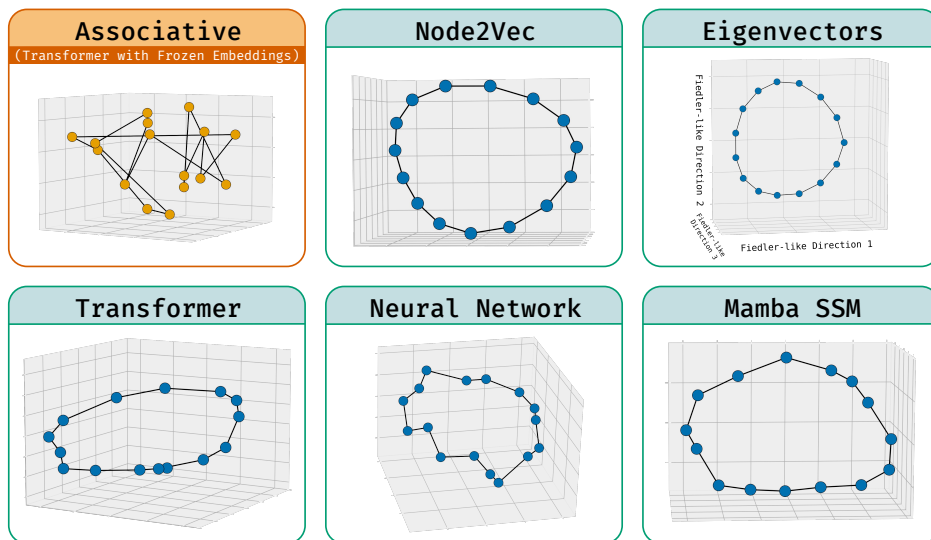


Figure 20: **Tiny cycle**: Geometries of various architectures on a small cycle graph. See Observation 5.

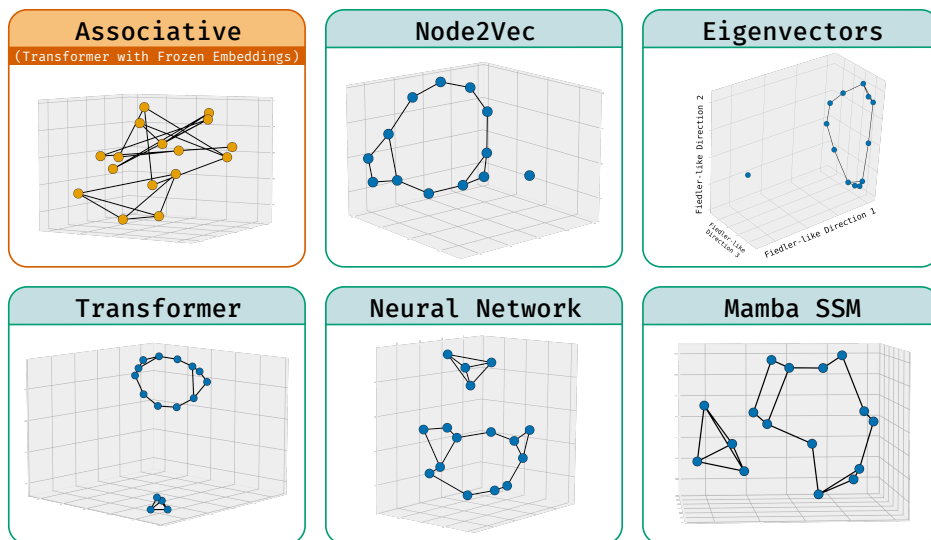


Figure 21: **Tiny irregular graph**: Geometries of various architectures on a small irregular graph of two connected components, both asymmetric. See Observation 5. Note that unlike in the other graphs, we do not use a 1-layer model here, but a 3-layered one.

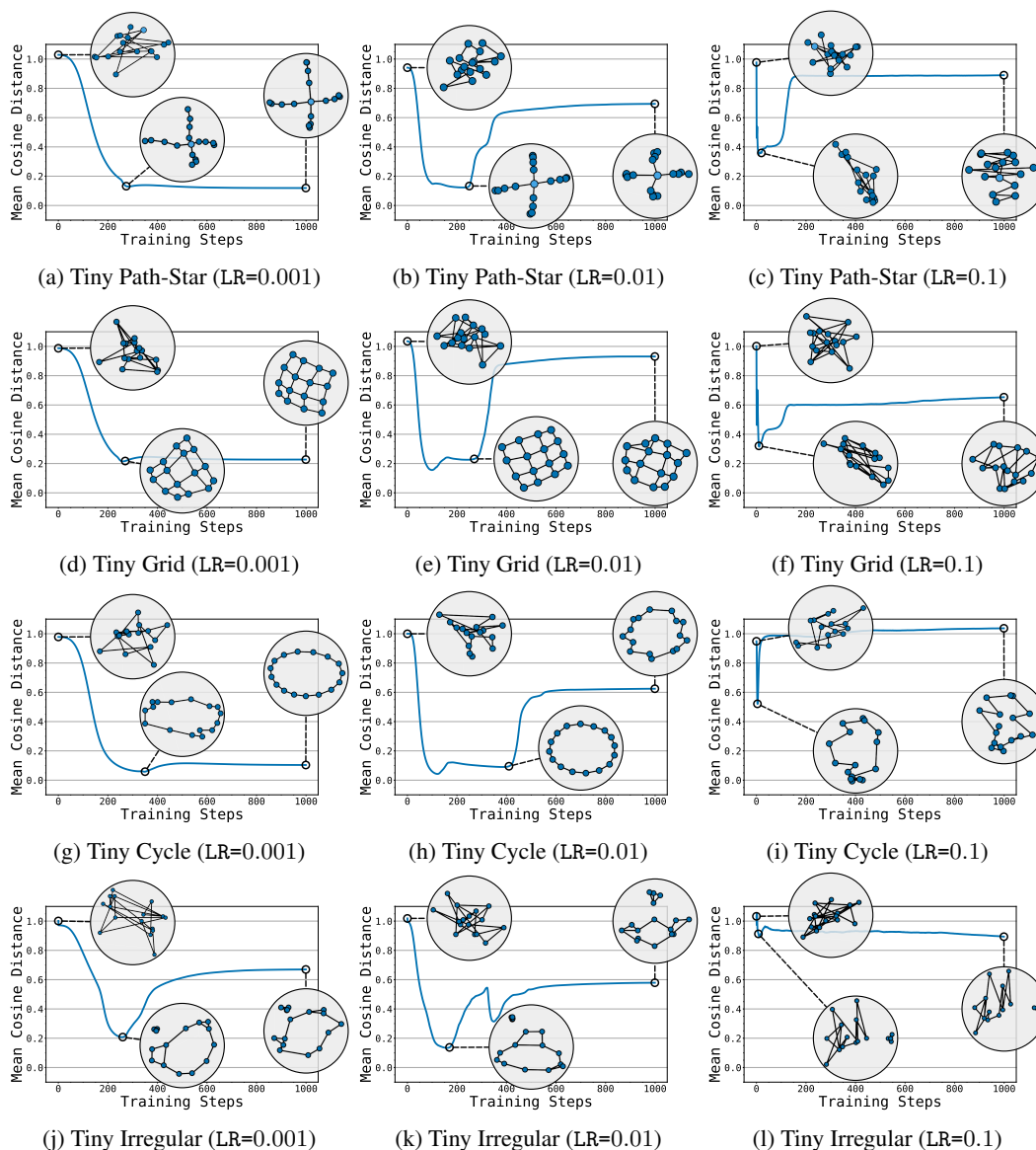


Figure 22: For various learning rates, geometric memorization takes much longer for gradient descent to discover: This is an extended version of Fig. 8 for two more learning rates. Recall that for the same TinyNN architecture as in Fig. 7 but without frozen embeddings, we roughly quantify geometric memorization over time via cosine distance across *all* pairs of vertices, alongside 2D visualizations. Each row is a different graph, and each column is a different learning rate. For both the learning rate 0.001 and 0.01, the geometries take about 200 steps to appear; the larger learning rate of 0.1 is too aggressive to create the geometry. Recall that, for associative memory, two steps with learning rate of 0.1 sufficed (Fig. 7). This is evidence for Refutation 3c: ease of discovery does not determine what sort of memory is preferred.

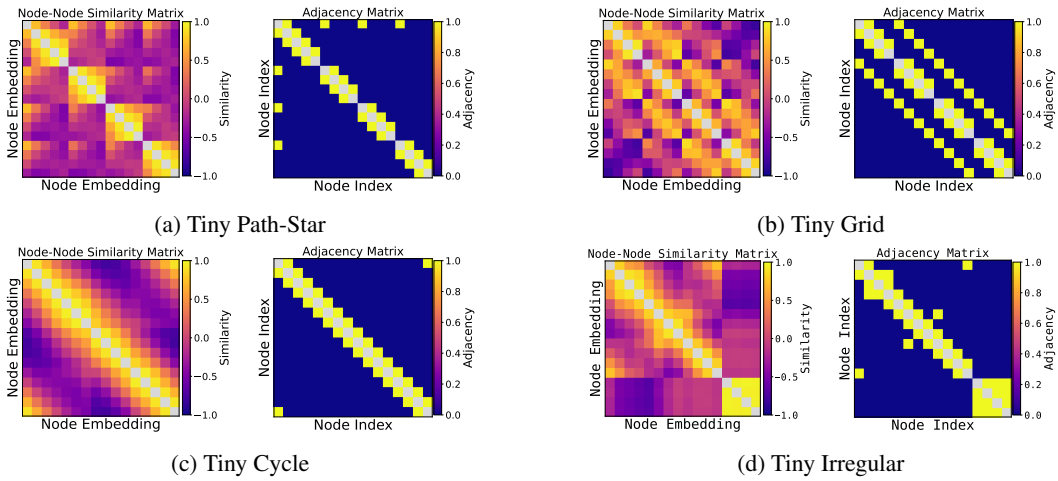


Figure 23: **Node-node cosine similarity vs. adjacency matrix for the Transformer**: For each graph, we plot the cosine similarity between all node embeddings and compare it against the adjacency matrix. Observe that the cosine similarities exhibit a richer structure than the adjacency matrix, reflecting some notion of multi-hop distance e.g., in the cycle graph, there is a gradual decrease in similarity as we walk towards the diametrically opposite node in any given row.

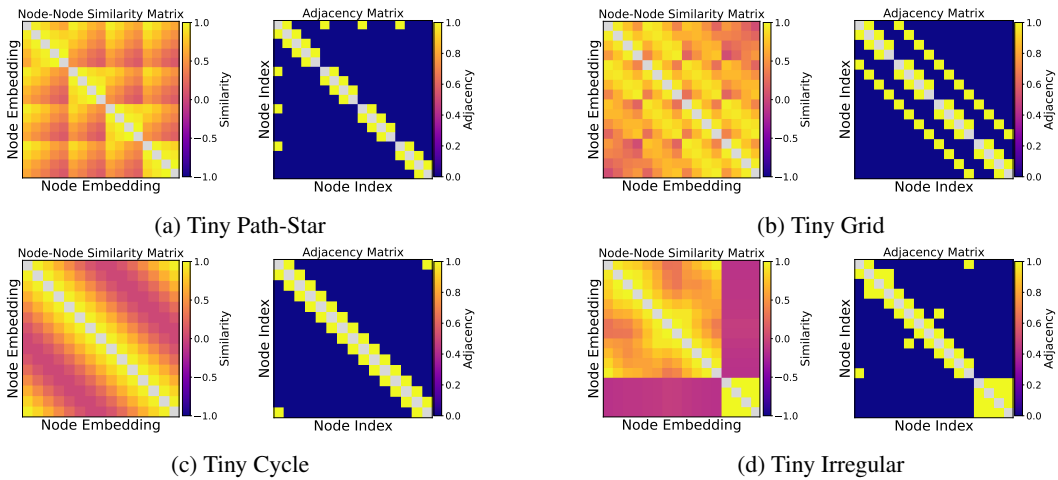


Figure 24: **Node-node cosine similarity vs. adjacency matrix for the Node2Vec model**: Like in the Transformer (Fig. 23), we again observe that cosine similarities exhibit a rich, multi-hop structure absent in the adjacency matrix.

C.4 Additional experiments on path-star geometry

In the main paper, we present heatmaps showcasing the distance between the leaf nodes and the first node in every path. We consolidate these below and also provide an additional path-to-path distance heatmap.

Leaf–first-hop distance (Fig. 25). In Fig. 25 (an extended version of the heatmaps in Fig. 6), entry (i, j) is the cosine distance between the *leaf* embedding of path i and the *first-hop* (*indecipherable token*) embedding of path j . Diagonal entries are low (a leaf lies close to its correct first hop), while off-diagonals are higher. This structure explains why the first-token-only objective succeeds in-weights (Fig. 4-(Right)): the k -fold composition map reduces to a local geometric step in the learned representation.

Path–by–path distance (Fig. 26). Instead of only analyzing the distance between the leaf and first nodes, we analyze the distance across all pairs of nodes in a path. For each pair of paths (i, j) , we compute the mean distance between *all* node embeddings on path i and all node embeddings on path j .

- **Diagonal — Intra-Path Distance ($i = j$):** This value is the average distance between all unique pairs of distinct nodes within a single path. It measures how tightly clustered the path’s nodes are. A smaller value indicates higher cohesion.

$$D_{i,i} = \frac{1}{\binom{\ell}{2}} \sum_{1 \leq k < m < \ell} d(v_k^{(i)}, v_m^{(i)})$$

- **Off-diagonal — Inter-Path Distance ($i \neq j$):** This value is the average distance between all nodes of one path and all nodes of another. It measures how separated two distinct paths are. A larger value indicates greater separation.

$$D_{i,j} = \frac{1}{\ell^2} \sum_{k=1}^{\ell-1} \sum_{m=1}^{\ell-1} d(v_k^{(i)}, v_m^{(j)})$$

We find a similar clustering of nodes within paths here, although the diagonal is generally less vivid. For the model trained only on edge-memorization, we do not see the diagonal at all.

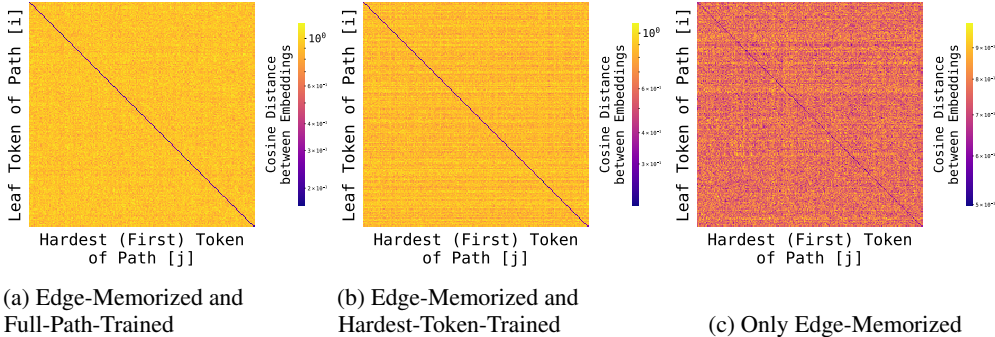


Figure 25: Evidence of global geometry in path-star task: Leaf-first-token cosine distance between node embeddings. We present again the heatmaps from Fig. 6 with an additional heatmap in the middle. Entry (i, j) is the mean cosine distance between the leaf token in (an unseen) path i (row) and first/hardest token on (an unseen) path j (col). Each heatmap corresponds to a different training objective: Left: trained on edges and path-finding task ($\mathcal{D}_{\text{edge}} \cup \mathcal{D}_{\text{path}}^{\rightarrow}$); Middle: trained on edges and hardest-token-finding task (not presented in the main paper); Right: edges only ($\mathcal{D}_{\text{edge}}$). We find that even on these unseen paths, the leaf and first token embeddings cluster together, regardless of whether path-finding supervision exists; however, the geometry is strongest with global supervision (however, in Mamba SSM, even the locally supervised model shows strong geometry; see Fig. 15).

UMAP projection (Fig. 27, zoomed in version of Fig. 6, middle). A different way to establish geometry is to directly visualize the paths. As done in Fig. 6, we do this by projecting the token

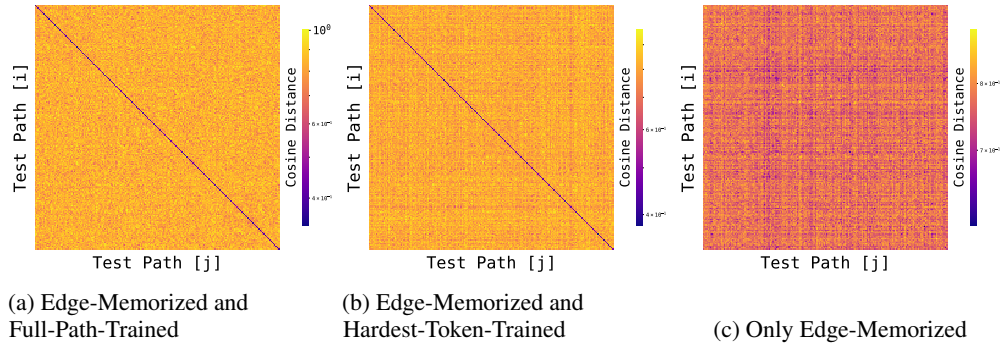


Figure 26: **Evidence of global geometry in path-star task: Pathwise average *cosine* distance between node embeddings.** While in Fig. 25, we reported the cosine distance between the embeddings of the *terminal* nodes of a pair of (unseen) paths, here we consider an average over all nodes in those (unseen) paths. In particular, entry (i, j) is the mean *cosine* distance between nodes on path i (row) and nodes on path j (col). On the first two settings, as before, we find that the diagonal cells are low, implying closer embeddings. Thus, a geometry has emerged on unseen paths. However, unlike in Fig. 6, we do not see any such signal when trained only on the edge memorization task.

embeddings of all nodes with default UMAP settings (`neighbors=15`, `min_dist=0.1`). A zoomed in version of this is presented in Fig. 27. We exclude the root token embedding in these projections since that is common to all paths. We find that different paths form well-separated clusters, and within each path cluster, nodes tend to arrange from leaf toward v_{root} .

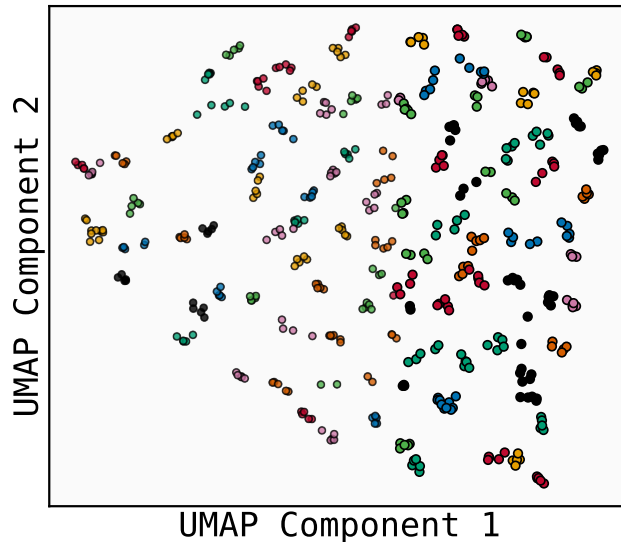


Figure 27: Zoomed in version of Fig. 6: UMAP **projection of token embeddings exhibits path-star topology.** Each point is a node embedding; color indicates path identity. Different paths form separated clusters; the central node v_{root} is excluded since it is shared across all paths. The graph has degree 10^4 and path length 6 (which includes the root). Axes are UMAP components (arbitrary units). Note that we have re-used the same color for multiple paths.

D Edge supervision and training dynamics

There are tangential aspects of our training that are worth elaborating on: the roles of reverse edges (§D.1), of pause tokens (§D.2), of interleaving edge-memorization (§D.3), of weight-tying (§D.4), and of the learning order of tokens (§D.5).

D.1 The role of reverse edges

Reverse edges seem to play a nuanced role in our observations. On the large path-star task in §2, we find it necessary to augment training on the reverse edges; on the other hand, for the tiny graphs, a geometry arises even without these reverse edges. Perhaps, reverse edges are needed for larger tasks; or perhaps, they are necessary to perform implicit reasoning and retrieval. We leave it for future work to gain greater clarity on this effect, which is tied to the reversal curse [18, 9].

D.1.1 The critical role of reverse edges in the large path-star task

Edge supervision regimes. We evaluate three edge supervision regimes for the fixed in-weights graph: (i) *forward-only* edges $\mathcal{D}_{\text{edge}}^{\rightarrow}$, (ii) *backward-only* edges $\mathcal{D}_{\text{edge}}^{\leftarrow}$, and (iii) their mixture $\mathcal{D}_{\text{edge}} = \mathcal{D}_{\text{edge}}^{\rightarrow} \cup \mathcal{D}_{\text{edge}}^{\leftarrow}$, each combined with path supervision.

We consider two types of path-finding tasks. The first, as discussed in Section 2.1, is a *forward generation* ($v_{\text{root}} \rightarrow v_{\text{leaf}}$) task defined by $\mathcal{D}_{\text{path}}^{\rightarrow}$. Another task is *reverse generation* ($v_{\text{leaf}} \rightarrow v_{\text{root}}$), denoted by $\mathcal{D}_{\text{path}}^{\leftarrow}$. Forward path generation is non-trivial to learn as it involves planning or look-ahead, and is adversarial towards next-token learning; the reverse path however is trivial to learn on path-star graphs because each node has a unique predecessor along the target path. We must also clarify that the presence of reverse edges in itself *does not trivialize* the forward path-finding task—these edges provide only local information; thus, the success of the global path-finding task is still *non-trivial*.

We enumerate our observations from these various edge-supervision regimes below:

Observation 6. (Role of reverse edges) We find in Fig. 28 that:

1. A Transformer trained on only the forward edges, struggles on both forward and reverse path-finding tasks (see the middle color in Fig. 28).
2. A Transformer trained on only the reverse edges, achieves non-trivial accuracy on the reverse path-finding task; however, it fails on the forward path-finding task (see the third color in Fig. 28).

We suspect that the lack of reverse edges either hurts the geometry *or* hurts the retrieval ability of the model. On the other hand, the success of the reverse path-finding task with reverse-only edge memorization could be explained by the fact that the task requires no planning, as discussed in the remark below.

Remark 4. We note that the asymmetry between forward and reversed path-generation tasks stems from their algorithmic complexity. The reversed path generation is algorithmically trivial on path-star graphs because each node has a unique predecessor along any target path—the model simply needs to follow the unique backward edges. Forward generation, however, requires planning (examine each outgoing path) or lookahead (track the reverse path without explicit chain-of-thought and reverse it). Indeed, for the in-context task of B&N’24, the model fails on the forward task, but strikingly succeeds on the reverse task, as corroborated in Fig. 29 (right). Even in the in-weights setting Fig. 29 (left), the reverse path is generally quicker to learn and yields higher accuracy.

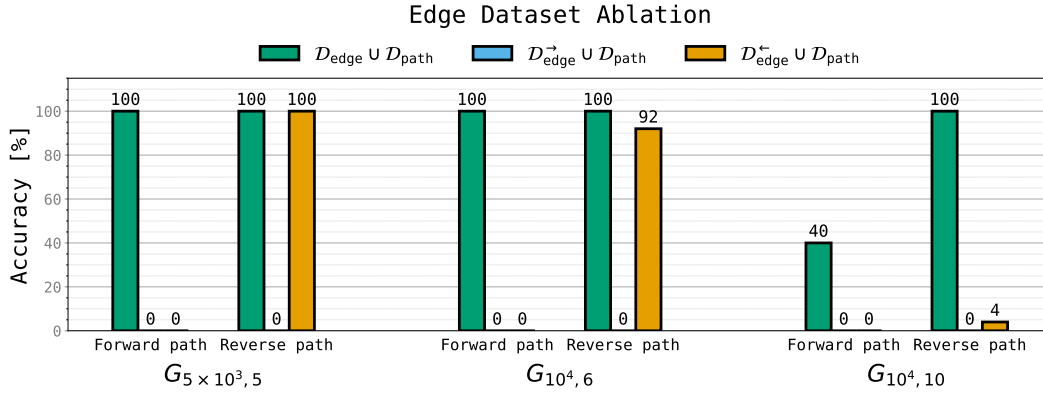


Figure 28: **Mixed edge supervision enables forward path generation while forward-only fails due to reversal curse.** Exact-match accuracy on held-out leaves for multiple path-star graphs (varying degree d and path length ℓ). As established, training on *mixed* edges D_{edge} yields high non-trivial *forward* accuracy across graphs. But training on *forward-only* D_{edge}^{\rightarrow} fails on both the forward and reverse tasks. This is indicative of the reversal curse. With *backward-only* edges (D_{edge}^{\leftarrow}) the model attains high accuracy primarily on *reverse* path generation for smaller graphs. This can be reconciled by noting that generating the reverse path is an easier retrieval task. Random forward path accuracy is $1/d$.

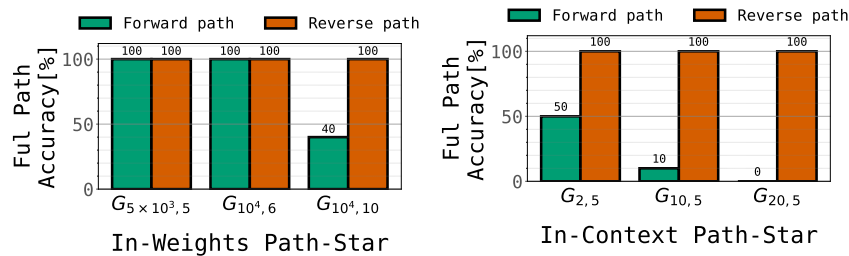


Figure 29: **Forward vs. reverse path generation:** The figure contrasts the model’s performance on forward (start→leaf) and reverse (leaf→start) path generation tasks for path-star graphs learned either **in-weights** (left) or **in-context** (right). While both methods achieve perfect accuracy on the algorithmically simple reverse path task, their performance on the forward task differs dramatically. **(left)** The in-weights model succeeds at the forward task, which requires planning and look-ahead, demonstrating high accuracy even on large graphs with thousands of nodes. **(right)** In contrast, the in-context model completely fails at forward path generation. This stark difference highlights the superior capability of in-weights learning to internalize and utilize complex graph structures.

D.1.2 Tiny graphs with uni-directional edge-memorization

In Fig. 30, we revisit our tiny graphs in §C.3, and examine the embeddings of a Transformer when it memorizes only one direction of the edges. We find that a geometry still arises, although a bit weaker.

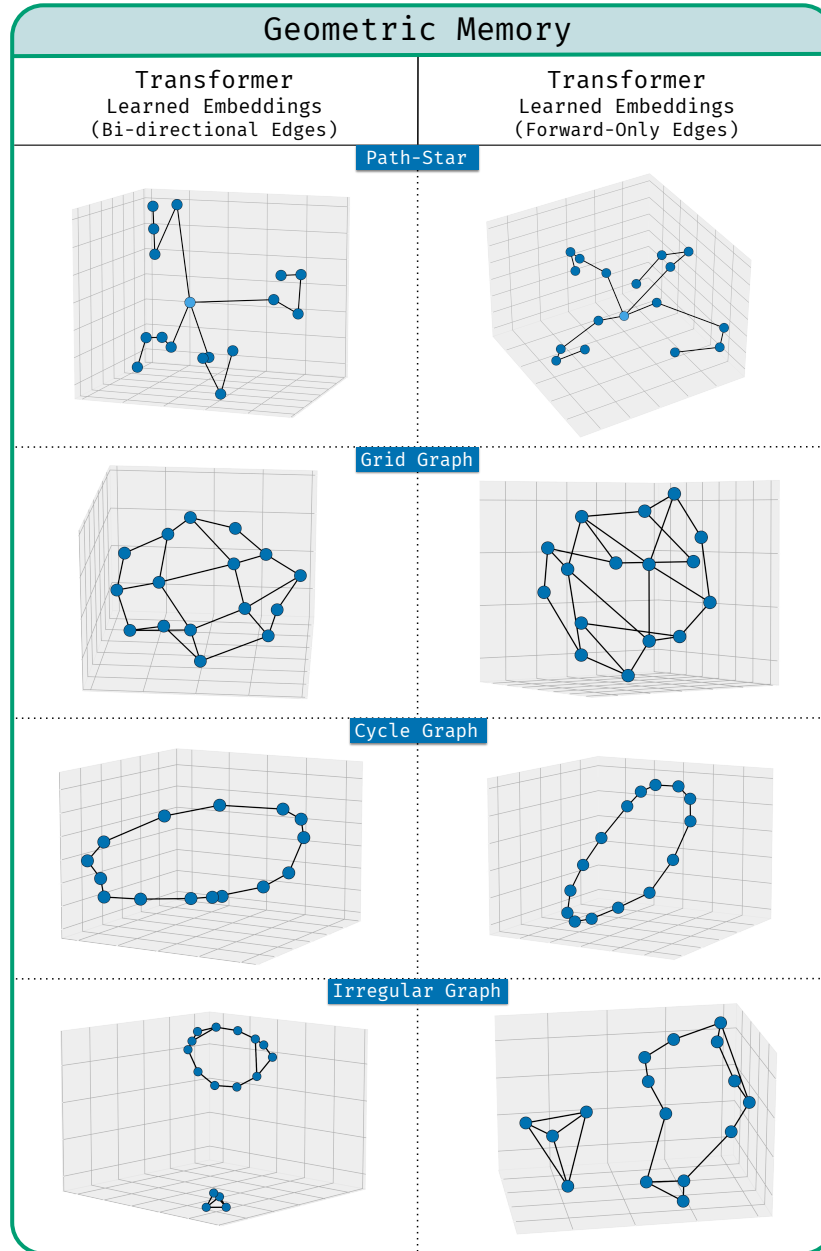


Figure 30: **Embeddings of a Transformer with bi-directional vs. uni-directional edge memorization.** With our smaller graphs, we find a geometry arise regardless of whether the model is made to memorize both or only one direction of each edge. However, the geometry is weaker (e.g., for the grid graph) under uni-directional memorization.

D.2 Pause tokens for computational slack

In the same in-weights path-finding task of §2, we find that it is helpful to insert pause tokens [25, 57] to achieve quicker accuracy gains during training. Pause tokens are added by appending dummy tokens to the prefix of the path-finding task both during training and inference.

Fig. 31 shows that adding a short sequence of pause tokens after the prompt reliably boosts exact-match accuracy across graphs, for a given amount of training time. Increasing the number of pause tokens increases speed of convergence.

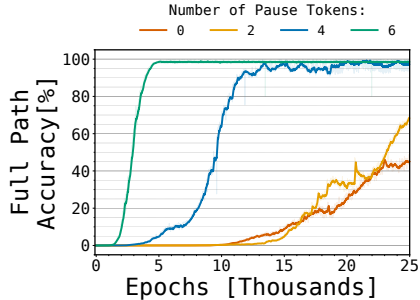


Figure 31: **Pause tokens boost convergence speed of in-weights path-star path-finding task of §2.**

D.3 (Not) Interleaving edge-memorization

In all our experiments, we have interleaved edge-memorization examples with path-finding examples. An alternative training method would be a two-phased approach, where we first enforce edge-memorization, and then follow up by finetuning on the path-finding task. We found this to be less stable, e.g., the model achieves a peak accuracy momentarily, only to deteriorate dramatically right after. This is a manifestation of the well-known effect that finetuning has on parametric memory [95, 103]. Since this is a confounding effect, we do not choose this regime for our experiments.

However, we confirm that even in this regime, our models do achieve a high peak accuracy (see Fig. 32). The fact that the composition task is learnable in this regime implies that the edge-pretrained model must have come with an adequate global geometry despite being trained only on local supervision (Refutation 3a).

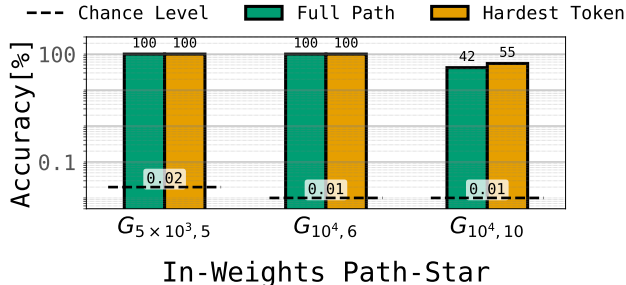


Figure 32: **Locally supervised model succeeds at path-finding task.** We report the *peak* accuracy under finetuning an edge-memorizing model on our path-finding task of §2. We emphasize that this accuracy value is only reached momentarily, and typically deteriorates quickly during further finetuning. Nevertheless, this suggests that local supervision alone was adequate to synthesize a global geometry (Refutation 3a). Learning rates of the two phases are given in §B.3.

D.4 Effect of weight-untying

As discussed in §4.4, weight-untied models do not produce an apparent geometry or exhibit high node-to-node cosine-similarities, since it corresponds to SVD directions. We demonstrate this for the Transformers in Fig. 11 and Fig. 34 and Node2Vec in Fig. 10 and Fig. 33.

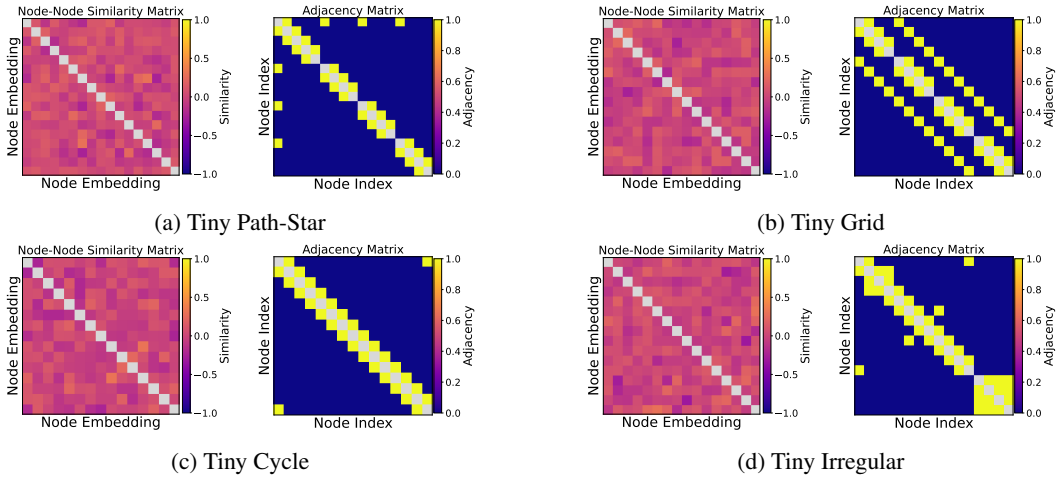


Figure 33: **Node-node cosine similarity vs. adjacency matrix for weight-untied Node2Vec.** As discussed in §4.4, observe that the node-to-node cosine-similarity matrix appears to be a bland near-zero matrix, lacking any information about the multi-hop connectivity of the underlying graph.

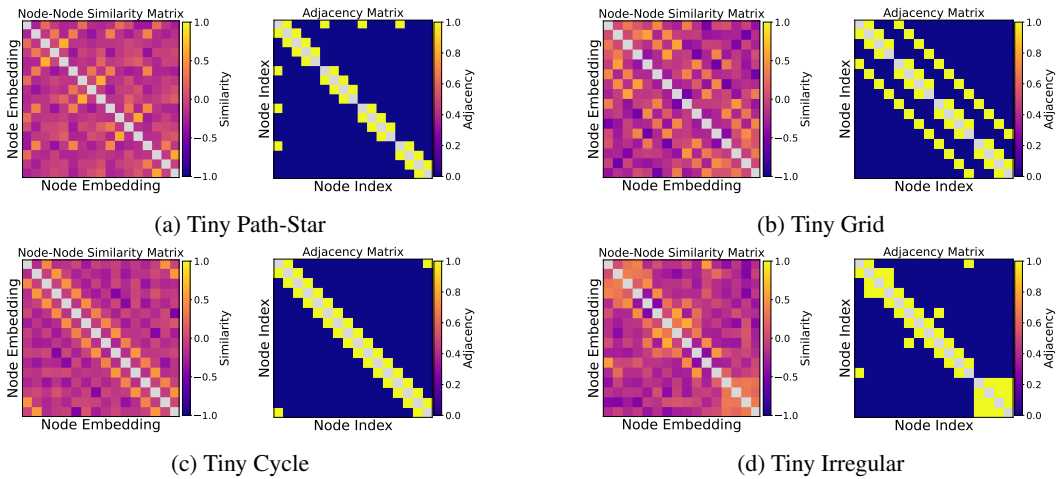


Figure 34: **Node-node cosine similarity vs. adjacency matrix for weight-untied Transformer.** As discussed in §4.4, observe that the node-to-node cosine-similarity matrix appears to be a bland near-zero matrix, lacking any information about the multi-hop connectivity of the underlying graph.

D.5 Learning order of tokens

For clarity, in Fig. 35, we provide a side-by-side contrast between the order in which tokens are learned in the in-weights setup (with next-token prediction) and the in-context setup (with multi-token prediction).

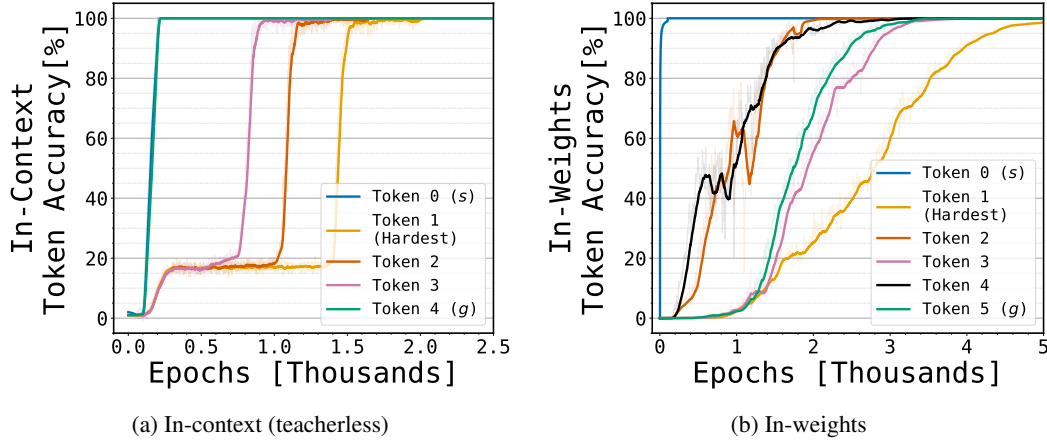


Figure 35: **Learning dynamics per token.** (a) In the in-context setting of $\mathcal{G}_{2,5}$ (trained with a multi-token, teacherless objective since standard next-token prediction fails), later tokens are learned first indicating strong reliance on future-token signals. (b) In the in-weights setting of $\mathcal{G}_{10^4,6}$ with next-token prediction, token accuracies rise largely in tandem (or in a somewhat confusing order); the first token is not selectively driven by future targets.

E Proofs about representational complexity

E.1 Empirical failure of composition learning under associative memory

As discussed in §2.3, it is well-known that certain compositional tasks are hard to learn empirically; theoretically, this has been proven in a certain sense. However, these prior discussions involve composing information available in the context, rather than in the weights. To test this intuition in our in-weights composition task, we design an experiment where we freeze the embeddings of a Transformer and train it on our path-star task. If the model succeeded in this task, it may mean one of two things: either the model develops a geometric memory in a subsequent layer, or the model does in fact efficiently learn how to compose associative matrix operations—going against our intuition derived from prior limits on composition learning. However, we find that even after 50,000 training epochs (using the same GPT-mid architecture described in Table 2 and §B.2.1, except with frozen token embeddings; and the optimization hyperparameter grid search reported in §B.3), the model fails to learn the in-weights path-star task. We believe, this is preliminary evidence that associative memory indeed struggles to learn compositional in-weights tasks. A fleshed-out proof of this negative result is left for future work.

E.2 Succinctness does not break the tie: Proof of Proposition 3d

In datasets where redundancies exist, the complexity of a lookup table scales quickly with the training set size (say n), whereas the more succinct solution does not (or at worst, grows polynomially slower). For example, if the data is linearly separable in some constant dimensionality, the linear classifier can be described in a constant number of bits, whereas a lookup table (such as a nearest neighbor model) would require n bits. However, this wide disparity in complexity does not necessarily surface in our setting, which is a *memorization* task without redundancies. Concretely, at least in terms of bits and ℓ_2 norms, there are simple graphs where both the geometric and associative views are equally complex—there is no factor of n , which in our case should be the edge count or the vertex count of our graph. We informally prove this below.

We first roughly derive the bit and norm complexity for a general graph, showing how an associative memory scales with the edge count, whereas a geometric memory scales with the vertex count. Then, we argue how this resolves to similar values for graphs like the path-star or a cycle, where the edge count and the vertex count are the same (almost).

Notation. We let $|V|$ be the number of entities and $|E|$ the number of associations.

Proposition 1. (Bit complexity) Storing a graph $\mathcal{G} = (V, E)$

- with associative memory requires $|E| \log |V|$ many bits (with a multiplicative factor of 2 if both direction of the edges must be stored).
- with geometric memory requires $|V|m \log \Delta$ many bits where m is the embedding dimensionality, and Δ is the number of cells along each dimension required to avoid collision. This is doubled if (un)embedding weights are not tied.

Proof. In the local associative view, given as input any vertex u , we must be able to lookup the vertex IDs of its neighbors. Thus, at the position of this vertex, we need a total of $d(u) \log |V|$ many bits (where $d(u)$ is the degree, and $\log |V|$ is the bit length of each ID). Summing this over all vertices gives us $|E| \log |V|$ many bits (since the sum of all degrees must equal the edge count). Note that an extra factor of 2 appears if both the direction of the edges must be stored.

In the geometric embedding, each vertex is stored as a vector in m dimensions. Each dimension must store one of Δ values, which requires $\log \Delta$ bits. Summing this up across all dimensions and vertices gives us the result. This is doubled if the unembedding matrix is not weight-tied. □

Proposition 2. (ℓ_2 norm complexity) Given a graph $\mathcal{G} = (V, E)$, and without loss of generality, given the margin constraint that if u is a neighbor of v , then $f(u)[v] - \arg \max_{w \notin \text{nbr}(u)} f(u)[w] \geq 1$ ($f(u)[v]$ denotes the logit of predicting v given u ; and w is a non-neighbor), then

1. associative memory requires ℓ_2 norm of at most $\sqrt{|E|}$ with an extra factor of $\sqrt{2}$ if both directions must be stored.
2. geometric memory requires an ℓ_2 norm of at least $\sqrt{|V|}$ with an extra factor of $\sqrt{2}$ if (un)embedding weights are not tied.

Proof. Recall that associative memory takes the form $f(u)[v] = \Phi(v)^T \mathbf{W}_{\text{assoc}} \Phi(u)$. Without loss of generality, if we assume that the embeddings are one-hot vectors in $\mathbb{R}^{|V|}$, we can set $\mathbf{W}_{\text{assoc}}$ to be the adjacency matrix to satisfy our margin constraint. The ℓ_2 norm (of the free parameters in $\mathbf{W}_{\text{assoc}}$) is $\sqrt{|E|}$.

In the geometric view, recall that $f(u)[v] = \Phi_{\text{geom}}(v)^T \Phi_{\text{geom}}(u)$. To have $\Phi_{\text{geom}}(v)^T \Phi_{\text{geom}}(u) > 1$, we need $\|\Phi_{\text{geom}}(v)\|^2 + \|\Phi_{\text{geom}}(u)\|^2 > 2$. Thus, roughly, all embedding norms must be at least 1, implying that $\sum_u \|\Phi_{\text{geom}}(u)\|^2 \geq |V|$. \square

Proof of Main Refutation 3d

Proof. Our proof follows from the fact that for graphs like the path-star graph and the cycle graph, the edge count and vertex count are nearly equal. Thus, both notions of complexity—the associative scaling with the edge count and the geometric with vertex count—can be shown to reduce to similar values here from the above propositions.

This is straightforward to see for ℓ_2 norm based complexity based on Lemma 2. For the bit complexity estimates, from Lemma 1, we know that associative memory costs $|V| \log |E|$ many bits; for the geometry, we need to pin down the values of the embedding dimension m and the cell count Δ .

The path-star graph can be embedded such that each path is stored along a unique dimension (thus totally $m = d$ dimensions), and each dimension can be gridded into ℓ many cells. This requires a bit complexity of $|V|d \log \ell$. For a more ambitious geometry, we could further squeeze this into $\log d$ dimensions while still keeping the paths well-separated (by the Johnson–Lindenstrauss lemma), resulting in $|V| \log d \log \ell$ bits. This is still greater than the cost of associative memory which is approximately $|V|(\log d \ell) = |V|(\log d + \log \ell)$.

A similar argument works for a cycle graph. Here, we can embed in $m = 2$ dimensions, with a cell count of $|V|/2$, thus totaling $2|V| \log(|V|/2)$ bits for geometric memory, again greater than $|V| \log |E|$ when $|V| = |E|$. \square

E.3 Weight-tied dual-encoder models can represent certain special or contrived forms of associative memory

In the standard associative memory view that we have discussed, associations are represented through the function $\Phi(v)^T \mathbf{W}_{\text{assoc}} \Phi(u)$. However, weight-tied dual encoder models like Node2Vec can only represent functions of the form $\Phi(v)^T \Phi(u)$. When weight-tied, this precludes the form of associative memory we care about; but it still allows two forms of associative memories under special conditions: if the graph is bipartite (Lemma 3) or if the embedding dimensionality is sufficiently large (in which case, the construction is contrived; see Lemma 5). We can also show that non-weight-tied models can represent any graph associatively (see Lemma 4). In all these results below, we will show that our constructions achieve a logit of 1 on adjacent vertices, but a logit of 0 on any non-adjacent vertices. In this sense, only local associations are captured, whereas no global geometry is.

Proposition 3. *Weight-tied dual encoder models of the form $\Phi(v) \cdot \Phi(u)$ can store a graph \mathcal{G} associatively when the graph is bipartite.*

Proof. Assume that the graph partition consists of vertices V_1 and V_2 . The construction is to represent one set of vertices with a one-hot representation, and the other by a one-hot adjacency vector. That is, consider an embedding $\Phi : V \rightarrow \mathbb{R}^{|V_1|}$ that has dimensionality $|V_1|$. For any $v_i \in V_1$, assume $\Phi(v)$ is such that it is 1 only at index i . For $w \in V_2$, $\Phi(w)$ at index i is 1 if and only if v is adjacent to v_i i.e., $\Phi(w)_i = \mathbf{1}[(w, v_i) \in E]$.

Thus, if w and v belong in the same partition $\Phi(v) \cdot \Phi(w) = 0$; if in different partitions, $\Phi(v) \cdot \Phi(w) = \mathbf{1}[(w, v) \in E]$. \square

Proposition 4. *Weight-untied dual encoder models of the form $\Phi_1(v) \cdot \Phi_2(u)$ can store any graph associatively when the embedding dimension is at least as large as the vertex count. Furthermore, this can be approximately learned in one-step of gradient descent under the correlation loss $\sum_{(u,v) \in E} (\Phi_1(u)) \cdot \Phi_2(v)$ with one tower frozen.*

Proof. The proof parallels that of Lemma 3. We set one of the embeddings to a one-hot representation of the vectors; the other is set to embed the adjacency row. In matrix notation, the resulting model (which outputs a vector of logits for a given input \mathbf{u}) looks like $f(\mathbf{u}) = \mathbf{W}_2 \mathbf{W}_1 \mathbf{u} = \mathbf{A} \mathbf{I} \mathbf{u} = \mathbf{A} \mathbf{u}$.

To show that this can be learned in one-step of gradient descent, consider Φ_1 initialized randomly. Given sufficiently high embedding size, these embeddings are orthogonal. Under the correlation loss, if one were to freeze Φ_1 , $\Phi_2(v)$ will be updated in the direction of $\sum_{u \in \text{nbr}(v)} \Phi_2(u)$, which is equivalent to the adjacency row up to a rotation. For a sufficiently large learning rate, the resulting model would effectively store \mathbf{A} up to a rotation defined by Φ_1 . \square

Now, for a generic graph, and for a weight-tied dual encoder model, we show that Node2Vec can represent a contrived form of associative memory when there is a much larger embedding dimensionality scaling with edge count. ¹⁴

Proposition 5. *Weight-tied dual encoder models of the form $\Phi(v) \cdot \Phi(u)$ can store a graph associatively given an embedding dimensionality of $|E|$ where E is the set of pairwise associations.*

Proof. For each node, we take its corresponding row from the “incidence” matrix. In other words, the embedding is $|E|$ -dimensional, where the i th dimension corresponds to the i th edge; for edge (u, v) , the embedding of u and v both are set to 1 along the dimension corresponding to (u, v) . Notationally, if the edges are indexed as $1, 2, \dots$, then $\Phi(u)_i = \mathbf{1}[u \in e_i]$, where $\mathbf{1}$ is the indicator function. Then, we have that $\Phi(u) \cdot \Phi(v) = \mathbf{1}[(u, v) \in E]$. Thus, the dot products capture only local information. \square

¹⁴We suspect this should also be a lower bound i.e., such a large dimensionality must be needed to represent associatively in Node2Vec.

F Detailed analysis of spectral bias in Node2Vec

Let G be a graph of n nodes $\{1, 2, \dots, n\}$. Let $\mathbf{A} \in \mathbb{R}^{n \times n}$ be the adjacency matrix, $\mathbf{D} \in \mathbb{R}^{n \times n}$ the diagonal degree matrix, and let the embedding of the nodes be denoted by $\mathbf{V} \in \mathbb{R}^{n \times m}$, where m is the embedding dimensionality. Let $\mathbf{L} = (\mathbf{I} - \mathbf{D}^{-1}\mathbf{A}) + (\mathbf{I} - \mathbf{D}^{-1}\mathbf{A})^T$ denote the *asymmetrically normalized random walk graph Laplacian*. The second topmost eigenvectors of $-\mathbf{L}$ are called the Fiedler vectors; we refer to them and the next few eigenvectors as Fiedler-like eigenvectors. The topmost eigenvector of $-\mathbf{L}$ is a degenerate eigenvector of (approximately) all 1s.

Node2Vec setup. We consider the simplest Node2Vec model, where the embeddings are directly parameterized by \mathbf{V} . We consider a 1-hop objective (where the neighborhood is defined by the immediate neighbors rather than by more distant ones discovered by a random walk). Note that our objective uses the full softmax loss:

$$\mathcal{J}_{\text{Node2Vec}}(\mathbf{V}) = \max_{\mathbf{V}} \sum_i \frac{1}{|\text{nbr}(\cdot)|} \sum_{j \in \text{nbr}(i)} \log \underbrace{\frac{\exp(\mathbf{v}_i^T \mathbf{v}_j)}{\sum_k \exp(\mathbf{v}_i^T \mathbf{v}_k)}}_{p(i,j)}, \quad (1)$$

where $\text{nbr}(\cdot)$ denotes the neighboring vertices in graph \mathcal{G} . The above (degree-normalized) objective resembles optimizing over a sequence dataset where we sample the first vertex uniformly, and the second vertex uniformly from its neighborhood.

Let $\mathbf{P} \in \mathbb{R}^{n \times n}$ be the matrix of probabilities $p(i, j)$, where:

$$\mathbf{P} = \text{row_softmax}(\mathbf{V}\mathbf{V}^T). \quad (2)$$

The dynamics of the Node2Vec algorithm can be expressed as below:

Lemma 6. *The update on the representations under gradient maximization of the Node2Vec objective in Eq 1 can be written as:*

$$\Delta \mathbf{V}(t) = \eta \mathbf{C}(t) \mathbf{V}(t) \text{ where, } \mathbf{C}(t) = \underbrace{(\mathbf{D}^{-1}\mathbf{A} - \mathbf{P}(t)) + (\mathbf{D}^{-1}\mathbf{A} - \mathbf{P}(t))^T}_{\text{co-efficient matrix}} \quad (3)$$

We prove this in §F.4.

F.1 Challenges of analyzing the dynamics

Unlike previously-studied dynamics which simplify nicely, this system may behave in one of many ways. For one, it may simply diverge, but if we are a bit lucky, it may at least converge in direction (like in logistic regression [162]); but then, this direction then may be degenerate—an all-one representation could potentially be a stable direction—and perhaps nice directions are visible only if we analyze with early-stopping. One way to get a handle on this would have been to show that, in the limit, we have $\mathbf{C}(t) \rightarrow 0$; solving this could then spell out the (limit) probability matrix \mathbf{P} , if not the inner products $\mathbf{V}\mathbf{V}^T$ themselves. However, we find that \mathbf{C} cannot be zero as that would require the self-probability term $p(i, i) = 0$, which is infeasible. This closes all obvious analytical routes to understanding this system, so we turn to an empirical study.

F.2 Empirical intuition of the dynamics

Empirically, we find that the model tends towards a gradient-zero state by working its way toward satisfying a two-fold constraint in Observation 7. First, the column space of $\mathbf{V}(t)$ converges to the top eigenvectors of $\mathbf{C}(0)$ —which is approximately the negative of the Laplacian \mathbf{L} . Concurrently, $\mathbf{C}(t)$ itself converges such that its null space matches these eigenvectors. Together then, the update $\Delta \mathbf{V}(t)$ in Lemma 6 must become zero.

Observation 7. *We find that $\Delta \mathbf{V}(t) \rightarrow 0$ through the following concurrent behaviors:*

- *The null space of $\mathbf{C}(t)$ spans the top eigenvectors of $-\mathbf{L}$.*

- The column space of $\mathbf{V}(t)$ converges to the top eigenvectors of $-\mathbf{L}$.

Crucially, we find that this can happen (a) even without a constraint on the dimensionality m and (b) this requires *no* early-stopping (see Remark 5 for a more nuanced discussion of this).

We lay out our empirical intuition below, deferring a more mathematical description of the same to the following section. First, we postulate a key invariant during training: the eigenvectors of the coefficient matrix $\mathbf{C}(t)$, the probability matrix $\mathbf{P}(t)$ and the embeddings $\mathbf{V}(t)$ all remain (inexplicably) stable during training. In particular, since the system begins with $\mathbf{P}(0) \approx \mathbf{I}$, and so $\mathbf{C}(0) \approx -\mathbf{L}$ all these eigenvectors are then fixed as the eigenvectors of the normalized random walk graph Laplacian.

Next, we find that the eigenvalues of the co-efficient matrix $\mathbf{C}(t)$ begin *negative*, gradually approaching zero. The top eigenvectors reach zero first, achieving the second condition in Observation 7. That the values begin negative follows from the fact that the co-efficient matrix begins as the negative graph Laplacian. That these values approach zero follows from the fact that embedding vectors become less orthogonal over time; this in turn reduces the eigenvalues of $\mathbf{P}(t)$, which increases the eigenvalues of $\mathbf{C}(t)$.

Next, due to the negative eigenvalues of $\mathbf{C}(t)$, the embeddings \mathbf{V} along the lowermost eigendirections quickly diminish, achieving our first condition. Note that this means we do not want early-stopping; unlike in the quadratic loss formulation of Karkada et al. [83], it is longer training that filters out the lower eigenvectors. (Although, the existence of a degenerate eigenvector complicates this; see Remark 5). This achieves the first condition in Observation 7.

Observe that this argument does not require any upper bound on the size of the embedding space. It is unclear if a more succinct, margin-maximizing or norm-minimizing view of these dynamics is expressible.

Remark 5. (The degenerate vector and early-stopping) *When the graph Laplacian is symmetrically normalized (e.g., $\mathbf{D}^{-1/2} \mathbf{A} \mathbf{D}^{-1/2} - \mathbf{I}$), the top-most eigenvector of the graph Laplacian is a degenerate vector that assigns a constant value to all nodes, and provably corresponds to a zero eigenvalue. However, in our setting, this eigenvalue is slightly above zero, likely due to the asymmetric nature of our Laplacian. Therefore, as we train for longer, the model would become degenerate thus requiring early-stopping. However, this is a conceptually different reason to early-stop than the one in Karkada et al. [83]. Here we may need to early-stop to prevent collapse to the top eigenvector; whereas in Karkada et al. [83], it is to prevent expansion to bottom eigenvectors.*

F.3 Mathematical description

Below, we provide a more mathematical description of the above summary by dividing it up into various propositions. Our proofs for these propositions are highly informal. However, our propositions hold in practice without our simplifying assumptions (at least in the graphs we study). We leave it for future work to deliver a rigorous proof and a more clearly characterized theorem statement.

First, we note that the co-efficient matrix approximately begins as the negative graph Laplacian for an appropriately large initialization. (Without this assumption, we may still make a connection to a graph Laplacian-like object).

Assumption 1. We assume a sufficiently large magnitude or embedding dimensionality of random initialization such that the initial embeddings are nearly orthogonal as $\mathbf{V}(0)\mathbf{V}(0)^T \approx c\mathbf{I}$.

Fact 1. Under Assumption 1,

$$\mathbf{C}(0) \approx -\mathbf{L} = (\mathbf{D}^{-1} \mathbf{A} + (\mathbf{D}^{-1} \mathbf{A})^T - 2\mathbf{I}). \quad (4)$$

Proof. At time $t = 0$, the embeddings $\mathbf{V}(0)$ are all random, and hence nearly orthogonal to each other i.e., $\mathbf{V}(0)\mathbf{V}(0)^T \approx c\mathbf{I}$, where c is some constant that depends upon the magnitude of the random initialization. Since $\mathbf{P} = \text{row_softmax}(\mathbf{V}\mathbf{V}^T(t))$, for a sufficiently large c , $\mathbf{P}(0) \approx \mathbf{I}$, proving our claim. \square

Next, we make the empirical observation that the eigenvectors of $\mathbf{P} + \mathbf{P}^T$ match the eigenvectors of the embedding inner products $\mathbf{V}\mathbf{V}^T$. Note that \mathbf{P} is related to the inner product via a non-linear row softmax operation, rendering a proof of this observation highly non-trivial. We assume this observation (without even an intuitive proof) for the rest of our discussion.

Observation 8. (Eigenvectors remain unchanged under a row-softmax transform) The eigenvectors of $\mathbf{P}(t) + \mathbf{P}(t)^T$ at any time t , are also approximately the eigenvectors of the embeddings $\mathbf{V}(t)\mathbf{V}(t)^T$, appearing in the same order.

From the above observation, we can conclude that the eigenvectors of the system match the Laplacian throughout training. This follows by how the updates reduce to multiplications between matrices sharing the same eigenspaces.

Proposition 7. (Time-invariant eigenvectors match that of the Laplacian) With Assumption 1 and by assuming Observation 8 as a given, we have that for all t , the quantities $\mathbf{C}(t), \mathbf{P}(t) + \mathbf{P}(t)^T, \mathbf{V}(t)\mathbf{V}(t)^T$ have the same eigenvectors as that of the negative Laplacian $-\mathbf{L}$.

Proof. At any time t , we can write the embedding vectors as

$$\mathbf{V}(T) = \prod_{t=0}^{T-1} (1 + \eta \mathbf{C}(t)) \mathbf{V}(0), \quad (5)$$

and so the inner product as

$$\mathbf{V}(T)\mathbf{V}(T)^T = \prod_{t=0}^{T-1} (1 + \eta \mathbf{C}(t)) \underbrace{\mathbf{V}(0)\mathbf{V}(0)^T}_{\approx c\mathbf{I} \text{ by Assumption 1}} \prod_{t=0}^{T-1} (1 + \eta \mathbf{C}(t))^T \quad (6)$$

$$\approx c \prod_{t=0}^{T-1} (1 + \eta \mathbf{C}(t))(1 + \eta \mathbf{C}(t))^T. \quad (7)$$

From here, we inductively prove our claim. At $t = 0$, it is indeed the case that $\mathbf{C}(t), \mathbf{P}(t), \mathbf{V}(t)\mathbf{V}(t)^T$ all have the same eigenvectors as \mathbf{L} either by Fact 1 for $\mathbf{C}(0)$, or trivially since $\mathbf{P}(t)$ and $\mathbf{V}(t)$ are orthogonal matrices. We assume this is true for all t until $T - 1$. Then, by the above equation, it is also true that the inner product $\mathbf{V}\mathbf{V}^T$ shares these eigenvectors. By invoking Observation 8, we can say that the same is true of the probability matrix $\mathbf{P} + \mathbf{P}^T$. Subsequently, this is true of $\mathbf{C}(t)$, which equals $\mathbf{D}^{-1}\mathbf{A} + (\mathbf{D}^{-1}\mathbf{A})^T + (\mathbf{P} + \mathbf{P}^T)$. (Note that the first term here has the same eigenvectors as $-\mathbf{L}$ as it is off only by the identity matrix.) This proves our inductive assumption. \square

Next, we begin to bound the eigenvalues of the system. For the sake of our informal proofs we make some simplifying assumptions that make our matrices approximately symmetric; however, we do not need these assumptions in practice.

Assumption 2. For theoretical convenience, we assume that:

- $\mathbf{P} \approx \mathbf{P}^T$.
- the embeddings (i.e., the rows of \mathbf{V}) are of equal ℓ_2 norms.
- the degrees of all nodes are roughly equal.

Now, we can observe a bound on the eigenvalues of the probability matrix.

Proposition 8. (Eigenvalues of the probability matrix) Under Assumption 2, the eigenvalues of $\mathbf{P}(t) + \mathbf{P}(t)^T$ are such that:

1. their sum is upper bounded by $2n$ (where n is the number of nodes).
2. they are each approximately bounded in $[0, 2]$

Proof. For the first result, recall the fact the sum of eigenvalues is the trace of the matrix. Since each diagonal term is at most 2 (it is $2p(i, i)$), the trace is at most $2n$. This requires no special assumptions.

For the bounds on each eigenvalue, we can rely on the Gershgorin Circle theorem, which states that the eigenvalues lie in the union of discs centered at the diagonals $p(i, i)$, each with radius equal to the sum of the absolute off-diagonal terms, $\sum_{j \neq i} p(i, j)$. The upper bound is then equal to the sum of the

rows. For $\mathbf{P}(t)$, this sum is equal to 1 due to the row-softmax operation. Assuming $\mathbf{P}^T \approx \mathbf{P}$ —which is approximately true in practice, especially if the node degrees are uniform (but not always)—, we can conclude that the upper bound is approximately 2.

For the lower bound, if we have that the self-probabilities $p(i, i)$ are the largest in any row, then the lower bound $p(i, i) - \sum_{j \neq i} p(i, j)$ is at least zero. This is indeed the case if the embeddings of all nodes are of approximately equal norms, in which case the inner product $\mathbf{V}\mathbf{V}^T$ is highest along the diagonal. \square

Proposition 9. *The eigenvalues of $\mathbf{D}^{-1}\mathbf{A} + (\mathbf{D}^{-1}\mathbf{A})^T$ approximately lie in $[-2, 2]$ assuming that the nodes have approximately uniform degree as in Assumption 2.*

Proof. The diagonal of $\mathbf{D}^{-1}\mathbf{A}$ is 0 (assuming no self-loops in the graph), while the off-diagonal values are all positive and sum up to 1 in each row. When the node degrees are approximately uniform, $\mathbf{D}^{-1}\mathbf{A} \approx (\mathbf{D}^{-1}\mathbf{A})^T$. From the Gergshgorin circle theorem, the eigenvalues lie in the union of discs centered at the diagonal (from the above, 0) with radii equal to the sum of the absolute off-diagonal terms (from the above, 2), thus proving our claim. \square

Now, we can establish the conditions in Observation 7, namely, the convergence of the null space of the co-efficient matrix from Observation 1, and then the convergence of the embedding vectors.

Proposition 10. *Under Assumption 2 and Assumption 1, at any time instant t , the eigenvalues of $\mathbf{C}(t)$ are all strictly negative (except for the topmost eigenvalue, which is of a degenerate all-1 eigenvector, and is approximately zero), and this is so until when the top eigenvectors of the Laplacian converge into the null space of $\mathbf{C}(t)$ (i.e., their eigenvalues become zero).*

Intuition. Recall that $\mathbf{C}(t) = \mathbf{D}^{-1}\mathbf{A} + (\mathbf{D}^{-1}\mathbf{A})^T - (\mathbf{P} + \mathbf{P}^T)$. The eigenvalues of the first term lie approximately in $[-2, 2]$ from Lemma 9, while that of the probability term lie in $[0, 2]$, from Lemma 8. Note that eigenvalues of the probability matrix all begin uniformly at 2 in the beginning (as $\mathbf{P}(0) = \mathbf{I}$, by Fact 1 under Assumption 1), as a result of which the initial eigenvalues of $\mathbf{C}(t)$ start at or below 0.

While the embeddings are initialized orthogonally under Assumption 1, they become less orthogonal during training, leading to a gradual decrease of the diagonal self-probability terms in $\mathbf{P} + \mathbf{P}^T$. Intuitively, this also means that the eigenvalues of $\mathbf{P} + \mathbf{P}^T$ must themselves all decrease from the initial value of 2 (based on Lemma 8). In turn, the eigenvalues of $\mathbf{C}(t)$, which begin negative must gradually inch toward zero. The topmost eigenvalues—which are closest to zero—are the first to reach zero.¹⁵ \square

Proposition 11. (Embeddings converge to top eigenvectors) *Assuming Observation 8 as a given, for a sufficiently small learning rate η , with increasing timestep t , the column space of $\mathbf{V}(t)$ converges to the top eigenvectors of the negative graph Laplacian $-\mathbf{L}$, independent of the embedding dimensionality.*

Proof. We can examine the dynamics of each embedding dimension separately.¹⁶ For the embedding dimension $j = 1, 2, \dots, m$, let $\mathbf{r}_j \in \mathbb{R}^n$ denote the j th column of the embedding matrix \mathbf{V} . The dynamics of this column (we drop the index j for the moment) at any timestep t can be isolated as:

$$\mathbf{r}(t) = \prod_{t=0}^T (1 + \eta \mathbf{C}(t)) \mathbf{r}(0). \quad (8)$$

Given that $\mathbf{C}(t)$ have time-invariant eigenvectors (by Lemma 7), this can be further simplified as

$$\mathbf{r}(t) = \mathbf{E} \left(\prod_{t=0}^T (1 + \eta \mathbf{\Lambda}(t)) \right) \mathbf{E}^T \mathbf{r}(0). \quad (9)$$

¹⁵Note that this is not straightforward to show. It is possible that even if the initial eigenvalues are very close to zero, they approach 0 slower than farther off values.

¹⁶This is possible only in a dual-encoder, Node2Vec style architecture. In a Transformer for example, there are cross-dimensional interactions, due to the associative weight matrix $\mathbf{W}_{\text{assoc}}$ that interfaces between the embedding and unembedding layers.

Given that the eigenvalues in Λ are all less than or equal to zero (by Lemma 10), the term $(1 + \eta\Lambda(t))$ must consist of a diagonal of values in $[0, 1]$ for an appropriately small learning rate. Furthermore, as T becomes large, the values of the top eigenvectors (which have the least eigenvalues, and therefore, the largest value of $1 + \eta\lambda_i(t)$) must come to dominate. Then, as t increases, we can express the embedding dimension as an affine combination of some top K eigenvectors (where the coefficients depend on how the embedding dimension was initialized):

$$\mathbf{r}(t) \approx \sum_{k=1}^K \left(\prod_t (1 + \eta\lambda_k(t)) \mathbf{r}(0) \cdot \mathbf{e}_k \right) \mathbf{e}_k. \quad (10)$$

□

F.4 Deriving the dynamics

We provide proof of Lemma 6 which expresses the dynamical system of our Node2Vec objective in Eq 1.

Proof. For a pair of nodes with embeddings $\mathbf{u} \in \mathbb{R}^m, \mathbf{v} \in \mathbb{R}^m$, the probability value of the edge (\mathbf{u}, \mathbf{v}) can be written as:

$$p(\mathbf{u}, \mathbf{v}) = \frac{\exp(\mathbf{u} \cdot \mathbf{v})}{\sum_{\mathbf{v}'} \exp(\mathbf{u}, \mathbf{v}')} \quad (11)$$

Let $N(u)$ denote the neighborhood of the node u , and N_u , its degree. Let \mathcal{J}_u denote the summand in the objective function specific to that node:

$$\mathcal{J}_u(\mathbf{V}) = \frac{1}{|N(u)|} \sum_{\mathbf{v} \in N(u)} \log p(\mathbf{u}, \mathbf{v}) \quad (12)$$

We now compute the derivative of \mathcal{J}_u with respect to itself \mathbf{u} :

$$\frac{\partial \mathcal{J}_u(\mathbf{V})}{\partial \mathbf{u}} = \frac{1}{N_u} \sum_{\mathbf{v} \in N(u)} \left(\underbrace{\mathbf{v}}_{\text{numerator}} - \underbrace{\sum_{\mathbf{v}' \neq \mathbf{u}} p(\mathbf{u}, \mathbf{v}') \mathbf{v}' - 2p(\mathbf{u}, \mathbf{u}) \mathbf{u}}_{\text{denominator}} \right) \quad (13)$$

$$= \frac{1}{N_u} \sum_{\mathbf{v} \in N(u)} \mathbf{v} - \sum_{\mathbf{v}' \neq \mathbf{u}} p(\mathbf{u}, \mathbf{v}') \mathbf{v}' - 2p(\mathbf{u}, \mathbf{u}) \mathbf{u} \quad (14)$$

Next, we compute the derivative of \mathcal{J}_w with respect to \mathbf{u} for nodes $w \neq u$:

$$\frac{\partial \mathcal{J}_w(\mathbf{V})}{\partial \mathbf{u}} = \frac{1}{N_w} \sum_{\mathbf{v} \in N(w)} \left(\underbrace{\mathbf{1}[u = v] \mathbf{w}}_{\text{numerator}} - \underbrace{p(\mathbf{w}, \mathbf{u}) \mathbf{w}}_{\text{denominator}} \right) \quad (15)$$

$$= \frac{1}{N_w} \sum_{\mathbf{v} \in N(w)} \mathbf{1}[u = v] \mathbf{w} - p(\mathbf{w}, \mathbf{u}) \mathbf{w} \quad (16)$$

$$(17)$$

By writing the above expressions as a matrix formula, we get the dynamical system claimed in Lemma 6. □